

การวิเคราะห์ไอออนปรอท(II) เซิงสเปกโทรเมตรีโดยใช้อนุภาคระดับนาโนเมตร  
ของทองคำที่ทำให้เสถียรด้วยลิแกนด์ไดไทอะ-ไดเอซา

นายวรวิทย์ จันทรสุวรรณ

วิทยานิพนธ์นี้เป็นส่วนหนึ่งของการศึกษาตามหลักสูตรปริญญาวิทยาศาสตรดุษฎีบัณฑิต

สาขาวิชาเคมี ภาควิชาเคมี

คณะวิทยาศาสตร์ จุฬาลงกรณ์มหาวิทยาลัย

ปีการศึกษา 2555

ลิขสิทธิ์ของจุฬาลงกรณ์มหาวิทยาลัย

บทคัดย่อและแฟ้มข้อมูลฉบับเต็มของวิทยานิพนธ์ตั้งแต่ปีการศึกษา 2554 ที่ให้บริการในคลังปัญญาจุฬาฯ (CUIR)

เป็นแฟ้มข้อมูลของนิสิตเจ้าของวิทยานิพนธ์ที่ส่งผ่านทางบัณฑิตวิทยาลัย

The abstract and full text of theses from the academic year 2011 in Chulalongkorn University Intellectual Repository (CUIR)

are the thesis authors' files submitted through the Graduate School.

SPECTROMETRIC ANALYSIS OF MERCURY(II) ION USING GOLD  
NANOPARTICLES STABILIZED BY DITHIA-DIAZA LIGANDS

Mr. Woravith Chansuvarn

A Dissertation Submitted in Partial Fulfillment of the Requirements  
for the Degree of Doctor of Philosophy Program in Chemistry

Department of Chemistry

Faculty of Science

Chulalongkorn University

Academic Year 2012

Copyright of Chulalongkorn University

Thesis Title                    SPECTROMETRIC ANALYSIS OF MERCURY(II) ION  
   USING GOLD NANOPARTICLES STABILIZED  
   BY DITHIA-DIAZA LIGANDS  
By                                    Mr. Woravith Chansuvarn  
Field of Study                    Chemistry  
Thesis Advisor                    Assistant Professor Apichat Imyim, Ph.D.

---

Accepted by the Faculty of Science, Chulalongkorn University in Partial  
Fulfillment of the Requirements for the Doctoral Degree

..... Dean of the Faculty of Science  
(Professor Supot Hannongbua, Dr.rer.nat.)

#### THESIS COMMITTEE

..... Chairman  
(Assistant Professor Warinthorn Chavasiri, Ph.D.)

..... Thesis Advisor  
(Assistant Professor Apichat Imyim, Ph.D.)

..... Examiner  
(Professor Thawatchai Tuntulani, Ph.D.)

..... Examiner  
(Associate Professor Orawon Chailapakul, Ph.D.)

..... External Examiner  
(Chatvalee Kalambaheti, Ph.D.)

วรวิทย์ จันทร์สุวรรณ : การวิเคราะห์ไอออนปรอท(II) เชิงสเปกโทรเมตรีโดยใช้อนุภาคระดับนาโนเมตรของทองคำที่ทำให้เสถียรด้วยลิแกนด์ไดไทอะ-ไดเอซา. (SPECTROMETRIC ANALYSIS OF MERCURY(II) ION USING GOLD NANOPARTICLES STABILIZED BY DITHIA-DIAZA LIGANDS) อ. ที่ปรึกษาวิทยานิพนธ์หลัก : ผศ.ดร.อภิชาติ อัมย์ม, 132 หน้า.

งานวิจัยนี้เสนอแนวทางการพัฒนาวิธีการวิเคราะห์ไอออนปรอท(II) เชิงสเปกโทรเมตรีและด้วยตาเปล่าโดยอาศัยการเกิดปฏิกิริยารีดักชันของทองคำ(III) เป็นอนุภาคระดับนาโนเมตรของทองคำที่ใช้ลิแกนด์ไดไทอะ-ไดเอซา 3 ชนิดคือ 3-AEPE, 4-AEBE และ 5-AEPE เป็นตัวทำให้อนุภาคระดับนาโนเมตรของทองคำมีความเสถียรและป้องกันไม่ให้อนุภาคเกาะรวมตัวกัน สารละลายของอนุภาคระดับนาโนเมตรของทองคำที่มีลิแกนด์ไดไทอะ-ไดเอซามีสีแดงอย่างชัดเจนและปรากฏเป็นสีม่วงและน้ำเงินเมื่อมีไอออนปรอท(II) การศึกษาสภาวะที่เหมาะสมของการเกิดอนุภาคระดับนาโนเมตรของทองคำที่ทำให้เสถียรด้วยลิแกนด์ 3-AEPE พบว่าความเข้มข้นของสารละลายทองคำ(III), ลิแกนด์ 3-AEPE,  $\text{NaBH}_4$  และ Triton X-100 เป็น 125 ไมโครโมลต่อลิตร 0.3 มิลลิโมลต่อลิตร 0.6 มิลลิโมลต่อลิตร และ 0.1% (ปริมาตรต่อปริมาตร) ตามลำดับ และ pH ที่เหมาะสมเท่ากับ 1.4 วิธีวิเคราะห์นี้มีความจำเพาะสูงต่อไอออนปรอท(II) โดยสามารถวัดการดูดกลืนแสงที่ความยาวคลื่น 680 นาโนเมตร และพบว่ากราฟความเป็นเส้นตรงแบ่งได้ 3 ช่วงได้แก่ ช่วงความเข้มข้นต่ำ (0 ถึง 1.25 ไมโครโมลต่อลิตร) ช่วงความเข้มข้นกลาง (1.25 ถึง 5.25 ไมโครโมลต่อลิตร) และช่วงความเข้มข้นสูง (5.25 ถึง 10.0 ไมโครโมลต่อลิตร) ชีดจำกัดการตรวจวัดเป็น 35 นาโนโมลต่อลิตร ร้อยละความเบี่ยงเบนมาตรฐานสัมพัทธ์เป็น 1.3 ( $n = 11$ ) และร้อยละของการกลับคืนอยู่ในช่วง 90.7 ถึง 106.7 ส่วนอนุภาคระดับนาโนเมตรของทองคำที่ทำให้เสถียรด้วยลิแกนด์ 4-AEBE และ 5-AEPE ให้ผลการทดลองเหมือนกับ 3-AEPE แต่ใช้ความเข้มข้นของลิแกนด์ 4-AEBE, 5-AEPE และ  $\text{NaBH}_4$  ไม่เท่ากัน เปรียบเทียบลิแกนด์ทั้ง 3 ชนิด พบว่าลิแกนด์ 3-AEPE มีสภาพไวในการวิเคราะห์มากกว่า 4-AEBE และ 5-AEPE และสังเกตการเปลี่ยนสีด้วยตาเปล่าได้ง่ายกว่า วิธีวิเคราะห์ที่พัฒนาขึ้นมีข้อดีเช่น สะดวก รวดเร็ว ราคาถูก และไม่จำเป็นต้องใช้เครื่องมือที่มีความซับซ้อนสูงและสามารถประยุกต์ในการวิเคราะห์ไอออนปรอท(II) ในน้ำดื่มบรรจุขวดได้ และวิธีวิเคราะห์นี้ไม่จำเป็นต้องเตรียมอนุภาคระดับนาโนเมตรของทองคำขึ้นมาก่อนและใช้เวลาในการวิเคราะห์น้อย

ภาควิชา.....เคมี..... ลายมือชื่อนิสิต.....  
 สาขาวิชา.....เคมี..... ลายมือชื่อ อ.ที่ปรึกษาวิทยานิพนธ์หลัก.....  
 ปีการศึกษา 2555.....

# # 5173853523 : MAJOR CHEMISTRY

KEYWORDS : GOLD NANOPARTICLE / MERCURY(II) / DITHIA-DIAZA LIGANDS / SPECTROMETRIC / NAKED-EYE

WORAVITH CHANSUVARN: SPECTROMETRIC ANALYSIS OF MERCURY(II) ION USING GOLD NANOPARTICLES STABILIZED BY DITHIA-DIAZA LIGANDS. ADVISOR: ASST. PROF. APICHAT IMYIM, Ph.D., 132 pp.

A novel method has been proposed to realize the visual and colorimetric detection of Hg(II) ions based on direct reduction of Au(III) solution to gold nanoparticle (AuNPs). Three dithia-diaza ligands: 3-AEPE, 4-AEBE and 5-AEPE, were synthesized and used as a stabilizer for preventing the aggregation of gold nanoparticles in the absence of Hg(II) ion, showing a rose-red color. In the presence of Hg(II) ion, gold nanoparticle stabilized by dithia-diaza ligand solution became purple and blue immediately when addition of reducing agent NaBH<sub>4</sub>. For spectrometric and naked eye detection, the suitable concentration of Au(III) solution, 3-AEPE, NaBH<sub>4</sub> and Triton X-100 was 125 μM, 0.3 mM, 0.6 mM and 0.1%(v/v), respectively. The suitable pH of 3-AEPE-stabilized gold nanoparticles was 1.4. By comparing with other metal ions, only Hg(II) ion can induce the aggregation of gold nanoparticles, resulting solution turns to blue rapidly. By measuring at a wavelength of 680 nm, absorbance values increased linearly as three levels of concentration of Hg(II) ion range of 0 - 1.25 μM (low), 1.25 - 5.25 μM (medium) and 2.25 - 10.0 μM (high). The limit of detection was estimated to be 35 nM, with a relative standard deviation of 1.3% (n = 11). The acceptable recoveries of spiked samples were found in the range of 90.7 - 106.7%. Similarly, 4-AEBE and 5-AEPE ligands were able to stabilize gold nanoparticles from aggregation, but some conditions were slightly different, such as the concentration of 4-AEBE, 5-AEPE and NaBH<sub>4</sub>. However, among three dithi-diaza ligands, 3-AEPE provided the highest sensitivity and was more easily observed by naked eye. This method offers advantages of simplicity, rapidity, cost effectiveness and no requirement of any sophisticated instruments and it is alternatively possible method for Hg(II) monitoring in bottled drinking water. Moreover, this method has several potential advantages as optical sensor, especially no as-prepared AuNPs synthesis and shorter observation time.

Department : Chemistry..... Student's Signature.....

Field of Study : Chemistry..... Advisor's Signature.....

Academic Year : 2012.....

## ACKNOWLEDGEMENTS

I would like to express my profound gratitude and appreciation to my advisor, Assistant Professor Dr.Apichat Imyim, for his invaluable guidance, grateful supervision, continual encouragement, and discussions of my study and research. Additionally, I am grateful to Assistant Professor Dr.Warinthorn Chavasiri, Professor Dr.Tawatchai Tuntulani, Associate Professor Dr.Orawon Chailapakul and Dr.Chatvalee Kalambaheti for their valuable suggestions as my thesis committee and examiners.

I would also especially my thanks to Assistant Professor Dr.Wanlapa Aeungmitrepirom, Assistant Professor Dr.Fuangfa Unob and Assistant Professor Dr.Narong Praphairaksit for their advices and helps throughout my study and conducting research in Environmental Analysis Research Unit (EARU). I would like to thank the Commission on Higher Education, Thailand for supporting by grant fund under the program Strategic Scholarships for Frontier Research Network for the Ph.D. Program Thai Doctoral degree and the 90<sup>th</sup> Year Chulalongkorn Scholarship, Ratchadaphiseksompot Endowment Fund, Chulalongkorn University (GRU-53-005-23-003 and FW002A) for financial supports which enabled this research to be carried out. In addition, I would like to thank the Department of Chemistry, Faculty of Science, Chulalongkorn University and Faculty of Science and Technology, Rajamangala University of Technology Phra Nakhon (RMUTP) for research facilities in analytical instruments and any financial supports.

I would like to thank those whose names are not listed here and those who have one way or another contributed to the success of this work. Finally, I am profoundly grateful to my family and my wife for their tender love, continual care, and encouragement during his study in the Ph.D. program.



	PAGE
2.3.5.2 Characterization of stabilizing ligands.....	20
2.4 Dithia-diaza ligands.....	21
2.5 Ionic liquids.....	23
2.6 Cold-vapor atomic absorption spectrometry.....	24
2.7 Methodology in spectrochemical analysis.....	25
2.7.1 External standard calibration curves.....	25
2.7.2 Standard addition method.....	25
2.7.3 Validation of spectroanalytical method.....	27
2.8 Literature review.....	30
 CHAPTER III EXPERIMENTAL SECTION.....	 41
3.1 Apparatus.....	41
3.2 Chemicals.....	43
3.3 Preparation of chemicals.....	44
3.4 Synthesis of dithia–diaza ligands.....	45
3.4.1 Synthesis of 3-AEPE.....	45
3.4.2 Synthesis of 4-AEBE.....	46
3.4.3 Synthesis of 5-AEPE.....	46
3.4.4 Synthesis of ionic liquid 1-butyl-3-methylimidazolium hexafluorophosphate ([C <sub>4</sub> mim][PF <sub>6</sub> ]).....	47
3.5 Optimization of gold nanoparticle stabilized by dithia-diaza ligands.....	48
3.5.1 Gold nanoparticle stabilized by 3-AEPE.....	48
3.5.1.1 Effect of the concentration of gold(III) solution.....	48
3.5.1.2 Effect of the concentration of 3-AEPE solution.....	48
3.5.1.3 Effect of the pH.....	49
3.5.1.4 Effect of the concentration of NaBH <sub>4</sub> .....	49

	PAGE
3.5.1.5 Effect of the concentration of Triton X-100 solution.....	49
3.5.1.6 Effect of reaction time.....	49
3.5.1.7 Effect of interfering metal ions.....	50
3.5.2 Gold nanoparticle stabilized by 4-AEBE.....	50
3.5.2.1 Effect of the concentration of gold(III) solution.....	50
3.5.2.2 Effect of the concentration of 4-AEBE solution.....	50
3.5.2.3 Effect of the concentration of NaBH <sub>4</sub> .....	50
3.5.3 Gold nanoparticle stabilized by 5-AEPE.....	50
3.5.3.1 Effect of the concentration of gold(III) solution.....	50
3.5.3.2 Effect of the concentration of 5-AEPE solution.....	50
3.5.1.4 Effects of the concentration of NaBH <sub>4</sub> .....	51
3.5.4 Gold nanoparticle stabilized by cysteamine hydrochloride.....	51
3.5.4.1 Effect of the concentration of gold(III) solution.....	51
3.5.4.2 Effect of the concentration of cysteamine hydrochloride.....	52
3.6 Method validation.....	52
3.7 Application to drinking water analysis.....	52
3.8 Determination of mercury(II) using ICP-OES.....	53
3.9 Extraction of mercury(II) ions by ionic liquid.....	53
CHAPTER IV RESULTS AND DISSCUSION.....	54
4.1 Synthesis and characterization of dithia-diaza ligands.....	54

	PAGE
4.2 Stabilization of the gold nanoparticles with dithia-diaza ligands.....	59
4.2.1 Gold nanoparticles stabilized by 3-AEPE.....	59
4.2.1.1 Effect of the concentration of gold(III) solution.....	59
4.2.1.2 Effect of 3-AEPE concentration.....	62
4.2.1.3 Effect of the pH.....	63
4.2.1.4 Effect of reducing agents.....	65
4.2.1.5 Effect of co-stabilizer concentration .....	70
4.2.1.6 Effect of reaction times.....	72
4.2.1.7 Characterization of 3-AEPE-stabilized gold nanoparticles.....	75
4.2.1.8 Selectivity and sensitivity.....	81
4.2.1.9 Calibration curve for mercury(II) ions.....	83
4.2.2 Gold nanoparticles stabilized by 4-AEBE.....	86
4.2.2.1 Effect of gold(III) concentration.....	87
4.2.2.2 Effect of 4-AEBE concentration.....	88
4.2.2.3 Effect of NaBH <sub>4</sub> concentration.....	89
4.2.2.4 Characterization of 4-AEBE-stabilized gold nanoparticles.....	91
4.2.2.5 Calibration of 4-AEBE-stabilized gold nanoparticles.....	92
4.2.3 Gold nanoparticles stabilized by 5-AEPE.....	93
4.2.3.1 Effect of gold(III) concentration.....	93
4.2.3.2 Effect of 5-AEPE concentration .....	94
4.2.3.3 Effect of NaBH <sub>4</sub> concentration .....	95
4.2.3.4 Characterization of 5-AEPE-stabilized gold nanoparticles.....	96
4.2.3.5 Calibration of 5-AEPE-stabilized gold nanoparticle.....	97

	PAGE
4.2.4 Gold nanoparticles stabilized by cysteamine hydrochloride.....	98
4.3 Method validation.....	99
4.4 Application in real drinking water.....	101
4.5 Extraction of mercury(II) ions by ionic liquid.....	103
4.5.1 Synthesis and characterization of ionic liquid.....	103
4.5.2 Optimization of the extraction of mercury(II) ions by ionic liquid.....	104
4.5.2.1 Effect of the volume of ionic liquid.....	104
4.5.2.2 Effect of pH.....	105
4.5.2.3 Effect of the concentration of 3-AEPE.....	106
4.5.2.4 Effect of extraction times.....	107
CHAPTER V CONCLUSION.....	109
REFERENCES.....	111
APPENDIX.....	128
VITA.....	132

## LIST OF TABLES

TABLE		PAGE
2.1	Analyte recovery and precision at different concentrations.....	28
2.2	Method comparison based on functionalized gold nanoparticle assays for determination of mercury(II) ions.....	37
2.2	Method comparison based on functionalized gold nanoparticle assays for determination of mercury(II) ions ( <i>continued</i> ).....	38
2.2	Method comparison based on functionalized gold nanoparticle assays for determination of mercury(II) ions ( <i>continued</i> ).....	39
2.3	Method comparison based on unmodified gold nanoparticle assays for mercury(II) ion detection.....	40
3.1	List of chemicals.....	43
4.1	Mole ratio of sodium borohydride and gold(III) ion.....	61
4.2	Mole ratio of gold(III) ion and 3-AEPE.....	63
4.3	Mole ratio of sodium borohydride and gold(III) ion.....	67
4.4	Optimum conditions of 3-AEPE-stabilized gold nanoparticle.....	75
4.5	Linearity ranges of different mercury(II) concentration levels at different measuring wavelengths.....	85
4.6	Mole ratio of gold(III) ion and 4-AEBE.....	88
4.7	Optimum conditions of 4-AEBE-stabilized gold nanoparticles.....	90
4.8	Linearity ranges of different mercury concentration levels of gold nanoparticles stabilized by 3-AEPE and 4-AEBE.....	93
4.9	Mole ratio of gold(III) ion and 5-AEPE.....	95
4.10	Optimum conditions of 5-AEPE-stabilized gold nanoparticles.....	96
4.11	Determination of mercury(II) ions in real samples.....	102

## LIST OF FIGURES

FIGURE		PAGE
2.1	Optical properties of gold nanoparticle interaction with light, resulting in the strong enhancement of the electric field, light absorption and scattering and surface enhancement luminescence.....	7
2.2	Schematic of plasmon oscillation for spherical nanoparticle, showing the displacement of the conduction electron charge cloud relative to the nuclei.....	8
2.3	SPR absorption band of spherical gold nanoparticles in different diameter sizes.....	10
2.4	The color of colloidal gold nanoparticles in a varied solvent refractive index. Refractive indices of the solutions (from left to right) are 1.336, 1.407, 1.481, 1.525 and 1.583.....	11
2.5	Schematic representation of colloidal stabilization through, (A) small charged molecules on the gold nanoparticle surface (electrostatic stabilization), (B) surface steric stabilization, and (C) surface electrosteric stabilization.....	16
2.6	Structure of 2-[3-(2-amino-ethylsulfanyl)-propylsulfanyl]-ethylamine (3-AEPE).....	22
2.7	Linear calibration graph for standard addition method.....	26
2.8	Definition terms of linearity, range, limit of quantitation and limit of detection.....	30
4.1	The $^1\text{H}$ -NMR spectrum of 3-AEPE in $\text{CDCl}_3$ .....	55
4.2	The $^{13}\text{C}$ -NMR spectrum of 3-AEPE in $\text{CDCl}_3$ .....	56
4.3	The $^1\text{H}$ -NMR spectrum of 4-AEPE in $\text{CDCl}_3$ .....	57
4.4	The $^{13}\text{C}$ -NMR spectrum of 4-AEPE in $\text{CDCl}_3$ .....	57
4.5	The $^1\text{H}$ -NMR spectrum of 5-AEPE in $\text{CDCl}_3$ .....	58
4.6	The $^{13}\text{C}$ -NMR spectrum of 5-AEPE in $\text{CDCl}_3$ .....	59

FIGURE	PAGE
4.7	Effect of the concentration of gold(III) solution on the formation of gold nanoparticle stabilized by 3-AEPE..... 61
4.8	Effect of the concentration of 3-AEPE ligand on the formation of gold nanoparticle stabilized by 3-AEPE..... 63
4.9	Effect of the pH on the formation of gold nanoparticle stabilized by 3-AEPE by addition of HNO <sub>3</sub> ..... 65
4.10	Effect of the pH on the formation of gold nanoparticle stabilized by 3-AEPE by addition of 0.1 M NaOH..... 65
4.11	Effect of the concentration of NaBH <sub>4</sub> on the formation of gold nanoparticle stabilized by 3-AEPE..... 67
4.12	Effect of different reducing agents on producing gold nanoparticles stabilized by 3-AEPE with 0.6 mM NaBH <sub>4</sub> , 72 mM NH <sub>2</sub> OH·HCl and 71 mM ascorbic acid. Experimental conditions: 125 μM gold(III), 0.3 mM 3-AEPE and 0.1% (v/v) Triton X-100..... 69
4.13	Comparison of reducing agents on the formation of gold nanoparticles stabilized by 3-AEPE. Experimental conditions: 125 μM gold(III), 0.3 mM 3-AEPE, 0.1% (v/v) Triton X-100, 0.6 mM NaBH <sub>4</sub> , 72 mM NH <sub>2</sub> OH·HCl and 71 mM ascorbic acid..... 69
4.14	Effect of Triton X-100 concentration on producing gold nanoparticles stabilized by 3-AEPE. Experimental conditions: 125 μM gold(III), 0.3 mM 3-AEPE and 0.6 mM NaBH <sub>4</sub> ..... 71
4.15	The aggregation degree of 3-AEPE-stabilized gold nanoparticles without (a) and with (b) the inclusion of 0.1% (v/v) Triton X-100. Experimental conditions: 125 μM gold(III), 0.3 mM 3-AEPE and 0.6 mM NaBH <sub>4</sub> ..... 72

FIGURE	PAGE	
4.16	The stability of 3-AEPE-stabilized gold nanoparticles without any mercury(II) ions ( $\Delta$ 517 nm and $\square$ 680 nm). Experimental conditions: 125 $\mu$ M gold(III), 0.3 mM 3-AEPE, 0.1% (v/v) Triton X-100 and 0.6 mM NaBH <sub>4</sub> .....	73
4.17	Reaction times of 3-AEPE-stabilized gold nanoparticles in the presence of different concentrations of mercury(II) ions. Experimental conditions; 125 $\mu$ M gold(III), 0.3 mM 3-AEPE, 0.1% (v/v) Triton X-100 and 0.6 mM NaBH <sub>4</sub> .....	74
4.18	Absorbance at 680 nm versus reaction times of 3-AEPE-stabilized gold nanoparticles in the presence of different concentrations of mercury(II) ions. Experimental conditions; 125 $\mu$ M gold(III), 0.3 mM 3-AEPE, 0.1% (v/v) Triton X-100 and 0.6 mM NaBH <sub>4</sub> .....	74
4.19	UV-vis absorption spectra of 3-AEPE stabilized-gold nanoparticles in the (a) absence and (b) presence of 5 $\mu$ M mercury(II) ion.....	76
4.20	TEM images (450,000 x magnification) of the 3-AEPE-stabilized gold nanoparticle solution in the (a) absence and (b) presence of 5 $\mu$ M mercury(II) ion.....	78
4.21	Size distributions and ( <i>insert</i> ) typical TEM image of 3-AEPE-stabilized gold nanoparticle with average diameter of $9 \pm 2$ nm.....	78
4.22	The possibility of forming of 3-AEPE-stabilized gold nanoparticles under conditions of 125 $\mu$ M gold(III), 0.3 mM 3-AEPE, 0.1% (v/v) Triton X-100 and 0.6 mM NaBH <sub>4</sub> .....	80
4.23	The proposed mechanism of 3-AEPE-stabilized gold nanoparticle formation in the (a) absence and (b) presence of mercury(II) ions, under conditions of 125 $\mu$ M gold(III), 0.3 mM 3-AEPE, 0.1% (v/v) Triton X-100 and 0.6 mM NaBH <sub>4</sub> .....	80

FIGURE	PAGE	
4.24	Absorption spectra of 3-AEPE-stabilized gold nanoparticles in the presence of various metal ions (250 $\mu$ M) or 2.5 $\mu$ M mercury(II) and ( <i>inset</i> ) the corresponding photo images, under conditions of 125 $\mu$ M gold(III), 0.3 mM AEPE, 0.1% (v/v) Triton X-100 and 0.6 mM NaBH <sub>4</sub> .....	82
4.25	Absorbance at 680 nm of 3-AEPE-stabilized gold nanoparticles in the presence of various metal ions (250 $\mu$ M) or 2.5 $\mu$ M mercury(II) (n=3), under conditions of 125 $\mu$ M gold(III), 0.3 mM AEPE, 0.1% (v/v) Triton X-100 and 0.6 mM NaBH <sub>4</sub> .....	82
4.26	Colorimetric responses of 3-AEPE-stabilized gold nanoparticle solution upon the addition of various concentration of mercury(II) ion.....	83
4.27	Absorption spectra of 3-AEPE-stabilized gold nanoparticle solution upon the addition of various concentrations of mercury(II) ions.....	84
4.28	The relationship between the concentrations of mercury(II) ions and their absorptions of 3-AEPE-stabilized gold nanoparticles at different wavelengths.....	85
4.29	Absorption values of 3-AEPE-stabilized gold nanoparticles at a wavelength of 680 nm versus mercury(II) concentrations.....	86
4.30	Three levels of calibration curves of 3-AEPE-stabilized gold nanoparticles.....	86
4.31	Effect of the concentration of gold(III) solution on the formation of gold nanoparticle stabilized by 4-AEPE.....	87
4.32	Effect of the concentration of 4-AEPE ligand on the formation of gold nanoparticle stabilized by 4-AEPE.....	89
4.33	Effect of the concentration of NaBH <sub>4</sub> on the formation of gold nanoparticle stabilized by 4-AEPE.....	90

FIGURE	PAGE	
4.34	TEM images (450,000x magnification) of 4-AEBE-stabilized gold nanoparticle solution in the (a) absence and (b) presence of 5 $\mu$ M mercury(II) ion.....	91
4.35	The calibration curve of 4-AEBE-stabilized gold nanoparticles.....	92
4.36	Effect of the concentration of gold(III) solution on the formation of gold nanoparticle stabilized by 5-AEPE.....	94
4.37	Effect of the concentration of 5-AEPE ligand on the formation of gold nanoparticle stabilized by 5-AEPE.....	95
4.38	Effect of the concentration of NaBH <sub>4</sub> on the formation of gold nanoparticle stabilized by 5-AEPE.....	96
4.39	TEM images (450,000x magnification) of the 5-AEPE-stabilized gold nanoparticle solution in the (a) absence and (b) presence of 5 $\mu$ M mercury(II) ion.....	97
4.40	The calibration curve of 5-AEPE-stabilized gold nanoparticles.....	98
4.41	Standard addition curve (solid and transparent shapes represent the calibration and matrix-matched curves, respectively).....	101
4.42	The <sup>1</sup> H-NMR spectrum of an ionic liquid [C <sub>4</sub> mim][PF <sub>6</sub> ] in CDCl <sub>3</sub> .....	103
4.43	Effect of ionic liquid volumes on the extraction efficiency of mercury(II) ions using ionic liquid [C <sub>4</sub> mim][PF <sub>6</sub> ] in the absence and presence of 3-AEPE.....	105
4.44	Effect of the pH on the extraction efficiency of mercury(II) ions using ionic liquid [C <sub>4</sub> mim][PF <sub>6</sub> ] in the absence and presence of 3-AEPE.....	106
4.45	Effect of the concentration of 3-AEPE on the extraction efficiency of mercury(II) ions using ionic liquid [C <sub>4</sub> mim][PF <sub>6</sub> ].....	106
4.46	Effect of extraction time on the extraction efficiency of mercury(II) ions using ionic liquid [C <sub>4</sub> mim][PF <sub>6</sub> ] in the absence and presence of 3-AEPE.....	107

FIGURE		PAGE
A.1	FT-IR spectra of dithia-diaza (a) 3-AEPE, (b) 4-AEBE and (c) 5-AEPE.....	129
A.2	Calibration curve of mercury from ICP-OES.....	130
A.3	Calibration curve of mercury from flow injection CV-AAS.....	130
A.4	Pictures of blue solutions and membranes (0.22 $\mu$ M) after the filtration and mercury (202 amu) and gold (197 amu) contents from LA-ICP-MS of 3-AEPE-stabilized gold nanoparticles with different concentration of mercury(II) ions. ....	131

**LIST OF SCHEME**

SCHEME		PAGE
3.1	Synthesis of 3-AEPE.....	45
3.2	Synthesis of 4-AEBE.....	46
3.3	Synthesis of 5-AEPE.....	46
3.4	Synthesis of ionic liquid [C <sub>4</sub> mim][PF <sub>6</sub> ].....	47
4.1	General schematic of synthesis of dithia-diaza ligands (n = 3, 4 and 5 for 3-AEPE, 4-AEBE and 5-AEPE, respectively).....	54

## LIST OF ABBREVIATIONS

3-AEPE	=	2-[3-(2-Amino-ethylsulfanyl)-propylsulfanyl]-ethylamine
4-AEBE	=	2-[4-(2-Amino-ethylsulfanyl)-butylsulfanyl]-ethylamine
5-AEPE	=	2-[5-(2-Amino-ethylsulfanyl)-pentylsulfanyl]-ethylamine
TEM	=	Transmission electron microscopy
UV-vis	=	Ultra violet-visible spectroscopy
NMR	=	Nuclear magnetic resonance spectroscopy
ICP-OES	=	Inductively coupled plasma-optical emission spectroscopy
CV-AAS	=	Cold vapor atomic absorption spectroscopy
FT-IR	=	Fourier transforms infrared spectroscopy
CMC	=	Critical micelle concentration
°C	=	Degree Celsius
HSAB	=	Hard and soft acid and bases
RSD	=	Relative standard deviation
LOD	=	Limit of detection
SERS	=	Surface enhanced raman spectroscopy
SPR	=	Surface plasmon resonance
AuNPs	=	Gold nanoparticles
LDR	=	Linear dynamic range
RTIL	=	Room temperature ionic liquid
mg L <sup>-1</sup>	=	Milligram per liter
µg L <sup>-1</sup>	=	Microgram per liter
mL	=	Milliliter
min	=	Minute
nm	=	Nanometer
V	=	Voltage
$E^0$	=	Standard reduction potential

# CHAPTER I

## INTRODUCTION

### 1.1 Statement of the problem

Currently, the contamination of toxic heavy metals in the environment causes highly serious environmental and human health problems. Among the toxic trace metals, mercury (Hg) is one of the most hazardous environmental pollutants affecting both human health and the degradation of the environment. The three most important chemical forms of mercury in the environment are (i) elemental mercury ( $\text{Hg}^0$ ), which has a high vapor pressure and relatively low solubility in water and is primarily present in the atmosphere; (ii) inorganic mercury in the form of mercurous ( $\text{Hg}_2^{2+}$ ) and mercuric ( $\text{Hg}^{2+}$ ) cations and their salts, which can be far more soluble and have a strong affinity for many inorganic and organic ligands, especially those containing sulfur; and (iii) organic mercury, including methylmercury ( $\text{CH}_3\text{Hg}^+$ ), dimethylmercury ( $\text{CH}_3\text{HgCH}_3$ ) and organometallic compounds having one or two alkyl-/aryl-substituents bound to the mercury atom [1-3].

All mercury species are toxic, with organic mercury compounds generally being more toxic than inorganic species, especially methylmercury that is the most toxic of all forms to living systems [4]. Depending on environmental conditions, mercury species may transform among the different forms in atmospheric and aquatic environments through biogeochemical processes. The distribution of inorganic mercury is mainly found in water and sediments and depends on pH of the solution. The toxic effects of mercury depend on its chemical form and the route of exposure. Nevertheless, mercury may affect the central neurological and renal systems, damage of chromosome, kidney and other organs and can result in long-term health disorders. Nervous system disorders include impaired vision, impairment of pulmonary function and physical impairments. The toxicity of mercury can cause irreversible damage areas of the brain and may ultimately cause death [5].

Due to their high toxicity even at low concentrations, the monitoring and measurement of mercury(II) is very important in many fields, such as environmental monitoring, waste management, food toxicity and clinical or biomedical diagnosis. Considering the extreme toxicity of mercury(II), the US Environmental Protection Agency (EPA) standard for the maximum allowable level of inorganic mercury in drinking water is  $2 \mu\text{g L}^{-1}$  (10 nM). A wide variety of analytical methods have been recommended for determination of trace mercury, such as spectrophotometry [6-9], cold-vapor atomic absorption spectroscopy (CV-AAS) [10-12], atomic fluorescence spectroscopy (AFS) [13, 14] and inductively coupled plasma–mass spectrometry (ICP-MS) [15]. Despite numerous advantages in many parts, such as simplicity, high sensitivity and precision, high speed and powerful performance, these methods are limited in several applications. The drawbacks of these methods are high cost of operation, expensive equipment, amount of time consumed, complicated sample preparation and non-portability.

Over the past years, the specifically mercury(II) chemosensors, such as chromogenic [16-21], fluorogenic [22-25], biosensors [26] and optodes [27, 28], have been designed and developed to detect trace mercury(II) levels. Among these methods, colorimetric sensors have become widely popular, due in part to their simplicity, rapidity, precision and the common uses of this basic equipment in laboratory and field, including applications based upon easy visual detection by the naked eye without resorting to any expensive instruments. Recently, the development of a colorimetric sensor based on the gold nanoparticles (AuNPs) has attracted much attention to selective and sensitive sensors to monitor and determine trace mercury(II) levels in real-time from biological and environmental samples because of its high extinction coefficient in the visible region and color changing effect depending on the interparticle distance.

## **1.2 Objectives of the thesis**

The aims of this research were focused on the development of mercury(II) analysis using gold nanoparticles stabilized with dithia–diazia ligands. Thus, the objectives of this research are (i) to synthesize and characterize the dithia–diazia

ligands, including 2-[3-(2-amino-ethylsulfanyl)-propylsulfanyl]-ethylamine (3-AEPE), 2-[4-(2-amino-ethylsulfanyl)-butylsulfanyl]-ethylamine (4-AEBE) and 2-[5-(2-amino-ethylsulfanyl)-pentylsulfanyl]-ethylamine (5-AEPE), (ii) to optimize the gold nanoparticle stabilization in the presence of dithia-diaza ligands, (iii) to compare stabilization efficiency of gold nanoparticles stabilized by three dithia-diaza ligands and (iv) to develop the method for the determination of mercury(II) ions in water sample.

### **1.3 Scope of the thesis**

In this work, simple reduction of gold(III) ions with sodium borohydride to form gold nanoparticles in the presence of dithia-diaza ligands was a novel development. Dithia-diaza ligands (3-AEPE, 4-AEBE and 5-AEPE) were used as stabilizer for dispersing gold nanoparticles against aggregation or degradation and at the same time to be a selective ligand for mercury(II) ions in aqueous media. The gold(III) precursor solution (in  $\text{HAuCl}_4$  form) in the presence of dithia-diaza ligands was directly reduced by sodium borohydride to form dithia-diaza- gold nanoparticles (D-AuNPs), showing a red color. On the other hand, the color of the system containing mercury(II) appeared blue in coloration immediately after reduction. The color of aggregated gold nanoparticles could be observed by UV-vis spectrophotometer and naked eye. The effect of stability parameters on the surface plasmon resonance (SPR) of gold nanoparticle, such as the concentration of gold(III) solution, dithia-diaza ligands, sodium borohydride and co-stabilizer, pH, reaction time and interfering effects were investigated. In addition, the proposed method was validated and also applied for bottled drinking water samples.

### **1.4 The benefit of this research**

A novel, simple, rapid and reliable sensing based on direct formation of gold nanoparticle for determination of mercury(II) levels using UV-vis spectrophotometer and naked eyes was obtained.

## CHAPTER II

### THEORY AND LITERATURE REVIEWS

#### 2.1 Mercury measurement

A wide variety of analytical methods have been developed to detect trace levels of mercury(II) ions in human and environmental samples. Cold vapor-atomic absorption spectrometry (CV-AAS) is one of the most famous methods for determination of mercury and it offers several advantages, such as good precision, accuracy and low cost of operation. However, the lack of sensitivity is a major concern. In order to improve sensitivity, the sample preparation, separation and/or preconcentration processes have been required, especially when mercury concentrations in the sample are too low to be determined directly by CV-AAS. For example, Rio Segade and Tyson [12] reported the determination of inorganic mercury and total mercury by developing the flow injection CV-AAS using sodium borohydride as reducing agent. The limit of detection of inorganic mercury and total mercury were found in the range of 1.2 - 19 ng g<sup>-1</sup> (6 - 95 nM) and 6.6 - 18 ng g<sup>-1</sup> (33 - 95 nM), respectively. Tavallali and NoroziKhah [29] designed the cold vapor system coupled with atomic absorption spectrometry (AAS) for determining mercury in waste water with the lowest detection limit of 51 ng L<sup>-1</sup> (0.255 nM). Martinis *et al.* [30] developed the determination of trace mercury by flow injection CV-AAS after preconcentration with ionic liquid 1-butyl-3-methylimidazolium hexafluorophosphate, [C<sub>4</sub>mim][PF<sub>6</sub>]. The limit of detection was as low as 2.3 ng L<sup>-1</sup>.

Atomic fluorescence spectroscopy (AFS) and inductively coupled plasma-mass spectrometry (ICP-MS) have been alternatively used for the determination of mercury due to their high sensitivity, high selectivity, and high sample throughput and they often provide direct and quantitative information about mercury concentration. However, they have several disadvantages, such as high cost of instrumentation, requiring specialist operation, being time-consuming, complicated sample preparation and they are not easily applied to on-filed applications or non-portable equipment.

Optical detection with a chemosensor, including fluorescence and colorimetric (or naked eye) assays have been widely developed based on the interaction of metal ions with the  $\pi$ -electron system of chromophore and/or fluorophore in the molecular-level host–guest concept in solution, resulting in complexation. The selectivity of receptors relies on the design of binding ligand with predominant recognition of guest or specific metal ions by binding-induced changes in spectroscopic or electrochemical properties. Thus, the design and synthesis of specific recognition receptors for metal ions is an extremely important subject in the application of sensing devices. For example, Cheng *et al.* [31] synthesized an azobenzene derivative for rapid naked eye detection of mercury(II). The lowest concentration of 20  $\mu\text{M}$  mercury(II) led to color change from yellow to deep-red. Tan and Yan [17] synthesized a 4-(4-fluoro-2,1,3-benzoxadiazol-7-ylthio)-7-mercapto-2,1,3-benzoxadiazole chromogenic sensor for determination of mercury(II) and copper(II) ions with the limit of detection of 0.34  $\mu\text{M}$  and 2.9  $\mu\text{M}$ , respectively. Cheng *et al.* [32] synthesized an azo derivative 5-(4-methylaminophenylazo)-2-methylquinolin-8-yl benzoate as a colorimetric and naked eye method for detection of mercury(II). Yang *et al.* [16] reported the synthesis of an anthraquinone derivative having two thiourea groups, exploited as a selective sensor to both UV-vis and colorimetric methods for mercury(II) and silver(I) ions. According to hard and soft acid and bases (HSAB) theory, thiourea and its derivatives containing sulfur and two nitrogen atoms were used as a sensitive receptor for the detection of mercury(II) ions by using colorimetric and fluorescence devices through the mercury-desulfurization reaction [33-36]. Yu *et al.* [22] synthesized a water-soluble fluoroionophore, *p*-dimethylaminobenzaldehyde thiosemicarbazone, for mercury(II) with the limit of detection of 0.77  $\mu\text{M}$ .

Colorimetric sensors have become extensively popular because of rapid detection and easy observation of the color change by naked eye. However, most of the chemosensor molecules have some disadvantages, such as the lack of water solubility, requiring the use of organic solvent mixtures, being cross-sensitive toward other metal ions and having complicated synthesis routes. Recently, the development of colorimetric sensors based on the aggregation of gold nanoparticles have become

popular as sensitive and selective sensors to determine mercury(II) levels in real-time from biological and environmental samples. Because of their unique optical properties, gold nanoparticles have been used as colorimetric nanoparticle sensor in rapid detection assays for several reasons. First, gold nanoparticles exhibit unique and tunable optical properties owing to the phenomenon of surface plasmon resonance (SPR); its SPR is an intense absorption band in the visible region. Second, gold nanoparticle has an extremely high molar absorptivity ( $\epsilon > 10^8 \text{ M}^{-1}\text{cm}^{-1}$ ) that is higher than organic molecules by about 3 - 5 orders. Thus, this property will increase the inherent limit of detection of the colorimetric method based on a measureable change in optical properties. Third, colloidal gold nanoparticle has a surface for easy modification by a variety of ligands in order to increase selectivity toward target analytes. Finally, the SPR depends on several parameters, such as size, shape, ligand capping, medium and interparticle distance; therefore, the change of any parameter leads to the color change that can be rapidly monitored via either UV-vis spectroscopy or naked eye. Mulvaney [37] overviewed theoretical and experimental studies by the use of optical measurements to monitor chemisorption, metal deposition and alloy formation of nanoparticles. It was indicated that the deposition of electropositive metal layers on the surface of nanoparticles resulted in a blue-shift to a longer wavelength of the SPR band.

## **2.2 Surface plasmon resonance in metallic nanoparticles**

Plasmon resonance is a prominent spectroscopic feature of noble metal nanoparticles that provide a sharp and intense absorption band in the visible region spectrum. The physical origin of the absorption is the coherent oscillation of the free conduction electrons at the surface of the particle with respect to the ionic core of the nanoparticle when nanoparticles are exposed to light radiation. The electric field of an incoming light which contains oscillating electronic and magnetic waves induces polarization of the electron at the surface of a spherical nanoparticle (6s electrons of the conduction band of gold nanoparticle), causing the collective oscillation of free conduction electrons [38]. The coherent oscillation of the metallic free electrons in resonance with the frequency of the electromagnetic field is called surface plasmon

resonance (SPR). The SPR of nanoparticles has a strong absorption band in the visible region and results in the origin of the observed color effect [39]. The plasmon resonance of the noble metals, such as copper (Cu), silver (Ag) and gold (Au) displays uniquely strong absorption bands in the visible region. Meanwhile, the plasmon frequency of other transition metals, such as lead (Pb), mercury (Hg), tin (Sn) and cadmium (Cd) appear in the UV region, but do not exhibit strong color effects and show a broad, low-intensity absorption band. The potential for achieving optical effects using strong SPR leads to the most important of the enhancement of light scattering and absorption cross-section of gold nanoparticle. As shown in Figure 2.1, the SPR of gold nanoparticle can relate to other applications, such as fluorescence and surface enhance raman scattering spectroscopy (SERS).

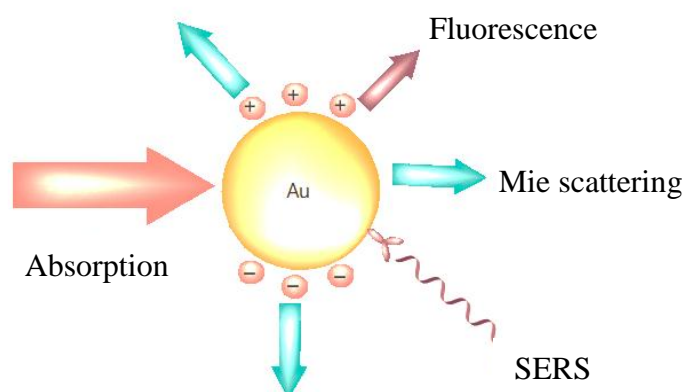


**Figure 2.1** Optical properties of gold nanoparticle interaction with light, resulting in the strong enhancement of the electric field, light absorption and scattering and surface enhancement luminescence [40].

A schematic presentation of the creation of SPR of metallic nanoparticles is depicted in Figure 2.2. The positive charges in the nanoparticles are assumed to be immobile while the negative charges (conduction electrons) move under the influence of external fields. A displacement of the negative charges from the positive charges occurs when the metallic nanoparticle is placed in an electric field. A dipolar oscillation of the electrons is created with respect to a particular time period. The collective oscillation of the electrons is also sometimes denoted as the “dipole particle plasmon resonance” [38, 41].

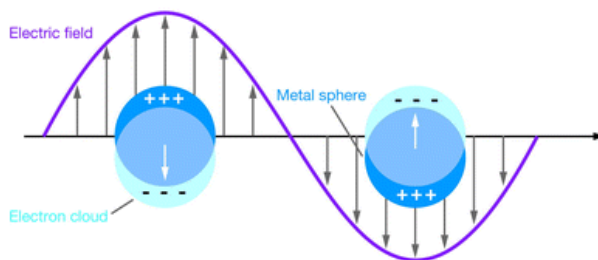


**Figure 2.2** Schematic of plasmon oscillation for spherical nanoparticle, showing the displacement of the conduction electron charge cloud relative to the nuclei [42].

The SPR effect of nanoparticles was first described quantitatively by classical Mie theory in 1908, by solving Maxwell's equation with appropriate boundary conditions for a small ( $< 100$  nm) spherical nanoparticle. A spherical nanoparticle that is much smaller than the wavelength of the incident light ( $2R \ll \lambda$ ,  $2R < 25$  nm of gold), only the dipole oscillation term contributes significantly to the light nanoparticle interaction, called extinction cross-section ( $\sigma_{ext}$ ) which includes both the light of absorption and scattering. For very small particles ( $R \ll \lambda$ ), the scattering cross-section is negligible and the extinction cross-section mainly dominated by absorption. The extinction cross-section from Mie theory then reduces to the following expression (dipole approximation) [38, 43, 44].

$$\sigma_{ext} = \frac{9 V \varepsilon_m^{3/2}}{c} \frac{\omega \varepsilon_2(\omega)}{[\varepsilon_1(\omega) + 2\varepsilon_m]^2 + \varepsilon_2(\omega)^2} \dots\dots\dots (2.1)$$

Where,  $V$  = is the spherical particle volume ( $V = 4\pi/3 \cdot R^3$ ),  $R$  is the radius of the particle,  $\omega$  is the angular frequency of the exciting electromagnetic radiation,  $c$  is the speed of light,  $\varepsilon_m$  is the dielectric functions of the surrounding medium and  $\varepsilon_1(\omega)$  and  $\varepsilon_2(\omega)$  are the real and imaginary parts of the material dielectric function, respectively [44]. As can be seen from Eq. 2.1, the extinction cross-section ( $\sigma_{ext}$ ) of a particle depends on the dielectric function ( $\varepsilon_m$ ) of the metal. The maximum value of  $\sigma_{ext}$ , or the SPR band, will occur when the denominator of the right-hand side of the equation becomes minimal, or in other word, when  $\varepsilon_1(\omega) = -2\varepsilon_m$ , and  $\varepsilon_2(\omega)$  is small or only weakly dependent on the frequency.

## 2.3 Gold nanoparticle

### 2.3.1 Properties of gold nanoparticle

One of the unique optical properties of gold nanoparticle is its SPR absorption or localized surface plasmon resonance (LSPR) band in the visible region (< 50 nm in diameter). The SPR absorption wavelength is strongly dependent on the particle's size, shape/geometry, refractive index of medium or environment and aggregation state in solution. Therefore, any change in these parameters allows changes of both the plasmon resonance frequency affecting the color as well as the strength of the plasmonic enhancement affecting the intensity [45]. For example, if the size or shape of nanoparticle changes, the surface geometry also changes, causing a shift in the electric field density on the surface and changing the oscillation frequency of the electrons. It leads to different cross-section optical properties. The color change effect is the result of the coupling of the SPR between particles in close proximity. When the distance between particles decreases, the effect of plasmonic coupling increases, thus resulting in a red shift of the plasmon band in the visible region and change in solution color [44]. The excitation of the SPR of gold nanoparticle results in the enhancement of the photophysical properties.

#### *Size-dependent optical properties*

It is well-known that the plasmon resonance of metal nanoparticles is strongly sensitive to their nanoparticle size, shape and the dielectric properties of the surrounding medium. Thus, optical properties of gold nanoparticle can be readily tuned by varying their size and shape. As the nanoparticle size increases, the number of electrons also increases in direct proportion to the volume, because of which the extinction of particles increases with volume (Eq. 2.1). For example, colloidal gold nanoparticle with diameters of 14 nm in aqueous solution displays a centered maximum absorption band in the visible region at an approximate 520 nm and exhibits a clear deep-red color. In aqueous media, the SPR is absent for gold nanoparticle with core diameter of less than 2 nm, as well as for bulk gold. A solution of smaller individual gold nanoparticle (5 - 20 nm) appears deep-red, while those of

larger particles or aggregates of smaller particles appear as purple to deep-blue [46]. For gold nanoparticles with mean diameter of 8.9, 14.8, 21.7, 48.3, and 99.3 nm, the maximum SPR absorption bands ( $\lambda_{spr}$ ) were observed at 517, 520, 521, 533 and 575 nm, respectively [43, 47]. The extinction spectra of gold nanoparticles of different sizes are shown in Figure 2.3. The plasmon resonance band is clearly visible and its center maximum absorption band shifts to longer wavelength with increasing particle diameter ( $D$ ).

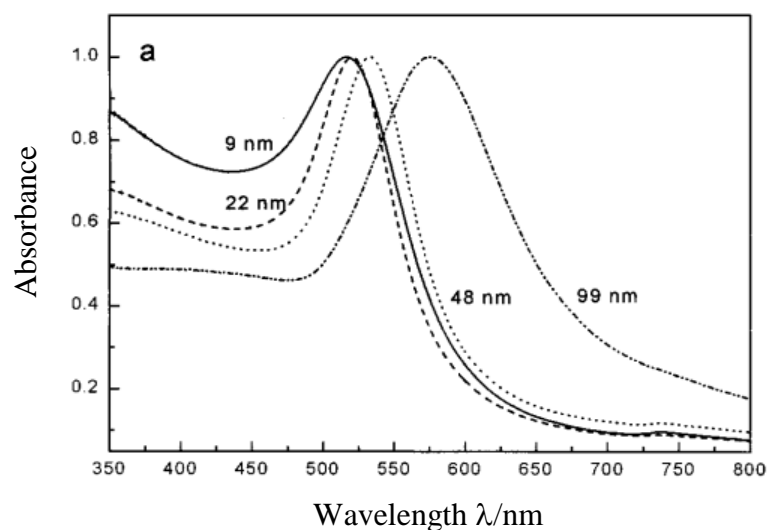


**Figure 2.3** SPR absorption band of spherical gold nanoparticles in different diameter sizes [43].

### *Effect of solvent medium*

From the expression of the Mie extinction cross-section (Eq. 2.1), medium or dielectric constant of the surrounding medium plays a predominant role in affecting the plasmon peak position and intensity of gold nanoparticle [37, 44, 48]. Changing the medium surrounding the nanoparticle another medium having a markedly different refractive index strongly alters the plasmon behavior of the nanoparticle due to the varying ability of the surface to accommodate electron charge density from nanoparticles. Underwood and Mulvaney [49] demonstrated the different color of the colloidal gold nanoparticles (16 nm in diameter) prepared in different solvent mediums, such as water and in mixtures of butyl acetate and carbon disulfide with different ratios, by using in a series of solvents with a refractive index from 1.30 to

1.60. As shown in Figure 2.4, the colloidal gold nanoparticles appeared in different colors and their SPR bands were variable in the range of 520 to 545 nm.



**Figure 2.4** The color of colloidal gold nanoparticles in a varied solvent refractive index. Refractive indices of the solutions (from left to right) are 1.336, 1.407, 1.481, 1.525 and 1.583 [49].

#### *Molar extinction coefficient of gold nanoparticle*

The main advantage of colorimetric sensor based on gold nanoparticles is their extremely high extinction coefficient,  $\epsilon$  ( $M^{-1} cm^{-1}$ ) which is called molar absorptivity in classical UV-visible spectroscopy. The  $\epsilon$  of gold nanoparticle is higher than the magnitude of conventional organic chromophores or dyes by about 3 - 5 orders. For example, the extinction coefficients of 13 and 50 nm diameter gold nanoparticles are  $2.7 \times 10^8$  and  $1.5 \times 10^{10} M^{-1}cm^{-1}$  (at  $\sim 520$  nm), respectively [44]. UV-vis absorption spectroscopy and transmission electron microscopy (TEM) have been used to determine the extinction coefficient of gold nanoparticles with different sizes and different capping ligand monolayers. The extinction coefficient is an important parameter that can be used to calculate the nanoparticle concentration or estimate nanoparticle sizes. The extinction coefficient of gold nanoparticles was determined according to the Beer-Lambert law. Jain *et al.* [50] reported a theoretical calculation of the extinction coefficient of gold nanoparticles and its dependence on nanoparticle size. Gold nanoparticle with diameter of 40 nm provided the molar absorption coefficient of  $7.66 \times 10^9 M^{-1}cm^{-1}$  at a plasmon resonance wavelength maximum ( $\lambda_{max}$ ) of 528 nm. This value is higher than other strongly absorbing dyes, such as an indocyanine green ( $\epsilon = 1.08 \times 10^4 M^{-1}cm^{-1}$ ), rhodamine-6G ( $\epsilon = 1.16 \times 10^5 M^{-1}cm^{-1}$ ) and malachite green ( $\epsilon = 1.49 \times 10^5 M^{-1}cm^{-1}$ ).

Liu *et al.* [51] reported a theoretical calculation of molar extinction coefficients of citrate-capped gold nanoparticle with different sizes by comparing extinction coefficients of well-known dyes. The different core sizes ( $D$ ) of citrate capped- gold nanoparticles ( $4.61 \pm 0.48$ ,  $8.55 \pm 0.79$ ,  $20.60 \pm 1.62$ ,  $25.67 \pm 5.62$  and  $34.46 \pm 4.34$  nm in diameter) in water display high molar extinction coefficients in the range of  $10^6$  to  $10^9$   $M^{-1}cm^{-1}$ . The increase in core diameter of gold nanoparticles provided dramatic and continuous increase in the extinction coefficient. For example, the extinction coefficient of 35 nm of citrate-capped gold nanoparticle is more increasingly than 4 nm by about three times. Maye *et al.* [52] demonstrated spectroscopic determination of extinction coefficient or molar absorptivity of gold nanoparticles (1.9 and 5.6 nm in diameter) capped with decanethiol and 13.4 nm of citrate-capped gold nanoparticles by calculating, with linear regression, that the  $\epsilon$  of 1.9 and 5.6 nm gold nanoparticles capped with decanethiol is  $4.43 \times 10^5$  and  $1.1 \times 10^7$   $M^{-1}cm^{-1}$ , respectively. For 13.4 nm of citrate-capped gold nanoparticle, the extinction coefficient is  $2.01 \times 10^8$   $M^{-1}cm^{-1}$ . Thus, gold nanoparticle in nanomolar concentration can be easily observed by visual naked eye, allowing sensitive detection with minimal consumption of reagents.

### ***Aggregation of gold nanoparticles***

Generally, a colloidal solution of gold nanoparticles with diameters of 5 - 20 nm exhibits a red color. Aggregation of gold nanoparticles leads to a shift of the absorption peak to longer wavelength and changes the color of the colloidal solution to purple or blue. The concept of gold nanoparticle aggregation has been applied to various target analytes, such as DNA, heavy metal ions, proteins, HIV and others. The aggregation mechanism may be mainly divided into two approaches [53, 54]. The first is interparticle crosslinking aggregation that occurs based on interparticle bonding formation, either by using crosslinker molecules to bind with the receptor ligand on gold nanoparticle, or without crosslinker (direct interaction between receptor modified gold nanoparticle and non-receptor gold nanoparticle). The possibility of interparticle bond formation, such as hydrogen bonding, electrostatic attraction, hydrophobic interaction and metal-ligand coordination can overcome the interparticle repulsive

forces (electrostatic and/or steric repulsion) of gold nanoparticles [55]. The other approach is non-crosslinking aggregation or destabilization-induced aggregation. This approach occurs by losing the electrostatic, steric, or electrosteric stabilization without the formation of interparticle bonds.

### *Colorimetric measurement of gold nanoparticle*

Within colorimetric analysis, the aggregation of gold nanoparticle is the main mechanism in gold nanoparticle, leading to a change in their SPR (color and absorbance). Using this concept, color changes of gold nanoparticles via analyte-induced aggregation have been widely developed for the detection of metal ions. The color change can be easily observed by colorimetric and naked eye methods that do not require sophisticated instruments for qualitative analysis. For quantitative analysis, the absorption spectra are usually recorded with the ratio of absorbance at 520 nm, which corresponds to dispersed particles, and a longer wavelength, corresponding to aggregated particles. Typically, the detection limit of gold nanoparticle-based colorimetric assays without signal amplification steps is in the range of nM to  $\mu$ M, depending on both the design of the system and the binding affinity of the biomolecule receptors. However, the sensitivity and selectivity of gold nanoparticle-based sensors also depends on several factors, such as the gold nanoparticle size, capping ligands, pH, ionic strength, medium and temperature [54, 56].

### **2.3.2 Preparation of gold nanoparticle**

The most commonly used method for the synthesis of gold nanoparticle is the chemical reduction of gold(III) salt to gold(0), yielding gold nanoparticle colloids. This method requires a reducing agent in the presence of a capping agent that can allow chemisorption and/or physisorption on the surface of gold nanoparticle to avoid their aggregation [45]. The reduction of  $\text{HAuCl}_4$  with tri-sodium citrate solution in water at boiling point is a well-known method for the synthesis of gold nanoparticle called as as-prepared gold nanoparticle, which was introduced by Turkevitch in 1951. The reduction reaction was done at high temperature until the solution changed from

yellow to red color, resulting in gold nanoparticle production approximately 20 nm in diameter [57]. The mechanism of this method occurs as a multi-step process [58]. The size of such nanoparticles is controlled by varying the reducing/stabilizing agent (tri-sodium citrate) to gold ratio from 5.0 to 0.5, to obtain the core size from 10 to 150 nm.

Brust *et al.* [59, 60] developed the two phase method, which is the most widely used for thiols stabilized gold nanoparticles in organic solvents. A solution of  $\text{HAuCl}_4$  was transferred into toluene containing tetraoctylammonium bromide (TOAB) and/or thiolalkanes or aminoalkanes as phase transfer agent. The toluene solution is thoroughly stirred with an aqueous solution of sodium borohydride, to obtain particle sizes in the range of 1 - 30 nm. The surface of gold nanoparticle was functionalized with specific functionalities of ligands by place-exchange reactions.

Although tri-sodium citrate is the most common reducing agent, spherical gold nanoparticles can also be synthesized by the use of borohydride and other reducing agents, such as ascorbic acid, hydroxylamine hydrochloride, monosodium glutamate, gallic acid and others [61]. While citrate is able to reduce gold(III) to gold(0) at high temperatures, sodium borohydride is a more powerful reducing agent with the capability to reduce gold(III) ions at room temperature [62]. Apart from chemical reduction methods, alternative methods for synthesizing gold nanoparticle were approached, such as microemulsion, reversed micelles, seeding growth and physical methods (photochemistry, sonochemistry, radiolysis, thermolysis etc.) [45].

### **2.3.3 Stabilization of gold nanoparticle**

The stability of gold nanoparticle can be related to its ability to prevent the aggregation or degradation of gold nanoparticles. There are several important factors that can influence the stability of colloidal gold nanoparticle, such as particle sizes, concentration, capping agent and local environment. Therefore, different capping agents have been developed for protecting gold nanoparticles from aggregation. They also display dual roles of effective reducing agents and stabilizing properties. The different types of reducing/capping agents have been investigated, such as those from

microorganisms and bacteria, plant extracts and physiological molecules, inorganic reagents and metal complexes, organic molecules, organic acids and salts, liposomes and polymers [61].

Gold nanoparticle prepared by the citrate reduction method is generally stabilized by charged citrate ions [54]. Citrate ions not only reduce gold(III) ions to form gold nanoparticles but also act as capping agents that stabilize gold nanoparticles by forming a negatively charged layer on its spherical surface. The repulsion force between the nanoparticles keeps them stable in suspension for long time without serious aggregation. Citrate species can stabilize gold nanoparticle; however, they are readily replaced by other desired ligands that form stronger interactions with the gold nanoparticle surface, especially thiols [63, 64].

Due to high surface susceptibility to displacement by various molecules, citrate-stabilized gold nanoparticle is simply exchanged by ligands. The possibility of using thiols of different lengths as stabilizers for gold nanoparticles was first reported by Mulvaney and Giersig [65]. However, the limitation of citrate reduction is particle size of gold nanoparticle obtained in the range over 15 nm. Yonezawa and Kunitake [66] demonstrated a ligand stabilization for preparing gold nanoparticle with diameter of 2.0 nm by adding sodium 3-mercaptopropionate during the refluxing citrate reduction reaction. Under these conditions, smaller particles were formed because of the stronger coordination of thiols to the nascent gold nanoparticle surface. While the citrate species is able to chemically reduce the gold(III) to gold(0), the thiol moieties will preferentially bind to the newly formed gold surface over the excess citrate to produce the diminished particles. Other chemical functional groups, such as amine, phosphine, alcohol and carboxylate have demonstrated the ability to bind onto the surface of gold nanoparticles [45, 67].

Common mechanisms of colloidal stabilizers stabilizing gold nanoparticle colloids are electrostatic, steric and electrosteric (a combination of electrostatic and steric) interactions. As shown in Figure 2.5, for example, electrostatic stabilization or charge stabilizing related to surface charges and the counter ions in the medium to produce a repulsive electric double layer that stabilizes colloids against van der Waals

attractive forces [11]. For charge stabilized particles, the zeta potential is a measure of the stability of the particle. Typically, nanoparticles with zeta potentials greater than 20 mV or less than -20 mV have sufficient electrostatic repulsion to remain stable in solution.

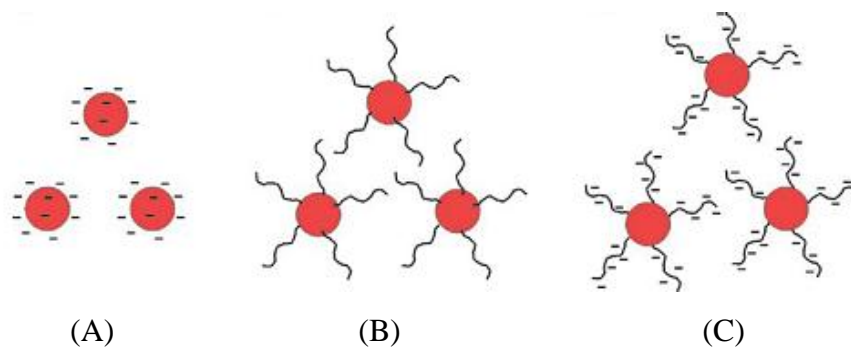


**Figure 2.5** Schematic representation of colloidal stabilization through, (A) small charged molecules on the gold nanoparticle surface (electrostatic stabilization), (B) surface steric stabilization and (C) surface electrosteric stabilization [54].

### 2.3.4 Functionalization of gold nanoparticle

The main objective of the functionalization of gold nanoparticle (or so-called modified-gold nanoparticles) is to preserve the stability, functionality and optical properties of gold nanoparticle. Gold nanoparticle should be able to retain its unique properties, such as strong plasmon absorption band and light scattering, whereas functionalized ligands should be stable and able to retain their specific recognition properties toward target analyte. The function of ligand modified on the surface of nanoparticle may be divided into two strategies. One strategy is stabilization of the dispersed gold nanoparticle against aggregation or degradation. The other is to increase the ability of gold nanoparticle to have high selectivity toward target analyte of interest. In both cases, recognition ligands will be also exchanged and capped on the surface of as prepared-gold nanoparticle fabrication via physico-chemical interactions [63, 68].

Generally, citrate ions are only weakly bound to the surface of gold nanoparticle; therefore, they can be easily replaced by substituting ligands through chemical interaction between the sensitive ligand molecules and nanoparticle surface.

Using this concept, various biological and non-biological molecules have effectively functionalized as both complete and partial surface substituents on the surface of gold nanoparticle through physical interactions (electrostatic and hydrophobic), covalent coupling bonds and specific recognition interactions [56].

#### **2.3.4.1 Functionalization with biological molecules**

Several ways have been exploited to attract biological molecules, especially DNA, to gold nanoparticle. The electrostatic interaction between gold nanoparticles and various biological molecules is one of the easiest ways to functionalize and stabilize gold nanoparticle. The positive charges of gold nanoparticles can bind to negatively charged and nucleophilic moieties with stable ionic interactions. Biological molecules containing simultaneous acidic and basic groups, such as DNA, oligonucleotides and proteins are efficient for functionalizing/stabilizing gold nanoparticles. Generally, the functionalization of gold nanoparticles by biological molecules occurs through passive adsorption of their ligands on the surface of gold nanoparticles by electrostatic and hydrophobic interactions. In the case of citrate-capped gold nanoparticle, a strong negative charge on the citrate-stabilized gold nanoparticle surface provides an opportunity for Coulombic interaction with amine ( $\text{NH}_2$ ) groups of biological ligands adsorbed on the nanoparticle surface. Meanwhile, thiolated biomolecules can be directly bound to the gold nanoparticle surface via thiol-gold affinity interactions [68].

DNA-functionalized gold nanoparticles (DNA-AuNPs) have been widely exploited as colorimetric sensors for monitoring mercury(II) ion based on high affinity of mercury(II) ion and thymine-thymine (T-T) base pairs in DNA duplex to form a thymine-mercury(II)-thymine ( $\text{T-Hg}^{2+}\text{-T}$ ) coordination [69, 70]. When mercury(II) ions interact with the thymine units of the DNA molecules, the formations of these DNA molecules also change from linear to hairpin structures, resulting in DNA molecule release from the surface of gold nanoparticles and then reducing the aggregation of gold nanoparticle. The colorimetric detection of mercury(II) in aqueous media based on DNA/DNAzyme-functionalized gold nanoparticle has been widely developed [71-80]. Apart from DNA or DNAzymes,

other biological ligands, such as oligonucleotides [74, 81-83], chitosan [84] and protein [85] have been recently reported.

#### **2.3.4.2 Functionalization with non-biological molecules**

Ligands containing one or more functional groups, such as thiolate, amines, carboxylates and sulfide can be functionalized on the surface of gold nanoparticle similar to DNA through a strong bonding of gold-sulfur (Au-S) and gold-nitrogen (Au-N). For example, recognition ligands containing at least a thiol group can be generally modified on the surface of gold nanoparticle as mercury(II) detection proves, such as 3-mercaptopropionic acid [86-88], 11-mercaptoundecanoic acid [89], cysteine [90, 91], dithioerythritol [92], (11-mercapto-undecyl)-trimethyl ammonium [93], triethylene glycol thiol [94], 4-mercaptobutanol [95] and glutathione [96]. Thiolate groups can be strongly bound onto the surface of gold nanoparticle via strong gold-sulfur covalent bonds, while their positive and/or negative charges act as stabilizers by electrostatic repulsion. Apart from thiolates, other functional groups or molecules, such as Tween-20 [97], peptides [98], amine [99], thymine derivative [100, 101] and nitrotriazole [102] were alternatively developed as colorimetric mercury(II) sensors.

### **2.3.5 Characterization techniques**

#### **2.3.5.1 Characterization of gold nanoparticle**

##### *UV-visible spectroscopy*

UV-vis spectroscopy (UV-vis) is a very useful and simple technique for characterizing the optical properties and electronic structure of gold nanoparticle by absorption band. This method has been widely used to estimate size, concentration, and aggregation level of gold nanoparticles based on peak position and peak intensity. The extinction spectra of gold nanoparticle are related to the diameter and aspect ratio of gold nanoparticle. A solution of spherical gold nanoparticle displays a distinctive red color [103-105]. In the case of non-spherical nanoparticles, there is typically more

than one plasmon resonance peak due to asymmetry, allowing for assessment of shape as well. According to Beer's law, the absorbance of dilute gold nanoparticle dispersion is proportional to the number of nanoparticles per unit volume of dispersion [37].

$$A = \frac{NdC_{ext}}{2.303} \dots\dots\dots (2.2)$$

Where,  $A$  is the absorbance,  $N$  is the number of nanoparticles per unit volume of dispersion,  $d$  is the path length (usually 1 cm) and  $C_{ext}$  is the extinction cross-section of a single particle. As seen in Eq. 2.2, when the other factors are identical, the number of gold nanoparticle per unit volume can be measured by absorbance of the dispersion based on the Beer's law. By using UV-vis technique, both theoretical and experimental calculation, Haiss *et al.* [106] demonstrated the determination of size and concentration of gold nanoparticles in the range of 3 - 120 nm in diameter. The optical method is well in agreement for gold nanoparticles with diameter of 5 to 100 nm, with the SPR peak appearing in the range between 520 to 580 nm.

### ***Transmission electron microscopy***

The most common characterization technique of gold nanoparticle is transmission electron microscopy (TEM), which obtains a photograph of gold core, size and shape of the gold nanoparticle. TEM operates on the same basic principles as the light microscope but uses electrons instead of light as a "light source" and their much lower wavelength makes it possible to get a resolution one thousand times higher than with a light microscope. In principle, the electrons are emitted by an electron gun, commonly fitted with a tungsten filament cathode as the electron source. The electron beam is accelerated through a vacuum in the column of the microscope by an anode typically at +100 keV (40 to 400 keV). The electromagnetic lenses are focused into a very thin electron beam. The electron beam then transmits through the specimen that is in part transparent to electrons and in part scatters them out of the beam, depending on the density of the material components. The electron beam carries information about the structure of the specimen that is magnified by the objective lens system of the microscope. The spatial variation in this information (the

"image") is viewed by projecting the magnified electron image onto a fluorescent viewing screen coated with a phosphor or scintillator material such as zinc sulfide. The image can be photographically recorded by exposing a photographic film or plate directly to the electron beam, or a high-resolution phosphor may be coupled by means of a lens optical system or a fiber optic light-guide to the sensor of a CCD (charge-coupled device) camera.

### **2.3.5.2 Characterization of stabilizing ligands**

#### ***Fourier transforms infrared spectroscopy***

Fourier transforms infrared (FT-IR) spectroscopy is a powerful technique, popularly used in the characterization of the structure of both organic and inorganic molecules based on functional groups or chemical bonds. A suitable prepared sample, which could be a solid, liquid or gas, is placed in the path of an infrared radiation source and its absorption of different infrared frequencies is measured. The infrared photon energies, in a range of  $4000\text{ cm}^{-1}$  to  $400\text{ cm}^{-1}$ , are insufficient to excite electrons to higher electronic energy states, but cause transitions in vibrational energy states. These states are associated with molecular bonds, and consequently each molecule has its own unique signatures.

#### ***Nuclear magnetic resonance spectroscopy***

Nuclear magnetic resonance (NMR) spectroscopy is a research technique that exploits the magnetic properties of certain atomic nuclei to determine physical and chemical properties of atoms or molecules in which they are contained. It relies on the phenomenon of nuclear magnetic resonance and can provide detailed information about the structure, dynamics, reaction state, and chemical environment of molecules. NMR spectroscopy is commonly used to investigate the properties of organic molecules, though it is applicable to any nucleus possessing spin. When placed in a strong magnetic field, certain nuclei resonate at a characteristic frequency in the radio frequency range of the electromagnetic spectrum. Slight variations in this

resonant frequency provide detailed information about the molecular structure in which the atom resides.

## 2.4 Dithia-diaza ligands

Specific recognition of ligand toward the target analyte is one of most significant concerns for the application of gold nanoparticle based-colorimetric sensors. Sensor mechanisms based theoretically on the interaction between electron donor atoms and electron acceptor metals by covalent or coordination bonds. The electron donor atoms are molecules capable of binding to metal ions by donating a pair of electrons. Some elements are classified as donor atoms, such as Group VB (nitrogen and phosphorus) and Group VIB (oxygen and sulfur). Several functional groups usually contain one or more donor atoms, such as amine, urea, thiourea, imine, thiol, thiocarbamate, carboxylic, phenolic etc. According to the hard and soft acids and bases theory (HSAB), metal ions can be divided into three groups [107, 108].

Group 1) Hard acid: the characteristic of the cations in this group is small in size and low charge polarizability. This group includes alkali and alkaline-earth metals.

Group 2) Borderline acid: cations in this group have an intermediate character in both size and charge (polarizability), such as iron(II), cobalt(II), nickel(II), copper(II), zinc(II), lead(II) and manganese(II). They possess affinity for both hard and soft ligands and have suitable geometry for complex formation.

Group 3) Soft acid: the characteristics of this group are large in size and high charge polarizability. These tend to form covalent bonds with the donor ligand. Hence, cadmium(II) and mercury(II) ions possess strong affinity for intermediate (nitrogen) and soft (sulfur) ligands.

Similarly, Lewis bases are also classified in the same manner as acids. The order of donor atom affinity for a soft acid is observed as  $O < N < S$ . A reversed order can be applied for hard acids. In the case of bidentate chelating ligands which contain two donor sites, there are various levels of the softness. The coupling of the donor site makes the selectivity of the chelating ligand better than monodentate ligands. The

softness of the bidentate donor site is  $(O, O) < (O, N) < (N, N) < (N, S)$ . Basically, the competition between Group 1 and Group 2 metals is observed in the case of O donor sites. With metal ions in Group 2 and Group 3, competition is always present in the case of N and S donor sites. However, the competition between Group 1 and Group 3 is weak. This principle can be applied to the ligand design for specific analytes in the different cases.

Dithia-diaza ligands containing two sulfur (2S) and two nitrogen (2N) atoms as electron donor atoms are classified as soft base ligands. According to HSAB principles, soft acid metal ions, such as silver(I) and mercury(II) ions display great affinities binding to soft base ligands which contain sulfur and/or nitrogen atoms. In past years, a dithia-diaza ligand, especially 2-[3-(2-amino-ethylsulfanyl)-propylsulfanyl]-ethylamine (3-AEPE) as shown in Figure 2.6, was reported as a chelating ligand used in solid phase extraction for mercury(II) ion by grafting on effective materials, such as silica gel/MCM-41 [109] and organo-clay minerals [110]. Additionally, 3-AEPE was also coated on polystyrene magnetic particles for extraction of gold(III) and silver(I) in wastewater [111]. Nutthanara *et al.* [112] synthesized cyclic dithia-diaza with dual Schiff-base linkage functionalized polystyrene-divinylbenzene (PS-DVB) resins for adsorption of lead(II), copper(II), cadmium(II), zinc(II), nickel(II), cobalt(II) and chromium(III) ions in aqueous solution. Moreover, 3-AEPE was used as a functional subunit group to prepare ionophore as dual optical chemosensor for detecting mercury(II) ions [20, 113]. Nevertheless, dithia-diaza ligands have not been reported as a stabilizer for preventing the aggregation of gold nanoparticles.

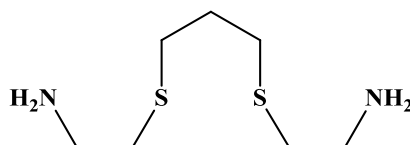


**Figure 2.6** Structure of 2-[3-(2-amino-ethylsulfanyl)-propylsulfanyl]-ethylamine (3-AEPE)

## 2.5 Ionic liquids

Room temperature ionic liquids (RTILs) are organic salts consisting of an organic cation with delocalized charge and organic or inorganic anions that are liquid at low temperature [114, 115]. Ionic liquids are widely considered as alternative organic solvents and have been applied in many fields, such as organic synthesis, liquid phase extraction and catalysis for clean technology. The unique properties of ionic liquids, such as water immiscibility, low vapor pressure under ambient conditions, miniscule volatility, tunable viscosity and non-flammability, mainly depend on their special structures [116]. Currently, ionic liquids have many uses as well as possessing great potential in many industrial applications with further research. Ionic liquids have the advantage of both homogenous and heterogeneous catalysts because they can be immiscible with reactants and products but dissolve the catalyst. They can also be used as an alternative to traditional organic and inorganic solvents. Recently, ionic liquids have been found to be able to remove metal ions such as cadmium and mercury from contaminated water because ionic liquids are insoluble in water making the two liquid phases being easy to separate. The biphasic system was shaken to ensure that it was fully mixed and then centrifuged to separate the two phases after extraction. Then, the upper aqueous phase was taken out and measured with spectroscopy techniques to determine the concentration of metal ions that was left in the aqueous phase. An extraction efficiency (*EE*) of metal ions with ionic liquids is calculated by [117];

$$EE(\%) = \frac{(C_i)_{aq} - (C_f)_{aq}}{(C_i)_{aq}} \times 100 \quad \dots\dots\dots (2.3)$$

where  $(C_i)_{aq}$  and  $(C_f)_{aq}$  are the concentration of metal ions in aqueous phase before and after extraction, respectively.

An ionic liquid 1-butyl-3-methylimidazolium hexafluorophosphate,  $[C_4mim][PF_6]$ , is considered as alternative organic solvent and has been attractively used as medium for extraction and preconcentration of mercury(II) ions [114, 118]. It is hydrophobic and immiscible in water. This makes the substance ideal for liquid-liquid extractions. If the solute is also hydrophobic, it easily dissolves into the ionic liquid upon contact with the solution. The classical ionic liquids ( $[C_nmim][PF_6]$ ,  $n =$

4, 6, 8) were reported as extractant for mercury(II) ions. Thus, all ionic liquids could extract mercury(II) ions from aqueous phase, but the extraction ability of them depended on their structure, extraction time and temperature [118]. The distribution ratio of mercury(II) ions between [C<sub>4</sub>mim][PF<sub>6</sub>] and aqueous phase is 0.84 [119, 120]. Therefore, coordinator or complexing agents, such as dithizone [117], 2-(5-bromo-2-pyridylazo)-5-diethylaminophenol (5-Br-PADAP) [30], *o*-carboxyphenyl diazoamino *p*-azobenzene (CDDA) [121], 2-mercaptobenzothiazole (2-MBT) [122], 1-(2-pyridylazo)-2-naphthol (PAN) [115, 123] were used to form with mercury(II) ions in order to improve the extraction efficiency.

## 2.6 Cold-vapor atomic absorption spectrometry

Cold vapor-atomic absorption spectrometry (CV-AAS) is traditionally the most widely used technique for mercury determination. Mercury in a liquid sample is reduced, normally with tin(II) chloride (SnCl<sub>2</sub>) or sodium borohydride, to elemental mercury. With an inert gas the mercury vapor is purged out of the solution and transported to an AAS where absorption at 253.7 or 185 nm is measured. A typical absorption cell for mercury determination with CV-AAS is made of quartz, is 25 cm long and has an inner diameter of about 0.5 cm. This method provides sensitivities approximately four orders of magnitude better than flame AAS. Tsalev *et al.* [124] reported the on-line treatment of liquid samples in a microwave oven digestion coupled with CV-AAS with the limits of detection of 0.01 and 0.2 µg L<sup>-1</sup> for mercury, with and without amalgamation, respectively. Limit of detection (LOD) of the developed sample preparation methods coupled with CV-AAS were reported as low as part per thousand (ppt) or ng L<sup>-1</sup> levels in water samples. The range of CV-AAS method is 0.2 - 10 µg L<sup>-1</sup> [29]. The range may be extended above or below the normal range by increasing or decreasing sample size. However, the actual method detection limit and linear working range are dependent on the sample matrix, type of instrumentation configuration, and selected operating conditions.

## 2.7 Methodology in spectrochemical analysis

Calibration is a very acceptable part in analytical procedures, using methods including external standard and standard addition calibration curves. External standard calibration curve is basically performed in analytical methods to calibrate instruments and procedures having no interference effect and matrices. Standard addition calibration curve is one alternative method for minimizing errors from matrix effect.

### 2.7.1 External standard method

An external standard curve between analytical signal  $S$  and known analyte concentration  $C_s$  is fitted, resulting in acceptable mathematical function using the least-squares method. Then,  $S$  obtained from the sample is used to determine unknown analyte concentration  $C_x$  from the calibration curve. However, the basic assumption of the external standard is that a standard and a sample with the same analyte concentration will yield the same analytical signal. After applying the appropriate sample preparation factors, the analyte concentration in sample can be found [125, 126].

### 2.7.2 Standard addition method

A standard addition method (often referred to as “spiking” the sample) is suitable for analyzing samples in which matrix effects are present. The addition of a known amount of analyte to the sample is done in order to determine the relative response of the detector to an analyte within the sample matrix. The relative response is then used to assess either an operative matrix effect or the sample analyte concentration. The procedure for going through the standard addition method is as follows: (1) several aliquots  $V_x$  of unknown with a concentration  $C_x$  of sample are transferred to a series of volumetric flasks having a volume  $V_t$ ; (2) a small volume of standard  $V_s$  with known concentration  $C_s$  is spiked in a series in another aliquot of analytical samples; (3) suitable reagents are added, and each solution is adjusted to the

marked volume; (4) each of the solutions is measured to yield a signal  $S$  (Eq. 2.4) [125, 126],

$$S = \frac{V_s C_s}{V_t} + \frac{V_x C_x}{V_t} \quad \dots\dots\dots(2.4)$$

Plotting between  $S$  and  $V_s$ , the slope  $m = \frac{C_s}{V_t}$  and intercept  $b = \frac{V_x C_x}{V_t}$  can be found from the graph, and  $C_x$  can be obtained from Eq. 2.5 - 2.6.

$$\frac{b}{m} = \frac{V_x C_x}{V_t} \times \frac{V_t}{C_s} \quad \dots\dots\dots(2.5)$$

$$C_x = \frac{b C_s}{m V_x} \quad \dots\dots\dots(2.6)$$

When the straight line is extrapolated to the  $x$ -axis, as shown in Figure 2.7, the difference between added standard volume at the origin and the volume at the intersection or  $x$ -intercept  $(V_s)_0$  is the volume of standard reagent equivalent to the amount of analyte in the sample. Besides, the  $x$ -intercept corresponds to null instrument response.  $C_x$  can also be obtained from Eq. 2.6 - 2.8 [125].

$$S = \frac{V_s C_s}{V_t} + \frac{V_x C_x}{V_t} = 0 \quad \dots\dots\dots(2.7)$$

$$C_x = - \frac{(V_s)_0 C_s}{V_x} \quad \dots\dots\dots(2.8)$$

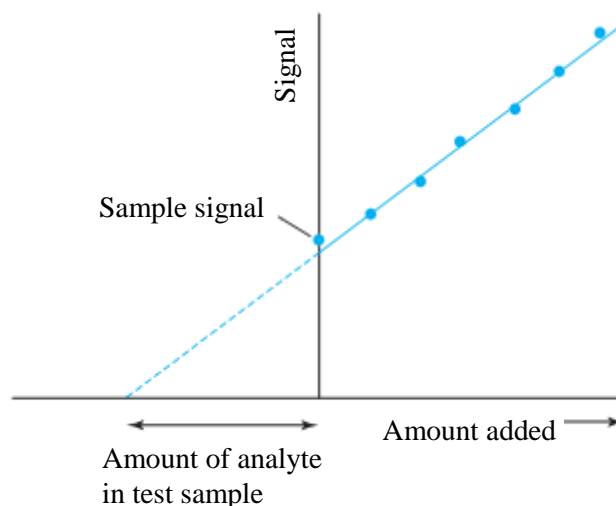


**Figure 2.7** Linear calibration graph for standard addition method.

### **2.7.3 Validation of spectroanalytical method**

For developed methods, the consistent, reliable and accurate data are extremely considered. Method validation is the process used to assure that the developed analytical technique or procedure applied for analysis is appropriate. Results from validation of the method are used to judge the consistency, reliability and accuracy of analytical results.

#### ***Accuracy***

The accuracy of an analytical method is the extent to which test results generated by the method and the true value agree [127]. Accuracy can also be described as the closeness of agreement between the value that is adopted, either as a conventional, true or accepted reference value and the value found. The true value for accuracy assessment can be obtained in several ways. Firstly, the results of the method and an established reference method are compared. Secondly, accuracy can be assessed by analyzing a sample with known concentration (e.g., a control sample or certified reference material) and comparing the measured value with the true value as supplied with the material. Finally, a blank sample matrix of interest can be spiked with a known concentration before calculating the recovery. Table 2.1 shows the range of acceptable recovery for different concentrations of the analyte.

#### ***Precision***

The precision of a method is the extent to which the individual test results of multiple experiments of a series of standards agree [127]. The measured standard deviation can be sub-divided into 3 categories: repeatability, intermediate precision and reproducibility. Repeatability is obtained when the analysis is carried out in a laboratory at least 6 determinations of 3 different matrices at 2 or 3 different concentrations. Intermediate precision is a term that has been defined as the long-term variability of the measurement process. It is determined by comparing the results of a method run within a single laboratory over a number of weeks. A method's intermediate precision may reflect discrepancies in results obtained. Reproducibility

represents the precision obtained between different laboratories. The objective is to verify that the method will provide the same results in different laboratories. The reproducibility of an analytical method is determined by analyzing aliquots from homogeneous lots in different laboratories with different analysts, and by using operational and environmental conditions that may differ from, but are still within, the specified parameters of the method. Validation of reproducibility is important if the method is to be used in different laboratories. The precision can be expressed as the standard deviation (SD) and relative standard deviation (RSD). The smaller the value of the relative standard deviation provides the greater the precision of an analysis. Table 2.1 shows the relationship between analyte concentrations and the acceptable relative standard deviation values.

**Table 2.1** Analyte recovery and precision at different concentrations [127]

<b>Analyte (%)</b>	<b>Analyte Ratio</b>	<b>Unit</b>	<b>Mean Recovery (%)</b>	<b>RSD (%)</b>
100	1	100%	98-102	1.3
10	$10^{-1}$	10%	98-102	2.8
1	$10^{-2}$	1 %	97-103	2.7
0.1	$10^{-3}$	0.1%	95-105	3.7
0.01	$10^{-4}$	100 ppm	90-107	5.3
0.001	$10^{-5}$	10 ppm	80-110	7.3
0.0001	$10^{-6}$	1 ppm	80-110	11
0.00001	$10^{-7}$	100 ppb	80-110	15
0.000001	$10^{-8}$	10 ppb	60-115	21
0.0000001	$10^{-9}$	1 ppb	40-120	30

#### *Limit of detection and limit of quantitation*

The limit of detection (LOD) is the point at which a measured value is larger than the uncertainty associated with it. It is the lowest concentration of analyte in a sample that can be detected but not necessarily quantified [127]. The limit of detection is frequently confused with the sensitivity of the method. The sensitivity of

an analytical method is the capability of the method to discriminate small differences in concentration or mass of the test analyte. In practical terms, sensitivity is the slope of the calibration curve that is obtained by plotting the response against the analyte concentration. The limit of detection of visual inspection is determined by the analysis of samples with known concentrations of analyte and by establishing the minimum level at which the analyte can be reliably detected. The limit of quantitation (LOQ) is a minimum amount that can be detected with acceptable precision. In general, the limit of detection and the limit of quantitation are estimated by 3 and 10 times, respectively, of blank signal or standard deviation of blank signal.

### ***Method detection limit***

Method detection limit (MDL) is the lowest concentration of an analyte in a sample that can be identified, measured, and reported with 99% confidence that the analyte concentration is greater than zero.

### ***Linearity and range***

The linearity of an analytical method is its ability to elicit test results that are directly proportional to the concentration of analytes in samples within a given range or proportional by means of well-defined mathematical transformations. It is determined by a series of 3 to 6 experiments of 5 or more standard solutions. A linear regression equation applied to the results should have an intercept not significantly different from zero. The linearity is generally evaluated as graphical relationship or as mathematical evaluation. The evaluation is made by visually inspecting a plot of signal responses as a function of analyte concentration as shown in Figure 2.8.

The range of an analytical method is the interval between the upper and lower levels (including these levels) that have been demonstrated to be determined with precision, accuracy and linearity using the method as written. The range is normally expressed in the same units as the test results (e.g., percentage, parts per million) obtained by the analytical method.

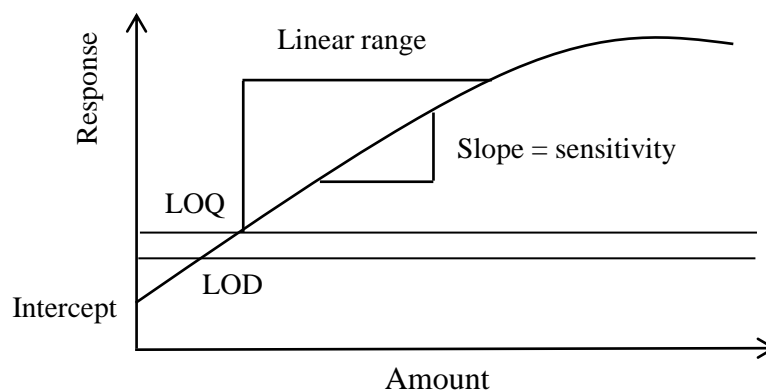


**Figure 2.8** Definition terms of linearity, range, limit of quantitation and limit of detection [127].

## 2.8 Literature review

Over past years, many publications of chemosensor (fluorescence and colorimetric sensors) used with gold nanoparticles for the detection of mercury(II) ions have been extensively reported. Colorimetric sensor use with gold nanoparticle may be divided into two strategies: chemical preparation and ligand modification. First, functionalized gold nanoparticle is as-prepared gold nanoparticle in which modified by ligand or receptor molecules on the surface of gold nanoparticle through gold-sulfur (Au-S) and/or gold-nitrogen (Au-N) bonds in order to increasingly recognize to the target analyte. Second, unmodified gold nanoparticle is as-prepared gold nanoparticle that can be exploited without ligand capping. However, in both strategies, the synthesis of as-prepared gold nanoparticle is first required. Herein, we summarize previous reports of colorimetric methods based on gold nanoparticles for determination of mercury(II) ions in various samples.

### *Colorimetric methods based on functionalized gold nanoparticle*

As described in section 2.3.4, the function of ligands in modifying the surface of gold nanoparticle has led many researchers to develop colorimetric detection methods for the determination of mercury(II) ions.

Huang and Chang [86] reported the 3-mercaptopropionic acid-functionalized gold nanoparticle (MPA-AuNPs) as chromophore-optical sensing for mercury(II) ions in the presence of 2,6-pyridinedicarboxylic acid (PDCA) acting as masking agent. The dispersed MPA-AuNPs in Tris-borate buffer pH 9.0 displayed an extinction absorption band at a wavelength of 520 nm. Following the addition of mercury(II) ions, the absorption underwent a red-shift with decreased extinction, while the intensity at a wavelength of 650 nm increased due to the aggregation of gold nanoparticle. Mercury(II)-induced aggregation of the MPA-AuNPs reached completion within 1 hour. The limit of detection of this method was 100 nM. In order to reduce the MPA-AuNPs aggregation in high-salt solutions, an adenosine monophosphate (AMP) was capped on the MPA-AuNPs as MPA/AMP-AuNPs [87]. MPA/AMP-AuNPs can disperse in high-salt concentration, while MPA-AuNPs can be aggregated. Following the addition of mercury(II) ions, the coordination between the carboxylic sub-unit of MPA and mercury(II) results in the aggregation of gold nanoparticle via bridging of neighboring nanoparticles. When using solutions containing phosphate buffer (pH 7.4) and without any masking agents, the lowest detectable concentration of mercury(II) was 500 nM by using colorimetric measurement of the ratio of absorption at 620 nm to 520 nm.

Hirayama *et al.* [94] reported colorimetric probe used to detect mercury(II) ion based on functionalizing a triethylene glycol thiol (HS-EG<sub>3</sub>) on the surface of gold nanoparticle (Au-S-EG<sub>3</sub>). The mercury(II)-induced color change of the dispersing Au-S-EG<sub>3</sub> changed from red to blue-shifted absorption band of UV-vis spectrum within 1 hour of the addition of mercury(II) ion. Mercury(II) played an important role in breaking the Au-S bonds prior to the aggregation process of gold nanoparticle. The kinetic behavior of Au-S-EG<sub>3</sub> aggregation appeared slowly due to the fact that the aggregation of Au-S-EG<sub>3</sub> with mercury(II) proceeded through several steps.

Kim *et al.* [92] developed a colorimetric sensor for mercury(II) ion in aqueous media based on the gold nanoparticle modified with dithioerythritol (DTET-AuNPs). Due to the fact that mercury(II)-induced processes through a specific S-Hg<sup>2+</sup>-S interaction, the colorimetric response of DTET-AuNPs changed from red (525 nm) to purple (670 nm). The mercury(II)-induced aggregation of the DTET-AuNPs

reached its completion within 10 minutes. To improve the selectivity toward mercury(II) ion, EDTA was added to remove interfering ions, such as lead(II), cadmium(II) and copper(II). The detection limit was 100 nM and the relative standard deviation (%RSD) was 1.2.

Lin *et al.* [97] synthesized the citrate-capped gold nanoparticle ( $13 \pm 1$  nm) by chemical reduction and then modified with Tween 20 (Tween 20-AuNPs) as a colorimetric sensor for mercury(II) and silver(I) ions. A neutral Tween 20 coating only shields around the surface of citrate-capped gold nanoparticles in order to protect against the aggregation of gold nanoparticles in high ionic strength conditions. Meanwhile, the citrate ions capped on the surface of Tween 20-AuNPs could still act as a reducing agent. In the presence of 10 mM phosphate buffer with pH 12.0 and a masking agent, mercury(II) and silver(I) ions were reduced to form mercury-gold alloy (Hg-Au) and silver(0) within 5 min. After the reducing process on the surface of the gold nanoparticles, Tween 20 molecules were also desorbed from the gold nanoparticles leading the aggregation of gold nanoparticles under high ionic strength. In the presence of sodium chloride (NaCl) and EDTA utilized as masking agent, the method showed the limit of detection for mercury(II) and silver(I) ions of 100 nM.

Similarly, in order to reduce incubation time and limit of detection, Lou *et al.* [128] used the same procedure reported by Lin *et al.* [97], but ascorbic acid was added into the system. With free metal ions, Tween 20-AuNPs could aggregate immediately following the addition of N-acetyl-L-cysteine ligand through a mercapto ligand self-assembly, resulting in color changes from red to blue. By contrast, mercury(II) and silver(I) ions could be increasingly reduced with the aid of ascorbic acid to form mercury-gold alloy (Hg-Au) or silver(0) coated on the surface of gold nanoparticles. The aggregation did not occur because both metal ions coated on the surface could block the ligand-induced aggregation. Thus, the color of gold nanoparticle turned from blue to red. This method could detect mercury(II) and silver(I) ions as low as 5 nM and 10 nM, respectively.

Liu *et al.* [93] reported a quaternary ammonium capped-gold nanoparticle (QA-AuNPs) as a selective mercury(II) ion sensor without the addition of any other

masking agents. A hydrophilic (11-mercapto-undecyl)-trimethylammonium (MTA) containing quaternary ammonium terminated thiol group was capped on the surface of gold nanoparticle via Au-S bonds. The quaternary ammonium group-terminated thiols can stabilize the dispersed gold nanoparticle only in acidic aqueous solution due to the electrostatic repulsion between the quaternary ammonium cations and the positively charged protons ( $H^+$ ). On the other hand, the QA-AuNPs aggregate rapidly in basic conditions because the quaternary ammonium cations on surface of gold nanoparticle can bind with hydroxide ion ( $OH^-$ ), which decrease the electrostatic repulsion among gold nanoparticles and, thus, cause aggregation, resulting in color change from red to blue immediately along with the appearance of the new absorption band at 600 nm. The aggregation of QA-AuNPs immediately appeared after the addition of mercury(II) in acidic solution because mercury(II) can abstract thiolates chemisorbed on gold nanoparticle surface, leading to the aggregation of gold nanoparticles and change of the color from red to blue within a minute. The lowest detectable concentration of mercury(II) by naked eye was 1  $\mu M$ . With the assistance of solar light irradiation for 30 seconds to improve sensitivity, the lowest detectable amount of this assay was lowered to 30 nM.

Si *et al.* [98] reported the discovery of carboxylated peptide ( $NH_2$ -Leu-Aib-Tyr-OMe) modified on the surface of gold nanoparticle (peptide-AuNPs). The peptide-AuNPs with a diameter of 20 nm showed a sharp SPR band at 527 nm. The assembly of peptide-AuNPs resulted in a change of color of the suspension from red to purple to blue. This color change is due to the development of a new SPR band at 670 nm.

Xiangjun *et al.* [100] reported a highly selective mercury(II) sensor based on thymine acetamidoethanethiol (T-SH) as a recognition unit to functionalize the surface of gold nanoparticles (T-S-AuNPs). Under conditions containing sodium borate buffer (pH 9.0) and incubation at 45-50  $^{\circ}C$  for 10 minutes, the dispersed T-SH modified gold nanoparticle displayed still red color, relating to the centered maximum absorption band at 520 nm. Upon the addition of mercury(II), the T-S-AuNPs were induced to aggregate via the formation of a stable  $T-Hg^{2+}-T$  complex, resulting in a color changed from red to blue-gray. The limit of detection using naked eye was as

low as 500 nM. By similarly aggregation concept, Chen *et al.* [101] synthesized *N*-1-(2-mercaptoethyl)thymine as T-S-AuNPs for mercury(II) ion with a limit of detection as low as 2.8 nM.

Chai *et al.* [91] reported the selectively detectable probe for mercury(II) ions based on the presence of modified L-cysteine on gold nanoparticles (Cys-AuNPs). The stabilized Cys-AuNPs in diameter of 16 nm appeared pink-red in color, displaying the SPR band at 518 nm. L-cysteine adsorbed on the surface of gold nanoparticles could prevent the aggregation of gold nanoparticles under high salt conditions. In addition of mercury(II) ions ( $> 20 \mu\text{M}$ ), the Cys-AuNPs solution changes to blue-gray immediately due to the aggregation of gold nanoparticle through the interaction of mercury(II) and L-cysteine. The kinetic of aggregated gold nanoparticles was slowly displayed when the concentration of mercury(II) ions less than  $20 \mu\text{M}$ . The lowest detectable concentration of mercury(II) by naked eye was  $15 \mu\text{M}$ . With the assistance of UV radiation to improve sensitivity, the detectable minimum concentration was lowered to 100 nM.

#### ***Colorimetric methods based on unmodified gold nanoparticle***

Due to some drawbacks of functionalized gold nanoparticle, such as requiring a surface modification step, separating and removing residual ligands and some limitations of ligands, unmodified gold nanoparticle or sometimes so-called “citrate-capped gold nanoparticle” (for citrate reduction preparation) as colorimetric assays have recently attracted more and more attention for many applications. Unmodified gold nanoparticles are gold nanoparticle prepared by anyway, but their surfaces were not modified with ligand molecules. Sometimes, this type was called as-prepared gold nanoparticles or bare gold nanoparticles. This strategy also relies on the target-triggered, interparticle distance dependent coloration similar to functionalized gold nanoparticle, but its aggregation is induced by removing protection from nanoparticles rather than by crosslinking.

Based on high affinity between mercury(II) ions and thymine through stable thymidine-mercury(II)-thymidine (T-Hg<sup>2+</sup>-T) coordination, Xu *et al.* [129] reported

the combination of unmodified gold nanoparticles (13 nm in diameter) and DNA oligonucleotides as a colorimetric method for mercury(II) ion with limit of detection of 500 nM. Li *et al.* [130] demonstrated that unmodified gold nanoparticle interacted differently with short single-strand DNA (ssDNA) and double-strand DNA (dsDNA). The limit of detection was as low as 0.6 nM. Wang *et al.* [131] demonstrated the citrate-capped gold nanoparticle ( $13.1 \pm 4.0$  nm) as a colorimetric probe for mercury(II) and lead(II) ions. An oligonucleotide of 15-mer thrombin binding aptamer (TBA), was used as a selective sensing element. TBA consists of 6 thymidine and 9 guanosine units, which are highly selective with mercury(II) and lead(II) ions to form hairpin-like or a quadruplex structure. TBA could be absorbed onto the citrate-capped gold nanoparticle and could also protect from the aggregation of gold nanoparticle under high salt condition. In the presence of Tris-HAc buffer (10 mM, pH 7.2) and 1 M NaCl, adding mercury(II) and lead(II) ions caused the structural forms of TBA to change, leading to the aggregation of gold nanoparticles. In order to avoid the interference of lead(II) and the need to use PDCA as masking agent, quantitative measurement was also measured at a wavelength of 800 nm, where the colorimetric response of TBA-AuNPs with lead(II) was negligible. The limit of detection was 200 nM and the linear dynamic range of mercury(II) concentration was in the range of 0.39 - 8.89  $\mu$ M.

Yang *et al.* [132] demonstrated a mercury(II)-inhibited aggregation mechanism of unmodified gold nanoparticle from pyridine-induced aggregation. The degree of inhibited aggregation was displayed by color progression change from blue to purple and then red, associating with mercury(II) concentration. The ratio value ( $E_{525}/E_{700}$ ) of the extinction increased linearly over the mercury(II) concentration range of 0.15 - 3.00  $\mu$ M with the limit of detection of 55 nM.

### ***Formation of gold nanoparticle by direct reduction***

Apart from both strategies of functionalize and unmodified gold nanoparticles, a novel strategy has been recently discovered and demonstrated by focusing on the direct formation of gold nanoparticle via simple reaction. This novel strategy has some advantages, such as its simple and rapid reaction, uncomplicated

experiments and very rapid detection with both spectrophotometry and visual naked eye assays. For example, Fan *et al.* [133] recently reported the direct formation of gold nanoparticle using a reduction reaction of  $\text{HAuCl}_4$  solution with  $\text{NH}_2\text{OH}\cdot\text{HCl}$  in the presence of Mops buffer pH 7.0 and Tween 20 stabilizer. In the absence of mercury(II), the color of the solution turned slowly to red after forming gold nanoparticles and exhibited a broadening absorption band at a wavelength of 492 nm. The speed of color change increased obviously with increasing mercury(II) concentration and it could be measured at a wavelength of 580 nm within 15 - 20 minutes. It was found that only 30 - 40% of mercury(II) was reduced and encapsulated inside or bound outside of the formed gold nanoparticles. This method provided to have a high sensitivity to mercury(II) with the detection limit of 10 nM and the recoveries were 106%, 94.7% and 66.8% for 20, 100 and 500 mM, respectively.

Properties and possibilities of functionalized and unmodified gold nanoparticle assays use as sensors for determination of mercury(II) ion in various samples are summarized in Table 2.2 and Table 2.3.

**Table 2.2** Method comparison based on functionalized gold nanoparticle assays for determination of mercury(II) ions

Modified AuNPs <sup>(a)</sup>	As-prepared AuNPs	Methods <sup>(b)</sup>	Masking agent <sup>(c)</sup>	LOD <sup>(d)</sup> (nM)	LDR (nM)	Time (min)	Co-stabilizer <sup>(e)</sup>	Buffer <sup>(f)</sup> / pH	Real sample	Ref.
CHD-AuNPs	Require	UV-vis	-	NA	0-3.4 $\mu$ M	10	SDS	-	-	[36]
dTTPs-AuNPs	Require	UV-vis	-	50	0.2-6.0 $\mu$ M	10	-	Tris-HCl / pH 7.2	Tab and river water	[80]
Chitosan-AuNPs	Require	UV-vis	-	50	50 nM-0.5 mM	-	-	-	-	[84]
MPA-AuNPs	Require	UV-vis	PDCA	100	250-500	60	-	Tris-borate pH 9	-	[86]
MPA/AMP-AuNPs	Require	UV-vis	-	500	0.5-3.5 $\mu$ M	30	-	PBS / pH 7.4	-	[87]
R6G/MPA/AMP-AuNPs	Require	FRET	-	50	50-1000	30	-	PBS / pH 7.4	Urine	[87]
MPA-HCys-PDCA-AuNPs	Require	HRS	PDCA	25	-	6-7	-	-	-	[88]
Cys-AuNPs	Require	UV-vis	-	100	0.1-2 $\mu$ M	4-6	-	-	-	[91]
DTET-AuNPs	Require	UV-vis	EDTA	100	100-600	10	-	Na <sub>3</sub> PO <sub>4</sub> / pH 6.6	-	[92]
QA-AuNPs	Require	UV-vis	-	1000 <sup>d1</sup> / 30 <sup>d2</sup>	30 nM - 0.01 M	1	-	pH 1.0	Drinking water	[93]
Au-S-EG <sub>3</sub>	Require	UV-vis	-	NA	NA	60	-	HEPES / pH 7.2	-	[94]

**Table 2.2** Method comparison based on functionalized gold nanoparticle assays for determination of mercury(II) ions (*continued*)

Modified AuNPs <sup>(a)</sup>	As-prepared AuNPs	Methods <sup>(b)</sup>	Masking agent <sup>(c)</sup>	LOD <sup>(d)</sup> (nM)	LDR (nM)	Time (min)	Co-stabilizer <sup>(e)</sup>	Buffer <sup>(f)</sup> / pH	Real sample	Ref.
4-MB-AuNPs	Require	UV-vis	-	500	1.0-7.5 $\mu$ M	120	-	pH 10	Water	[95]
Peptide-AuNPs	Require	UV-vis	EDTA	20000	2-9 ppm	10	PVA	-	-	[98]
Tween 20-AuNPs	Require	UV-vis	NaCl	100	0.2 -0.6 $\mu$ M	5	Tween 20	Na <sub>3</sub> PO <sub>4</sub> / pH 7.9	Drinking water	[97]
AP-AuNPs	Require	UV-vis	-	50	0.05-0.5	NA	-	pH 3.2	-	[99]
T-AuNPs	Require	UV-vis	-	500 <sup>d1</sup> 148 <sup>d2</sup>	0.1-1.0	10 (50°C)	-	-	Tap	[100]
NTA-AuNPs	Require	UV-vis	PDCA	7	10-500	-	-	Tris pH 8.0	Lake water	[102]
Tween 20-AuNPs	Require	UV-vis	-	5	0.5 -10 $\mu$ M	30	AA	PBS/pH 7.2	Tap and drinking water	[128]
TBA-AuNPs	Require	UV-vis	-	200	0.39-8.89	10	-	Tris-HAc / pH 7.2	Lake water	[131]
PDDA-AuNPs <sup>l</sup>	Require	UV-vis	-	25	50 nM-10 $\mu$ M	-	-	pH 5.0	Drinking water	[134]
MET-AuNPs	Require	UV-vis	-	5.6	5-1000 nM	5	-	pH 7.4	Tap water	[135]
T <sub>33</sub> -AuNPs	Require	UV-vis	-	10	10-30 nM	5	-	PBS/pH 7.4	Pond water	[83]
CA-AuNPs <sup>l</sup>	Require	UV-vis	-	-	1.6-16 $\mu$ M	5	-	pH 7.4	-	[136]

**Table 2.2** Method comparison based on functionalized gold nanoparticle assays for determination of mercury(II) ions (*continued*)

Modified AuNPs <sup>(a)</sup>	As-prepared AuNPs	Methods <sup>(b)</sup>	Masking agent <sup>(c)</sup>	LOD <sup>(d)</sup> (nM)	LDR (nM)	Time (min)	Co-stabilizer <sup>(e)</sup>	Buffer <sup>(f)</sup> / pH	Real sample	Ref.
P-AuNPs	Require	UV-vis	-	200	-	-	-	pH 7	Lake and tap water	[85]
DNA-AuNPs	Require	UV-vis	-	60	0.1-1.0 $\mu$ M	10	-	pH 7	-	[79]

<sup>a</sup>CHD; chemodosimeter, dTTPs; deoxythymidine triphosphates, MPA; 3-mercaptopropionic acid, HCys; homocysteine, R6G; rhodamine 6G, 4-MB; 4-mercaptopbutanol, QA; quaternary ammonium, S-EG<sub>3</sub>; triethylene glycol thiol, DTET; dithioerythritol, AP; aminopyrazole, T; thymine, Cys; cysteine, NTA; 3-nitro-1*H*-1,2,4-triazole, PDDA; poly(diallyldimethylammonium) chloride, MET; *N*-1-(2-mercaptoethyl)thymine, CA; cyanuric acid, T<sub>33</sub>; polythymine oligonucleotide, P; protien.

<sup>b</sup>Colorimetric (UV-vis and naked eye), HRS; hyper-Rayleigh scattering, FRET; fluorescence resonance energy transfer.

<sup>c</sup>PDCA; pyridine-2,6-dicarboxylic acid.

<sup>d1</sup>naked-eye and UV-Vis, <sup>d2</sup>solar light radiation assistance.

<sup>e</sup>SDS; sodium dodecyl sulfate, AA; ascorbic acid.

<sup>f</sup>HEPES; 4-(2-hydroxyethyl)-1-piperazineethanesulfonic acid, PBS; phosphate buffer silane, MOPS; 3-(*N*-morpholino)propanesulfonic acid.

**Table 2.3** Method comparison based on unmodified gold nanoparticle assays for mercury(II) ion detection

As-prepared AuNPs <sup>a</sup>	Ligand/reducing	Methods <sup>(b)</sup>	Masking agent <sup>(c)</sup>	LOD <sup>(d)</sup> (nM)	LDR (nM)	Time (min)	Co-stabilizer <sup>(e)</sup>	Buffer <sup>(f)</sup> / pH	Real sample	Ref.
AuNPs	DNA	UV-vis	-	500	0-5 $\mu$ M	30	-	HEPES / pH 7.4	no	[129]
AuNPs	DNA	UV-vis	-	0.6	0.1 mM - 1.0 nM	10	-	Tris-HCl/ pH 8	Tap and lake water	[137]
AuNPs <sup>l</sup>	Pyridine	UV-vis	-	55	0.15-3.0	10	-	-	Drinking water	[138]
AuNPs	H <sub>2</sub> S	UV-vis	-	0.485	10 nM-80 $\mu$ M	90	CTAB	pH 3.57	Pond water	[139]
AuNPs	DNA	UV-vis	-	250	0.75-1.5 $\mu$ M	20	-	Tris-AOc/ pH 7.4	Artificial water	[140]
AuNPs <sup>l</sup>	Thymine	UV-vis	-	2	2-12 $\mu$ M	10	-	Tris-HCl/ pH 8	Tap water	[141]
HAuCl <sub>4</sub>	NH <sub>2</sub> OH·HCl	UV-vis	-	10	10-1000	20	Tween 20	MOPs / pH 7	Lake water	[133]
Au(III)	AEPE/ NaBH <sub>4</sub>	UV-vis	-	35	0.5-10 $\mu$ M	1	Triton X-100	pH 1.4	Drinking water	[142]

<sup>a</sup>AuNPs<sup>l</sup>; anti-aggregation AuNPs assay

## CHAPTER III

### EXPERIMENTAL SECTION

#### 3.1 Apparatus

##### 3.1.1 UV-visible spectrophotometer

A UV-visible spectrophotometer (UV-vis) model UV-1700 (Shimadzu, Japan) over the wavelength range of 400 to 900 nm was used to characterize and to measure the SPR band of gold nanoparticles stabilized by dithia-diaza ligands and the aggregated gold nanoparticles.

##### 3.1.2 Cold-vapor atomic absorption spectrometer

An atomic absorption spectrometer (AAS) (model AAnalyst 100; PerkinElmer, USA) coupled with a flow injection analysis system (FIAS 100) was used to determine mercury using cold vapor (CV) technique. A mercury hollow cathode lamp (HCL, PerkinElmer, USA) operated at a current of 6 mA and a wavelength of 253.7 nm with a spectral band pass 0.7 nm were employed. Experimental conditions of CV-AAS analysis were performed as follows: 0.2% (w/v)  $\text{NaBH}_4$  (in 0.05% (w/v) NaOH) or 8% (w/v)  $\text{SnCl}_2$  at a flow rate of 5 mL  $\text{min}^{-1}$ , 3% (v/v) HCl at a flow rate of 8 mL  $\text{min}^{-1}$ , and argon gas (99.9%) as a carrier gas and 500  $\mu\text{L}$  of injection volume of sample solution.

##### 3.1.3 Fourier transforms infrared spectrometer

A Fourier transforms infrared (FT-IR) spectrometer (model Nicolet 6700; Thermo, USA) was used to characterize dithia-diaza ligands.

##### 3.1.4 Ultra-pure water

Ultra-pure water (Milli-Q) was produced using a model TKA, Germany.

### **3.1.5 Nuclear magnetic resonance spectrometer**

A characterization of dithia-diaza ligands was carried out by a nuclear magnetic resonance spectrometer (NMR) (model mercury 400; Varian, Germany). All chemical shifts were reported in part per million (ppm) using the residual proton in deuterated solvent as internal reference.

### **3.1.6 pH meter**

The pH of solution was measured by pH meter (model Lab 860; Schott Germany).

### **3.1.7 Inductively coupled plasma optical emission spectrometer**

An inductively coupled plasma optical emission spectrometer (ICP-OES) (model *i*CAP 6000 series; Thermo, USA) was used to determine mercury(II) ions in real samples.

### **3.1.8 Transmission electron microscopy**

The morphology and size of the anhydrous nanoparticles were photographed by transmission electron microscopy (TEM) (model JEM-2100; JEOL, Japan).

### **3.1.9 Mixer**

A vertex mixer (model VM-300, USA) was employed.

### 3.2 Chemicals

All chemicals used in this research are listed in Table 3.1.

**Table 3.1** List of chemicals

<b>Chemicals</b>	<b>Supplier / grade</b>
Gold standard solution (1000 mg L <sup>-1</sup> )	Merck / AR
Mercury standard solution (1000 mg L <sup>-1</sup> )	BDH / spectrosol
Silver standard solution (1000 mg L <sup>-1</sup> )	Merck / AR
Other metal solution (1000 mg L <sup>-1</sup> )	Merck / AR
Cysteamine hydrochloride	Fluka / purum > 97%
1,3-Dibromopropane	Merck / for analysis
Sodium hydroxide	Merck / for analysis
Dichloromethane	Fisher Chemicals / AR
Sodium sulfate anhydrous	Fisher Chemicals / AR
1,4-Dibromobutane	Aldrich / AR
1,5-Dibromopentane	Fluka (India) / AR
Ethanol	Merck / for analysis
Chloroform D1	Merck / 99.8% for NMR spectroscopy
Nitric acid	Merck / for analysis
Hydrochloric acid	Merck / for analysis
Sodium borohydride	Merck / for analysis
Triton X-100	Fluka / AR
1-Butyl-3-methylimidazolium chloride	Fluka / AR
Hexafluorophosphoric acid	Aldrich / AR
Tin(II) chloride dehydrate	Merck / for analysis
Sodium metal	RDH / lab

### **3.3 Preparation of chemicals**

All chemicals and organic solvents were of analytical grade and used without further purification. All solutions were prepared by using ultra-pure water (Milli-Q).

#### **Gold(III) ion solution**

A 100 mg L<sup>-1</sup> gold(III) standard solution was prepared by dilution of 1000 mg L<sup>-1</sup> with ultra-pure water.

#### **Metal ions of standard solutions**

All metal ion solutions were prepared by dilution of 1000 mg L<sup>-1</sup> stock standard solution to desired concentrations with ultra-pure water.

#### **Triton X-100 solution**

Triton X-100 solution (5 % v/v) was prepared daily by dissolving 5 mL of Triton X-100 in 100 mL of ultra-pure water.

#### **Sodium borohydride solution**

Sodium borohydride solution (8 mM) was daily prepared by dissolving 7.6 mg of NaBH<sub>4</sub> in 25 mL of 0.01 M NaOH solution. The reagent was used as reducing agent for gold nanoparticle formation.

#### **Hydrochloric carrier**

Hydrochloric acid solution (3 % v/v) was prepared by dilution of conc. HCl with ultra-pure water. The acid carrier was used for mercury analysis by flow injection CV-AAS.

### Tin(II) chloride solution

Tin(II) chloride solution was prepared daily by dissolving 80 g of SnCl<sub>2</sub> in 200 mL of conc. HCl. Then, the volume was adjusted to 1000 mL using deionized water. The solution was used to determine mercury(II) ions by flow injection CV-AAS.

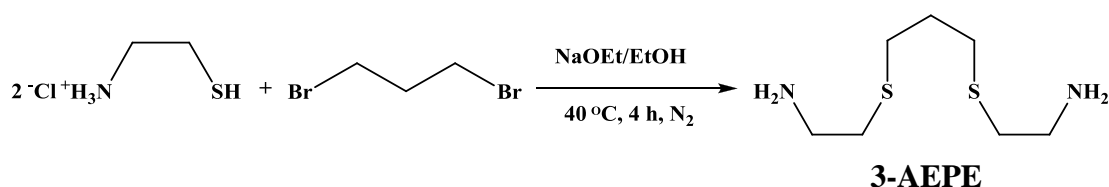
### Dithia-diaza ligands

Dithia-diaza ligands (3-AEPE, 4-AEBE and 5-AEPE) were dissolved in absolute ethanol to desired concentrations.

## 3.4 Synthesis of dithia–diaza ligands

### 3.4.1 Synthesis of 3-AEPE

The synthesis procedure of 2-[3-(2-aminoethylsulfanyl)-propylsulfanyl]-ethylamine (3-AEPE) was adapted from the previously reported procedure by Choudhury *et al.* [143] as shown in Scheme 3.1.



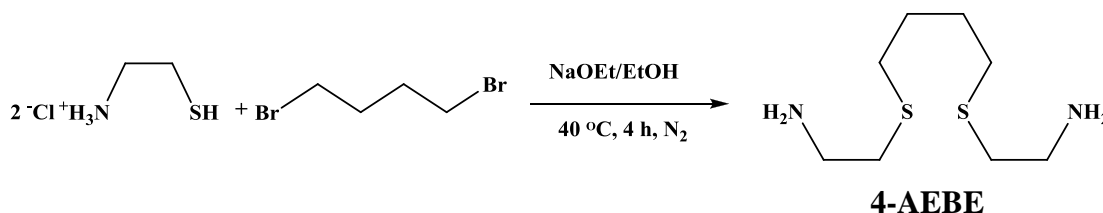
**Scheme 3.1** Synthesis of 3-AEPE.

Sodium metal (1 g, 42.9 mmol) was dissolved in 20 mL of absolute ethanol in a 150 mL two-necked round bottom flask and the solution was kept at 10-20 °C. Cysteamine hydrochloride (2.3 g, 20 mmol) was added to the solution. The mixture was stirred for 15 minutes under nitrogen atmosphere. Then, 1,3-dibromopropane (1 mL, 9.8 mmol) was slowly added using additional funnel and stirred for an additional 4 hours at 40 °C. Afterward the solvent was removed by a rotary vacuum evaporator, sodium hydroxide (5 g in 15 mL of deionized water) was added to the residue and the resulting mixture was stored in a refrigerator overnight. Then, the mixture was

transferred into a separatory funnel and extracted with dichloromethane (3 x 20 mL). The dichloromethane phase was washed twice with 20 mL of deionized water and then dried over anhydrous  $\text{Na}_2\text{SO}_4$ . After removing and drying in vacuum to give a quantitative yield of 80%, the yellow oil product was used without further purification. The 3-AEPE was characterized by FT-IR,  $^1\text{H-NMR}$  and  $^{13}\text{C-NMR}$ .

### 3.4.2 Synthesis of 4-AEBE

The synthesis procedure of 2-[4-(2-aminoethylsulfanyl)-butylsulfanyl]-ethylamine (4-AEBE) as shown in Scheme 3.2 was performed by the same synthesis steps as 3-AEPE, but 1,3-dibromopropane was replaced with 1,4-dibromobutane with the mole ratio of cysteamine hydrochloride and 1,4-dibromobutane equal to 2 : 1. A quantitative yield of 68 % was achieved and the yellow oil product was used without further purification. The 4-AEBE was characterized by  $^1\text{H-NMR}$  and  $^{13}\text{C-NMR}$ .



**Scheme 3.2** Synthesis of 4-AEBE.

### 3.4.3 Synthesis of 5-AEPE

The synthesis procedure of 2-[5-(2-aminoethylsulfanyl)-pentylsulfanyl]-ethylamine (5-AEPE) as shown in Scheme 3.3 was performed by the same synthesis steps as 3-AEPE, but 1,3-dibromopropane was replaced with 1,5-dibromopentane with the mole ratio of cysteamine hydrochloride and 1,5-dibromopentane equal to 2 : 1. After attaining a quantitative yield of 65 %, the yellow oil product was used without further purification. The 5-AEPE was characterized by  $^1\text{H-NMR}$  and  $^{13}\text{C-NMR}$ .



### **3.5 Optimization of gold nanoparticle stabilized by dithia-diaza ligands**

#### **3.5.1 Gold nanoparticle stabilized by 3-AEPE**

In a typical experiment, 0.5 mM gold(III) precursor solution, 4 mM 3-AEPE and 5% (v/v) Triton X-100 were mixed and transferred to a test tube. Next, an appropriate volume of ultra-pure water was added in order to correct the volume to 4.00 mL, but this is before adding  $\text{NaBH}_4$  reducing agent. Finally, a freshly prepared 8 mM  $\text{NaBH}_4$  solution in 0.01 M NaOH was slowly added into the solution. After adding the  $\text{NaBH}_4$  reducing agent, the color of the solution changed immediately from colorless to red within a few second. The absorption spectra of gold nanoparticle formation were measured by UV-vis in the wavelength range of 400 - 900 nm. The measurement of absorption spectra of gold nanoparticle stabilized by 3-AEPE was performed within a minute after reduction with  $\text{NaBH}_4$ . The red coloration of gold nanoparticles can be easily observed by naked eye and their images were also recorded using a digital camera (SONY, DSC-W50).

##### **3.5.1.1 Effect of the concentration of gold(III) solution**

The effect of the concentration of gold(III) was investigated by monitoring the absorption characteristic of the SPR band of gold nanoparticle stabilized by 3-AEPE. The different volumes of 0.5 mM gold(III) solution were varied in the range of 0.1 - 1.5 mL (25 - 200  $\mu\text{M}$ ), while maintaining a constant 3-AEPE, Triton X-100 and  $\text{NaBH}_4$  concentration of 0.3 mM, 0.1% (v/v) and 0.6 mM, respectively.

##### **3.5.1.2 Effect of the concentration of 3-AEPE solution**

The effect of the concentration of 3-AEPE on the SPR of gold nanoparticle formation stabilized by 3-AEPE was investigated. The different volumes of 4 mM 3-AEPE solution were varied in the range of 0.1 - 1.0 mL (0.1 - 1.0 mM) while maintaining a constant gold(III), Triton X-100 and  $\text{NaBH}_4$  concentrations of 125  $\mu\text{M}$ , 0.1% (v/v) and 0.6 mM, respectively.

### **3.5.1.3 Effect of the pH**

The effect of pH on the SPR of gold nanoparticle formation stabilized by 3-AEPE was studied by varying the pH in the range of 1 - 8. The pH of the solution was adjusted by adding different volumes of 5% (v/v) HNO<sub>3</sub> or 5% (w/v) NaOH. The pH of the solution was measured immediately after adding the reducing agent to form gold nanoparticle. Meanwhile, the concentration of gold(III), 3-AEPE, Triton X-100 and NaBH<sub>4</sub> were maintained at 125 μM, 0.3 mM, 0.1% (v/v) and 0.6 mM, respectively.

### **3.5.1.4 Effect of the concentration of NaBH<sub>4</sub>**

The effect of the concentration of NaBH<sub>4</sub> on the SPR of gold nanoparticle formation stabilized by 3-AEPE was studied. The different volumes of 8 mM NaBH<sub>4</sub> in 0.01 M NaOH were used in the range of 0.1 - 1.0 mL, with the final concentration of 0.1 - 1.0 mM, while maintaining constant gold(III), 3-AEPE and Triton X-100 concentrations of 125 μM, 0.4 mM and 0.1% (v/v), respectively.

### **3.5.1.5 Effect of the concentration of Triton X-100 solution**

The effect of the concentration of Triton X-100 co-stabilizer on the SPR of dispersed gold nanoparticle formation stabilized by 3-AEPE was studied. The different volumes of 5% (v/v) Triton X-100 solution was used in the range of 0.1 - 1.0 mL with the final concentration of 0.1 - 1.2 % (v/v), while maintaining constant gold(III), 3-AEPE and NaBH<sub>4</sub> concentrations of 125 μM, 0.3 mM and 0.6 mM, respectively.

### **3.5.1.6 Effect of reaction time**

An influence of reaction time on the formation of gold nanoparticle stabilized by 3-AEPE was studied by varying the allotted reaction time from 1 - 60 minutes. After a minute of reduction, gold nanoparticle stabilized by 3-AEPE in the absence of mercury(II) ion was monitored at a wavelength of 517 nm, while the solution with mercury(II) ion was measured at a wavelength of 680 nm.

### **3.5.1.7 Effect of interfering metal ions**

The effect of interfering metal ions was individually investigated under identical conditions of mercury(II) ion (2.5  $\mu\text{M}$ ), by the addition of 250  $\mu\text{M}$  of metal ions, including Pb(II), Cd(II), Cu(II), Co(II), Zn(II), Mn(II), Ni(II), Fe(III), Cr(III), Al(III), Mg(II), Ca(II), K(I) and Na(I). After a minute of reduction, gold nanoparticle stabilized by 3-AEPE in the presence of interfering metal ions, the absorption spectra were also recorded within the wavelength of 400 - 800 nm.

## **3.5.2 Gold nanoparticle stabilized by 4-AEBE**

### **3.5.2.1 Effect of the concentration of gold(III) solution**

The effect of the concentration of gold(III) was investigated by monitoring the absorption characteristic of the SPR band of gold nanoparticle stabilized by 4-AEBE. The experiments were performed by the same procedure as 3-AEPE (Section 3.5.1.1), but 3-AEPE was replaced with 4-AEBE.

### **3.5.2.2 Effect of the concentration of 4-AEBE solution**

The effect of the concentration of 4-AEBE on the SPR of the formation gold nanoparticle stabilized by 4-AEBE was investigated by the same procedure as 3-AEPE (Section 3.5.1.2), but 3-AEPE was replaced with 4-AEBE.

### **3.5.2.3 Effect of the concentration of $\text{NaBH}_4$**

The effect of the concentration of  $\text{NaBH}_4$  on the SPR of the formation gold nanoparticle stabilized by 4-AEBE was studied by the same procedure as 3-AEPE (Section 3.5.1.4), but 3-AEPE was replaced with 4-AEBE.

### **3.5.3 Gold nanoparticle stabilized by 5-AEPE**

#### **3.5.3.1 Effect of the concentration of gold(III) solution**

The effect of the concentration of gold(III) was investigated by monitoring the absorption characteristic of the SPR band of gold nanoparticle stabilized by 5-AEPE. The experiments were performed by the same procedure as 3-AEPE (Section 3.5.1.1), but 3-AEPE was replaced with 5-AEPE.

#### **3.5.3.2 Effect of the concentration of 5-AEPE solution**

The effect of the concentration of 5-AEPE on the SPR of gold nanoparticle formation stabilized by 5-AEPE was investigated by the same procedure as 3-AEPE (Section 3.5.1.2), but 3-AEPE was replaced with 5-AEPE.

#### **3.5.1.4 Effect of the concentration of NaBH<sub>4</sub>**

The effect of the concentration of NaBH<sub>4</sub> on the SPR of gold nanoparticle formation stabilized by 5-AEPE was studied by the same procedure as 3-AEPE (Section 3.5.1.4), but 3-AEPE was replaced with 5-AEPE.

### **3.5.4 Gold nanoparticle stabilized by cysteamine hydrochloride**

Cysteamine hydrochloride salt (HSCH<sub>2</sub>CH<sub>2</sub>NH<sub>2</sub>·HCl) is a precursor reagent to synthesize the three dithia-diaza ligands (3-AEPE, 4-AEPE, 5-AEPE). As it contains amine and thiol groups, it may be able to bind on the gold nanoparticle surface. Moreover, it may also stabilize and prevent the gold nanoparticles from the aggregation.

#### **3.5.4.1 Effect of the concentration of gold(III) solution**

The effect of the concentration of gold(III) was investigated by monitoring the absorption characteristic of the SPR band of gold nanoparticle stabilized by cysteamine hydrochloride. The experiments were performed by the same procedure as

described in Section 3.5.1.1, but 3-AEPE was replaced with cysteamine hydrochloride.

#### **3.5.4.2 Effect of the concentration of cysteamine hydrochloride**

Effect of concentration of cysteamine hydrochloride on the SPR of gold nanoparticle formation stabilized by 3-AEPE was investigated. Different volumes of 4 mM cysteamine hydrochloride solution was varied in the range of 0.1 - 1.0 mL (0.1 - 1.0 mM) while maintaining a constant gold(III), Triton X-100 and NaBH<sub>4</sub> concentration of 125 μM, 0.1% (v/v) and 0.6 mM, respectively.

### **3.6 Method validation**

In this part, this protocol was validated by using standard mercury(II) ions at various concentration levels. The analysis was repeated 11 times for each concentration level under optimal conditions. The calibration curve was obtained by analyzing 0, 0.75, 1.25, 2.25, 3.00, 3.75, 5.25, 6.00, 7.50 and 9.00 μM. Standard addition method was performed by spiking a series of mercury(II) standard into the real sample. The accuracy and the precision were presented as the percentage of recovery and the percentage of relative standard deviation, respectively. The limit of detection was calculated from standard deviation of 3 measurements of a reagent blank.

### **3.7 Application to drinking water analysis**

To demonstrate the performance of developed colorimetric method based on gold nanoparticle stabilized by 3-AEPE, real drinking water samples were spiked with mercury(II) concentrations over the range of 2 - 6 μM. Then, bottled drinking water and spiked samples were investigated as proposed protocol. An aliquot of 2.30 mL of sample was added into a test tube containing the mixture of 1000 μL of 0.5 mM gold (III), 300 μL of 4 mM 3-AEPE and 100 μL of 5% (v/v) Triton X-100. The solution was mixed thoroughly and then added slowly with 300 μL 8 mM NaBH<sub>4</sub> in 0.01 M NaOH. The color of 3-AEPE-stabilized gold nanoparticle solution developed

suddenly and the extinction absorbance at a wavelength of 680 nm was measured within a minute.

### **3.8 Determination of mercury(II) using ICP-OES**

To determine total content of mercury in drinking water samples, an inductively coupled plasma-optical emission spectrometer was operated in order to compare with the proposed method. The sample was filtered by membrane filter of 0.22  $\mu\text{m}$ . A series of standard mercury(II) over the range of 2 - 120  $\mu\text{g L}^{-1}$  was prepared using ultra-pure water.

### **3.9 Extraction of mercury(II) ions by ionic liquid**

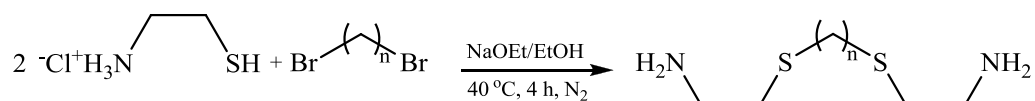
In this part, an ionic liquid  $[\text{C}_4\text{mim}][\text{PF}_6]$  was used to extract mercury(II) ions from aqueous phase. The initial concentration mercury(II) ion was 100  $\mu\text{g L}^{-1}$ . Under a constant stirring rate at room temperature, the extraction efficiency of mercury(II) using ionic liquid  $[\text{C}_4\text{mim}][\text{PF}_6]$  was investigated. The effects of volume of ionic liquid  $[\text{C}_4\text{mim}][\text{PF}_6]$ , pH, the concentration of 3-AEPE and extraction time were studied. Generally, the ionic liquid  $[\text{C}_4\text{mim}][\text{PF}_6]$  and mercury(II) ion solution was stirred thoroughly for 30 minutes with a constant stirring rate by means of a magnetic stirrer. After centrifugation for 5 minutes at 2500 rpm, the aqueous solution was collected by a dropper and then determined the residual mercury(II) ions using flow injection-cold vapor atomic absorption spectrophotometer (FI-CV-AAS).

## CHAPTER IV

### RESULTS AND DISCUSSION

#### 4.1 Synthesis and characterization of dithia–diaz ligands

Three dithia–diaz ligands, 2-[3-(2-amino-ethylsulfanyl)-propylsulfanyl]-ethylamine (3-AEPE), 2-[4-(2-amino-ethylsulfanyl)-butylsulfanyl]-ethylamine (4-AEPE) and 2-[5-(2-amino-ethylsulfanyl)-pentylsulfanyl]-ethylamine (5-AEPE) were synthesized via nucleophilic substitution reaction. These ligands differ in the number of carbon atoms between adjacent sulfur atoms. The synthesis of dithia-diaz ligands is shown in Scheme 4.1.



**Scheme 4.1** General schematic of synthesis of dithia-diaz ligands ( $n = 3, 4$  and  $5$  for 3-AEPE, 4-AEPE and 5-AEPE, respectively) [143].

#### 2-[3-(2-Amino-ethylsulfanyl)-propylsulfanyl]-ethylamine (3-AEPE)

3-AEPE was synthesized by the alkylation of cysteamine hydrochloride and 1,3-dibromopropane. The synthesis of 3-AEPE is shown in Scheme 4.1. The nucleophile was generated by ethoxide that abstracted the proton of  $-\text{SH}$  and then reacted with 1,3-dibromopropane, which has bromide as leaving groups. The synthesis of 3-AEPE was done at a mole ratio of cysteamine hydrochloride : 1,3-dibromopropane equal to 2 : 1. The product was obtained as yellow oil. The yield of 3-AEPE was 80%.

The  $^1\text{H-NMR}$  spectrum of 3-AEPE was recorded in  $\text{CDCl}_3$ .  $^1\text{H-NMR}$  spectrum of the aliphatic proton region showed three multiplets due to the symmetrical structure of dithia-diaz ligand as follows:  $\delta$  (ppm) 1.78 (2H, *t*,

$\text{CH}_2\text{CH}_2\text{CH}_2$ ,  $J = 7.02$  Hz), 2.53 (8H,  $t$ ,  $\text{SCH}_2$ ,  $J = 6.24$  Hz) and 2.78 (4H,  $t$ ,  $\text{CH}_2\text{NH}_2$ ,  $J = 6.24$  Hz). The  $^1\text{H}$ -NMR spectrum of 3-AEPE is presented in Figure 4.1.

The  $^{13}\text{C}$ -NMR spectrum of 3-AEPE was recorded in  $\text{CDCl}_3$  and was obtained with chemical shifts as follows:  $\delta$  (ppm) 27.57 ( $\text{CH}_2\text{CH}_2\text{CH}_2$ ), 30.18 ( $\text{SCH}_2\text{CH}_2\text{NH}_2$ ), 34.87 ( $\text{CH}_2\text{SCH}_2\text{CH}_2\text{NH}_2$ ) and 39.87 ( $\text{SCH}_2\text{CH}_2\text{NH}_2$ ). The  $^{13}\text{C}$ -NMR spectrum of 3-AEPE is depicted in Figure 4.2.

The FT-IR spectrum of 3-AEPE showed absorption bands or primary amine N-H stretching at  $3354 - 3280$   $\text{cm}^{-1}$ , primary amine N-H bending at  $1592$   $\text{cm}^{-1}$ , primary amine C-N stretching at  $1069$   $\text{cm}^{-1}$ , aliphatic C-H stretching at  $2856 - 2915$   $\text{cm}^{-1}$ , aliphatic C-H stretching at  $1069$   $\text{cm}^{-1}$ . The FT-IR spectrum of 3-AEPE is illustrated in Appendices (see in Figure A.1).

These results indicated that 3-AEPE was successfully synthesized.

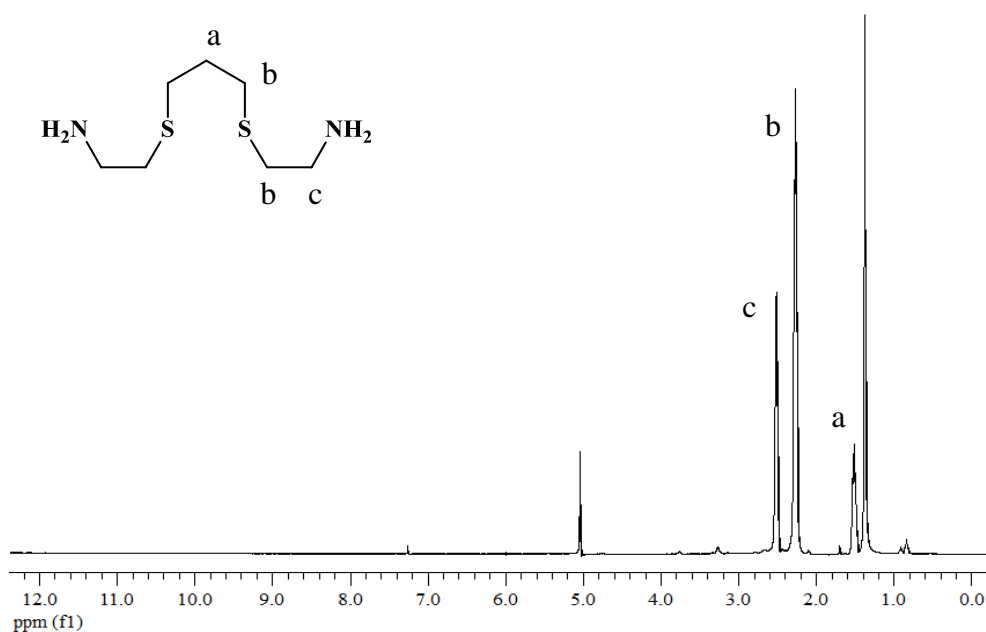


**Figure 4.1** The  $^1\text{H}$ -NMR spectrum of 3-AEPE in  $\text{CDCl}_3$ .

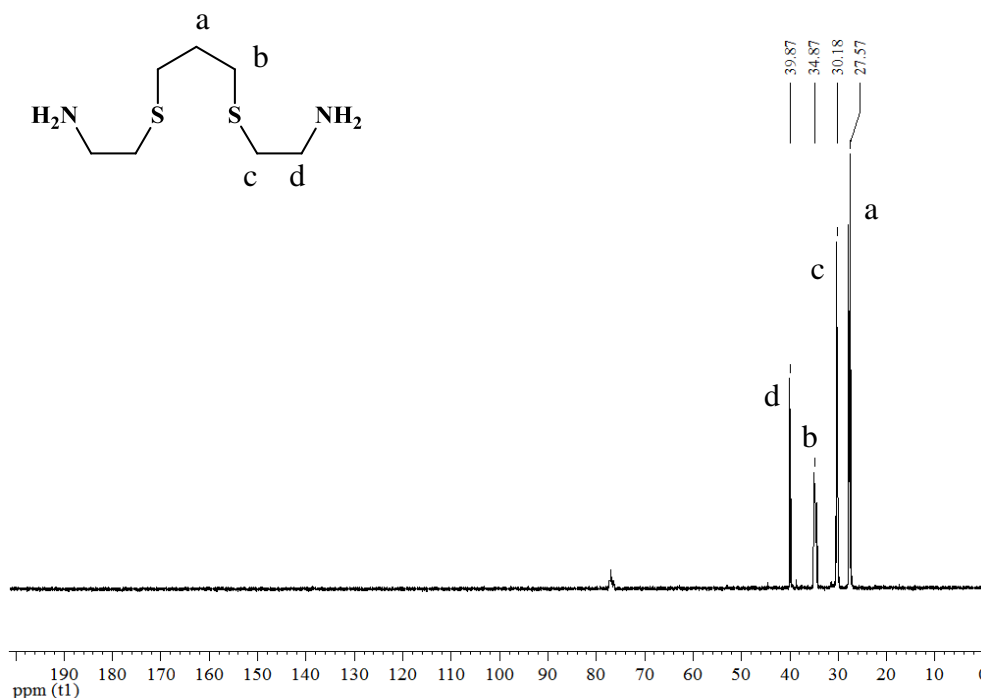


**Figure 4.2** The  $^{13}\text{C}$ -NMR spectrum of 3-AEPE in  $\text{CDCl}_3$ .

#### **2-[4-(2-Amino-ethylsulfanyl)-butylsulfanyl]-ethylamine (4-AEBE)**

Preparation of 4-AEBE was done using the same methodology as 3-AEPE, but 1,3-dibromopropane was replaced with 1,4-dibromobutane with a mole ratio of cysteamine hydrochloride : 1,4-dibromobutane equal to 2 : 1. The product was obtained as yellow oil. The yield of 4-AEBE was 70%.

The  $^1\text{H}$ -NMR spectrum of 4-AEBE was recorded in  $\text{CDCl}_3$ .  $^1\text{H}$ -NMR spectrum of the aliphatic proton region showed four multiplets due to the symmetrical structure of 4-AEBE ligand as follows:  $\delta$  (ppm) 1.56 - 1.60 (4H, *m*,  $\text{CH}_2\text{CH}_2\text{CH}_2$ ), 2.40 - 2.43 (4H, *m*,  $\text{SCH}_2\text{CH}_2$ ), 2.43 - 2.54 (4H, *m*,  $\text{SCH}_2\text{CH}_2\text{NH}_2$ ) and 2.71 - 2.80 (4H, *m*,  $\text{CH}_2\text{CH}_2\text{NH}_2$ ). The  $^1\text{H}$ -NMR spectrum of 4-AEBE is presented in Figure 4.3.

The  $^{13}\text{C}$ -NMR spectrum of 4-AEBE was recorded in  $\text{CDCl}_3$  and was obtained with chemical shifts as follows:  $\delta$  (ppm) 28.40 ( $\text{CH}_2\text{CH}_2\text{CH}_2$ ), 31.04 ( $\text{SCH}_2\text{CH}_2\text{NH}_2$ ), 35.89 ( $\text{CH}_2\text{SCH}_2\text{CH}_2\text{NH}_2$ ) and 40.72 ( $\text{SCH}_2\text{CH}_2\text{NH}_2$ ). The  $^{13}\text{C}$ -NMR spectrum of 4-AEBE is presented in Figure 4.4.

These results indicated that 4-AEBE was successfully synthesized.

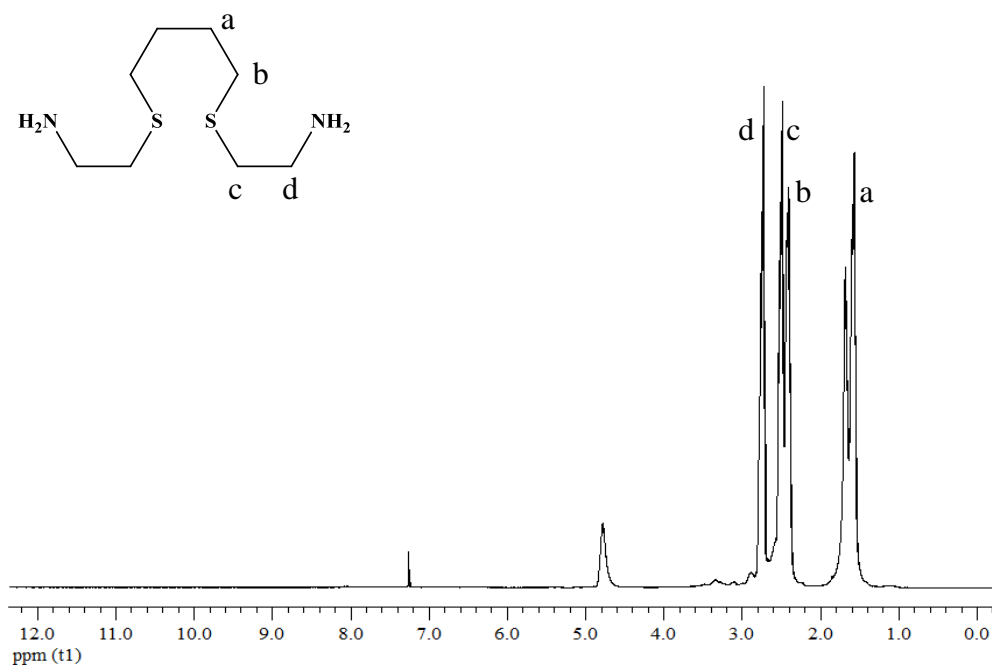


**Figure 4.3** The  $^1\text{H-NMR}$  spectrum of 4-AEBE in  $\text{CDCl}_3$ .

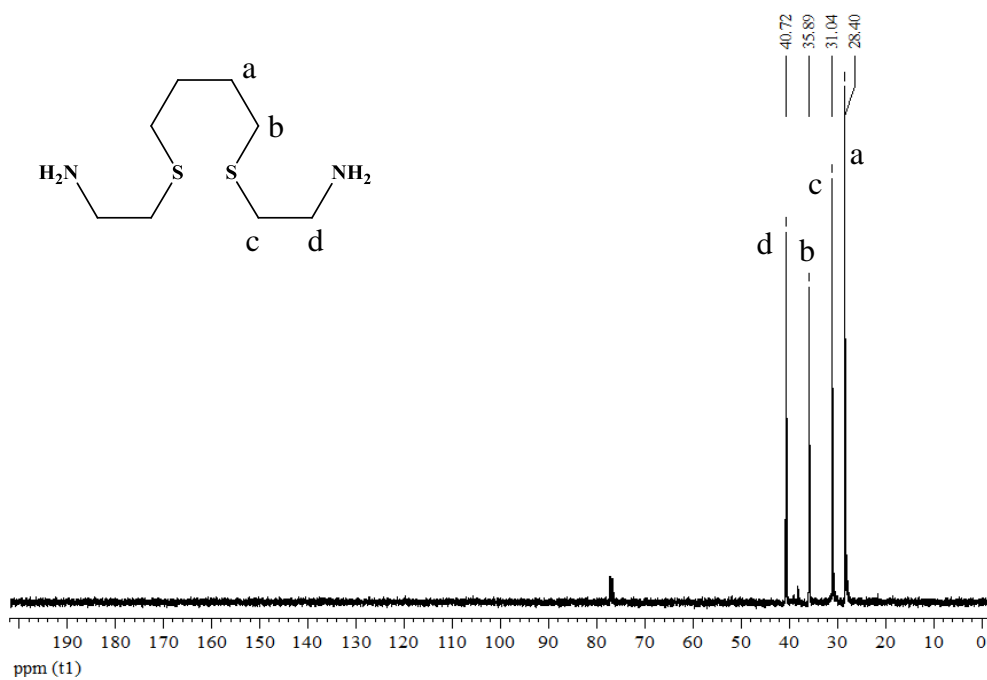


**Figure 4.4** The  $^{13}\text{C-NMR}$  spectrum of 4-AEBE in  $\text{CDCl}_3$ .

## 2-[5-(2-Amino-ethylsulfanyl)-pentylsulfanyl]-ethylamine (5-AEPE)

The preparation of 5-AEPE was achieved using the same methodology as 3-AEPE, but 1,3-dibromopropane was replaced with 1,5-dibromopentane with a mole ratio of cysteamine hydrochloride : 1,5-dibromopentane equal to 2 : 1. The product was obtained as yellow oil. The yield of 5-AEPE was 70%.

The  $^1\text{H-NMR}$  spectrum of 5-AEPE was recorded in  $\text{CDCl}_3$ .  $^1\text{H-NMR}$  spectrum of the aliphatic proton region showed five multiplets due to the symmetrical structure of 5-AEPE ligand as follows:  $\delta$  (ppm) 1.33 - 1.37 (2H, *m*,  $\text{CH}_2\text{CH}_2\text{CH}_2$ ), 1.41 - 1.47 (4H, *m*,  $\text{SCH}_2\text{CH}_2\text{NH}_2$ ), 2.34 - 2.37 (4H, *m*,  $\text{CH}_2\text{CH}_2\text{CH}_2\text{S}$ ), 2.46 (4H, *t*,  $\text{CH}_2\text{CH}_2\text{S}$ ,  $J = 6.30$  Hz), and 2.71 (4H, *t*,  $\text{CH}_2\text{NH}_2$ ,  $J = 6.30$  Hz). The  $^1\text{H-NMR}$  spectrum of 5-AEPE is presented in Figure 4.5.

The  $^{13}\text{C-NMR}$  spectrum of 5-AEPE was recorded in  $\text{CDCl}_3$  and was obtained with chemical shifts as follows:  $\delta$  (ppm) 27.61 ( $\text{CH}_2\text{CH}_2\text{CH}_2$ ), 28.96 ( $\text{CH}_2\text{CH}_2\text{NH}_2\text{S}$ ), 31.27 ( $\text{SCH}_2\text{CH}_2$ ), 35.89 ( $\text{CH}_2\text{CH}_2\text{S}$ ) and 40.64 ( $\text{SCH}_2\text{CH}_2\text{NH}_2$ ). The  $^{13}\text{C-NMR}$  spectrum of 5-AEPE is presented in Figure 4.6.

The results indicated that 5-AEPE was successfully synthesized.

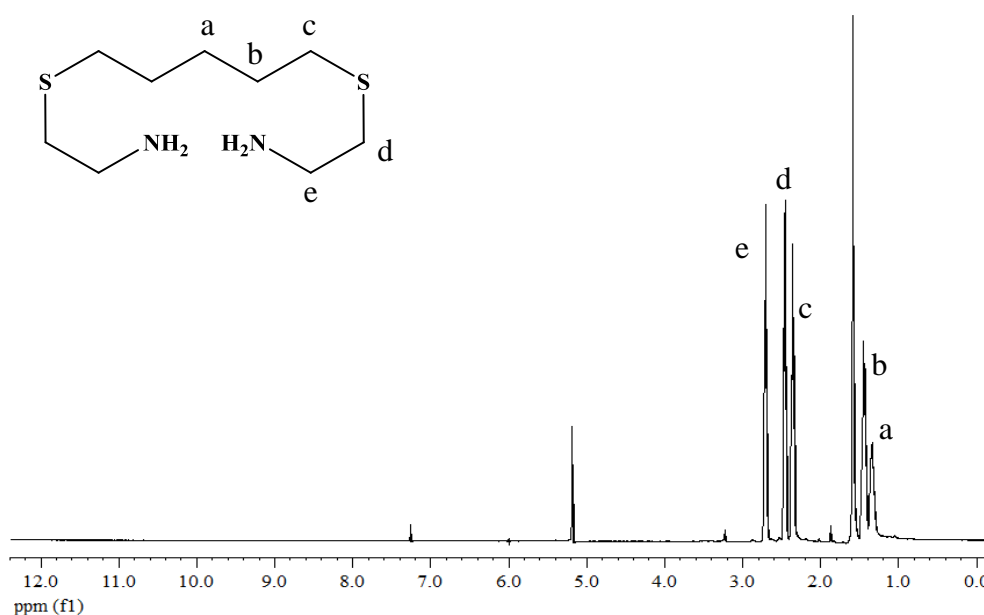


**Figure 4.5** The  $^1\text{H-NMR}$  spectrum of 5-AEPE in  $\text{CDCl}_3$ .

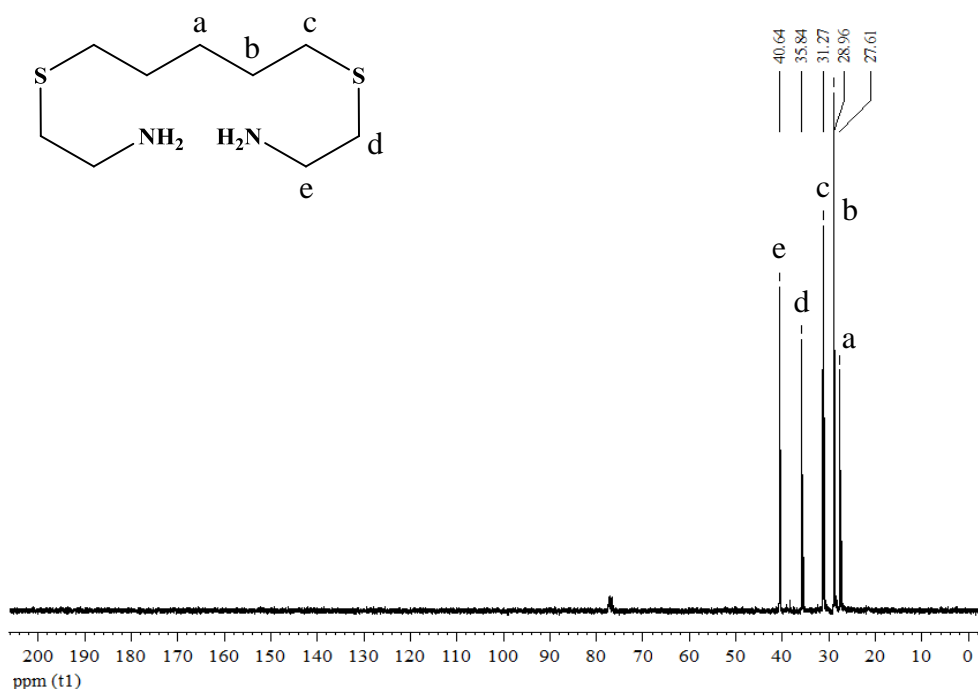


**Figure 4.6** The  $^{13}\text{C}$ -NMR spectrum of 5-AEPE in  $\text{CDCl}_3$ .

## 4.2 Stabilization of the gold nanoparticles with dithia-diaza ligands

Generally, gold nanoparticles obtained from direct reduction using the reducing agents, such as  $\text{NH}_2\text{OH}\cdot\text{HCl}$  and  $\text{NaBH}_4$  can easily aggregate rapidly, resulting in the change of SPR and coloration. Therefore, in this work, dithia-diaza ligands (3-AEPE, 4-AEPE and 5-AEPE) were used to stabilize gold nanoparticles preventing aggregation in the absence of mercury(II) ion.

### 4.2.1 Gold nanoparticles stabilized by 3-AEPE

#### 4.2.1.1 Effect of the concentration of gold(III) solution

Because the SPR characteristic of gold nanoparticles depends on gold(III) ion precursor solution, the concentration of gold(III) ion solution was first studied with a constant concentration of 0.3 mM 3-AEPE, 0.6 mM  $\text{NaBH}_4$  and 0.1% (v/v) Triton X-100. The mole ratio of sodium borohydride and gold(III) ion is shown in Table 4.1. By using a constant 2.4  $\mu\text{mol}$  sodium borohydride amount, gold(III) ion concentrations were varied in the range of 25 - 200  $\mu\text{M}$ . The result of the SPR absorption band of gold nanoparticles stabilized by 3-AEPE as a function of different

concentrations of gold(III) ion is shown in Figure 4.7. The UV-vis absorption bands can be used to confirm the formation of gold nanoparticles stabilized by 3-AEPE by showing the maximum absorption band at around 520 nm. It was found that the concentration of gold(III) ion at 25  $\mu\text{M}$  did not show the characteristic SPR band, indicating average particle size less than 2 nm [37, 51, 145]. Because of the high mole ratio between sodium borohydride and gold(III) ion (with 24 : 1), gold(III) ions can be reduced to colloidal gold instead of gold nanoparticles.

When the concentration of gold(III) was increased from 50 - 125  $\mu\text{M}$  (mole ratio of  $\text{NaBH}_4$  to gold(III) ion by 12 - 4.8 orders), a broad plasmon resonance band (517 nm) of gold nanoparticles appeared and also increased with increasing gold(III) ion concentrations. This resulted in an immediate change in the coloration of solution, becoming an obvious red color. These results also indicated that the formation of gold nanoparticles in the presence of 3-AEPE increased with increasing gold(III) ion concentrations. The optimum concentration of gold(III) ion was 125  $\mu\text{M}$  (mole ratio of gold(III) :  $\text{NaBH}_4$  was 0.2) because gold nanoparticle remained red in coloration. This implies that 3-AEPE can stabilize gold nanoparticles well. Corresponding with previous reports of reducing with  $\text{NaBH}_4$  [146] and hydroxylamine hydrochloride [133], the formation of gold nanoparticles was greatly dependent on the initial concentration of  $\text{HAuCl}_4$ . The gold nanoparticles also appeared when the lowest concentration of  $\text{HAuCl}_4$  was 1.5 mM (with a mole ratio of  $\text{NaBH}_4$  and gold(III) ion was 12:1). In the case of  $\text{NH}_2\text{OH}$ , the lowest concentration of  $\text{HAuCl}_4$  to form gold nanoparticles was 1 mM with a mole ratio of 4.5 relative to  $\text{HAuCl}_4$  [130, 133, 147].

In contrast, the color of the solution turned to blue rapidly, and the precipitation occurred with gold(III) ion concentrations over 125  $\mu\text{M}$  (mole ratio of  $\text{NaBH}_4$  to gold(III) ion less than 4.8). These results revealed that the concentration of gold(III) was too high, thus the aggregation could rapidly occur. The gold nanoparticles might occur at large nanoparticle sizes (>100 nm), causing them to aggregate easily. It was reasoned that the aggregated gold nanoparticles obtained from gold(III) ion concentrations over 150  $\mu\text{M}$  (0.6  $\mu\text{mol}$ ) appeared rapidly because 3-

AEPE could not prevent the aggregation mechanism. Thus, the optimum concentration of gold(III) ion was 125  $\mu\text{M}$ .

**Table 4.1** Mole ratio of sodium borohydride and gold(III) ion

$\text{Au}^{3+}$ ( $\mu\text{M}$ )	$\text{Au}^{3+}$ ( $\mu\text{mol}$ )	$\text{NaBH}_4$ (mM)	$\text{NaBH}_4$ ( $\mu\text{mol}$ )	Mole ratio $\text{Au}^{3+}:\text{NaBH}_4$
25	0.1	0.6	2.4	0.04
50	0.2	0.6	2.4	0.08
75	0.3	0.6	2.4	0.12
100	0.4	0.6	2.4	0.16
125	0.5	0.6	2.4	0.20
150	0.6	0.6	2.4	0.25
175	0.7	0.6	2.4	0.30
200	0.8	0.6	2.4	0.34

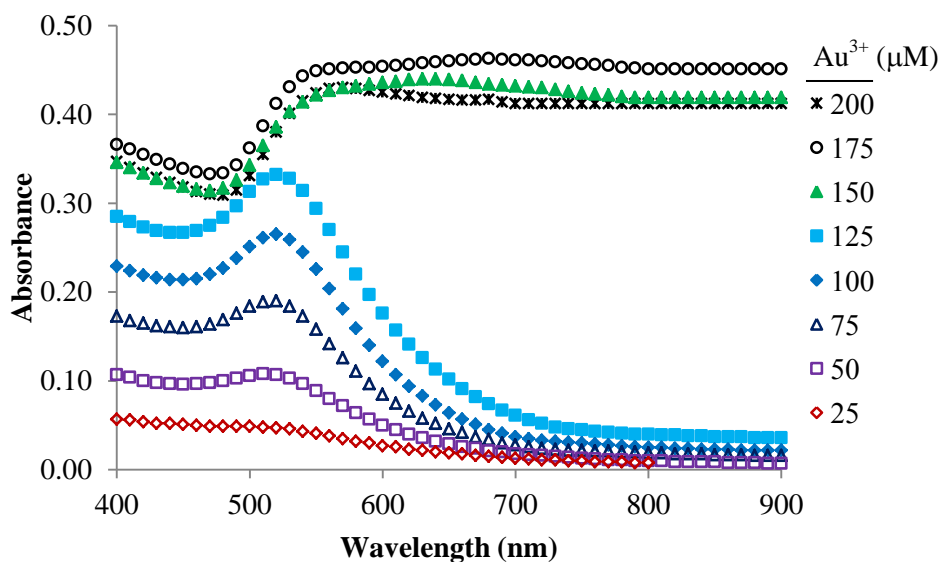


**Figure 4.7** Effect of the concentration of gold(III) solution on the formation of gold nanoparticle stabilized by 3-AEPE.

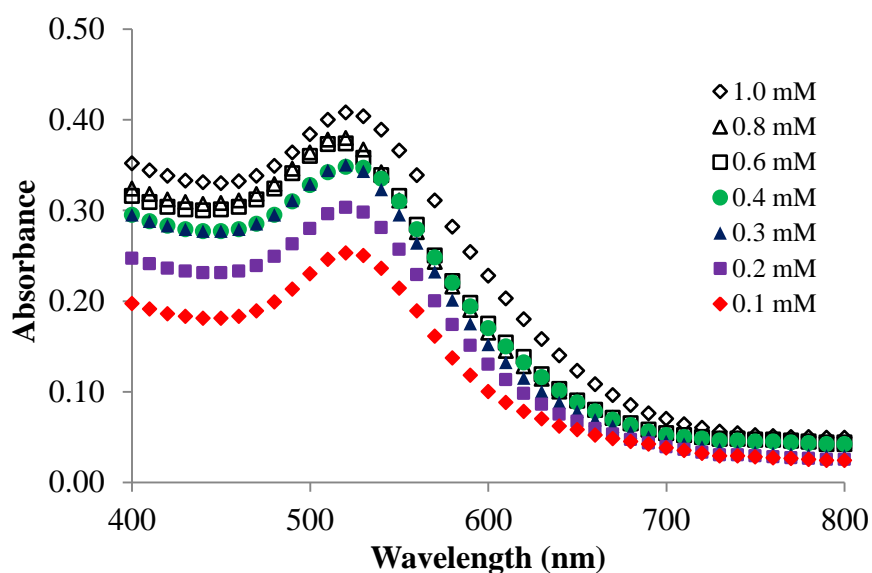
#### 4.2.1.2 Effect of 3-AEPE concentration

In this work, 3-AEPE displays a dual role; (i) it was used as a stabilizer to prevent the aggregation of gold nanoparticles and (ii) it offers a high selectivity towards mercury(II) by coordination with mercury(II) ions over other metal ions as previously reported [20, 109, 110, 113]. We first investigated the ability of 3-AEPE to stabilize gold nanoparticles by comparing the SPR band of the conditions with and without 3-AEPE ligand. It was found that the coloration of gold nanoparticle solution without 3-AEPE immediately changed to purple or blue after addition of the reducing agent due to the aggregation of the gold nanoparticles. On the other hand, the color of gold nanoparticle solution containing 3-AEPE quickly became rose-red.

Table 4.2 summarized the mole ratio of gold(III) ion and 3-AEPE (range of 0.1 - 1.0 mM) in the presence of a constant 125  $\mu$ M gold(III), 0.1% (v/v) Triton X-100 and 0.6 mM NaBH<sub>4</sub>. The absorption spectra of the gold nanoparticle stabilized by 3-AEPE solution obtained from using different 3-AEPE concentrations are shown in Figure 4.8. It was found that the absorption values at a wavelength of 517 nm increased with increasing concentrations of 3-AEPE. However, the color of solution rapidly changed from red to light blue and then changed to a more intense blue when concentration of 3-AEPE was below 0.3 mM. It could be assumed that concentrations of 0.1 - 0.2 mM 3-AEPE (mole ratio of gold(III) : 3-AEPE range of 12.5 - 3.19) could not protect against the aggregation of gold nanoparticles. On the other hand, the solution slowly changed from red to pale purple color when the 3-AEPE concentration was increased to 0.6 mM and higher (mole ratio of gold(III) : 3-AEPE less than 0.78). By visual observation, 0.3 mM of 3-AEPE exhibited a clearly red color that could be observed more easily than the other concentrations. Hence, 0.3 mM 3-AEPE was selected for further studies, which with 125  $\mu$ M gold(III) yields a 1.39 : 1 mole ratio of gold(III) : 3-AEPE.

**Table 4.2** Mole ratio of gold(III) ion and 3-AEPE

Au <sup>3+</sup> ( $\mu$ M)	Au <sup>3+</sup> ( $\mu$ mol)	3-AEPE (mM)	3-AEPE ( $\mu$ mol)	Mole ratio Au <sup>3+</sup> : 3-AEPE
125	0.5	0.1	0.04	12.5
125	0.5	0.2	0.16	3.13
125	0.5	0.3	0.36	1.39
125	0.5	0.4	0.64	0.78
125	0.5	0.6	1.44	0.35
125	0.5	0.8	2.56	0.20
125	0.5	1.0	4.00	0.13

**Figure 4.8** Effect of the concentration of 3-AEPE ligand on the formation of gold nanoparticle stabilized by 3-AEPE.

#### 4.2.1.3 Effect of the pH

In this section, the pH of gold nanoparticle stabilized by 3-AEPE solution obtained after addition of the reducing agent was measured within a minute using a pH meter. It was found that the pH of gold nanoparticle stabilized by 3-AEPE solution with constant concentrations of 125  $\mu$ M gold(III), 0.3 mM 3-AEPE, 0.1% (v/v) Triton X-100 and 0.6 mM NaBH<sub>4</sub> was about 1.4. The most acidic solution

detained from gold(III) standard precursor solution contained  $\text{HAuCl}_4$  at a concentration 0.5 mM, with a pH of 1. To investigate the effect of pH on the SPR band of gold nanoparticles stabilized by 3-AEPE, different pH values were added into the solution. The absorption spectra of gold nanoparticles stabilized by 3-AEPE in different volumes of 5%(w/v)  $\text{HNO}_3$  and 0.1 M NaOH are shown in Figure 4.9 and Figure 4.10, respectively. It was found that the SPR band shifted to a longer wavelength when the pH of the solution decreased comparing to the original solution without addition of acid and base (un-adjusted solution). The color of solution changed immediately to purple or deep-blue with a pH less than 1.14. This implied that protonated ammonium and positively charged hydrogen ions ( $\text{H}^+$ ) in acidic aqueous solution can be electrostatic repulsion; meanwhile, coordination could form through gold-sulfur (Au-S) bonds.

Oppositely, the pH values of solutions containing different volumes of NaOH (0.1 - 0.5 mL) were in the range of 1.4 - 10. These results showed that the color of the solution did not change when its pH value remained in the range of 1.38 - 2.02, but the color of the solution immediately changed from red to purple or deep-blue when the pH values of the solution increased up to the range of 2.52 to 7.02. In basic conditions (pH 9 - 10), the color of gold nanoparticles stabilized by 3-AEPE solution became pale-yellow shortly after the addition of reducing agent. Shortly afterward, the solutions appeared colorless because of precipitation in agreement with the previous report [135]. In basic conditions, 3-AEPE-stabilized gold nanoparticle aggregated rapidly because the amine groups on the surface of gold nanoparticle can bind with hydroxide ions ( $\text{OH}^-$ ) via dipole-dipole interaction [93].

The result indicated that 3-AEPE-stabilized gold nanoparticle could be stable in a narrow pH range of 1.4 to 2. Furthermore, the pH of un-adjusted solution of 3-AEPE-stabilized gold nanoparticles was about 1.4. Thus, the pH at 1.4 was selected for further investigations.

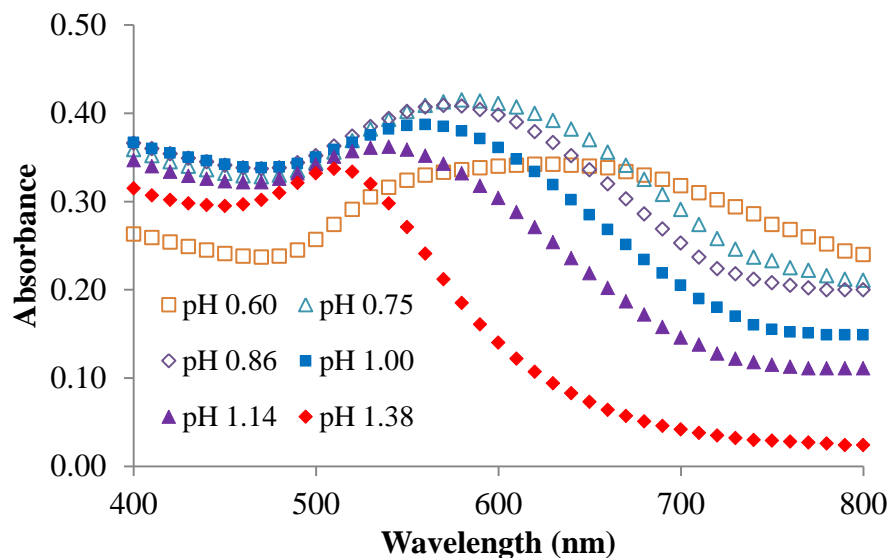


**Figure 4.9** Effect of the pH on the formation of gold nanoparticle stabilized by 3-AEPE by addition of  $\text{HNO}_3$ .

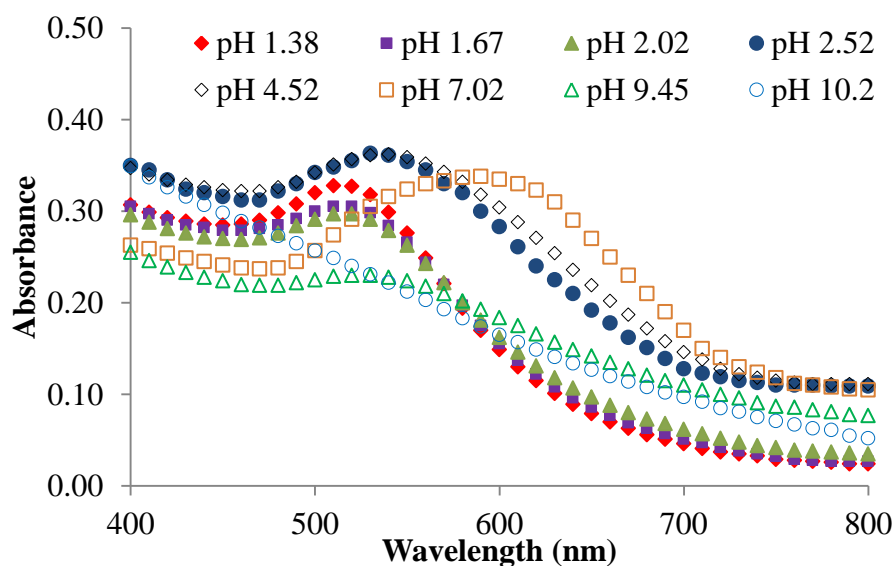


**Figure 4.10** Effect of the pH on the formation of gold nanoparticle stabilized by 3-AEPE by addition of 0.1 M NaOH.

#### 4.2.1.4 Effect of reducing agents

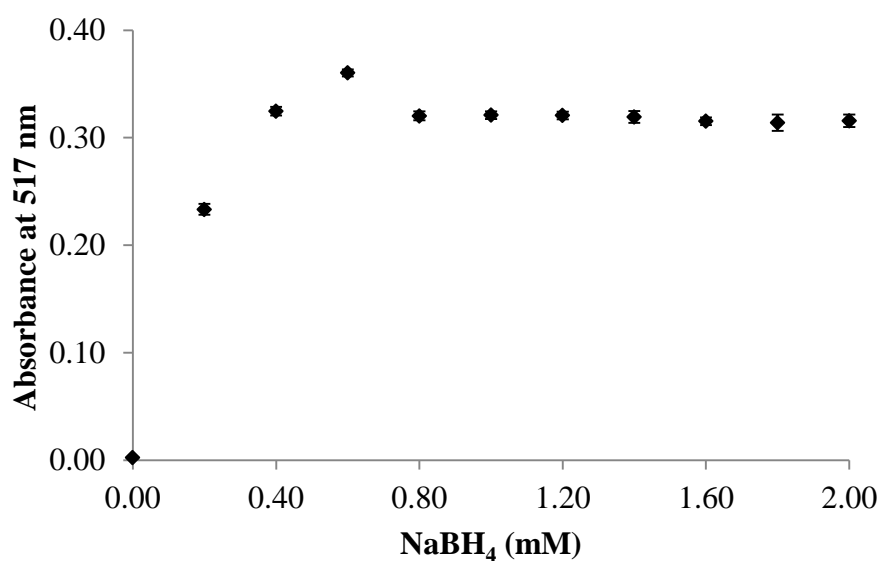
Sodium borohydride ( $\text{NaBH}_4$ ) is well known as a strong reducing agent. The standard reduction potential ( $E^0$ ) is -1.24 V in alkaline solutions and -0.48 V in acidic solutions. Sodium borohydride has been used to reduce many inorganic metal ions

such as cesium(IV), mercury(II), silver(I), copper(II) and gold(III) [148, 149]. Small spherical sizes (2 - 38 nm in diameters) of gold nanoparticles have been usually prepared by reducing tetrachloroauric acid with tri-sodium citrate and  $\text{NaBH}_4$ . A small number of  $\text{NaBH}_4$  concentrations were used to control gold nanoparticle size. However, influence on the SPR of gold nanoparticles depends mainly on the initial concentration of tetrachloroauric acid [101, 150]. Sodium borohydride changes optical and chemical properties with high efficiency by utilizing electron transfer into the nanoparticles. However, unsuitable concentrations of  $\text{NaBH}_4$  can greatly induce the aggregation of gold nanoparticles also [151].

The influence of  $\text{NaBH}_4$  concentration on gold nanoparticles was investigated by varying its concentration in the range of 0 - 2.0 mM (mole ratio of  $\text{NaBH}_4$  : gold(III) to be 0 - 16) with a constant concentration of 125  $\mu\text{M}$  gold(III), 0.3 mM 3-AEPE and 0.1%(v/v) Triton X-100, as seen in Table 4.3. The effect of the concentration of  $\text{NaBH}_4$  on the formation of gold nanoparticles stabilized by 3-AEPE is shown in Figure 4.11. It was found that the absorbance values increase sharply at the beginning with increasing  $\text{NaBH}_4$  concentration, and they show the highest absorption at the concentration of  $\text{NaBH}_4$  of 0.6 mM (mole ratio of  $\text{NaBH}_4$  : gold(III) of 4.8). At concentrations over 0.6 mM (mole ratio of  $\text{NaBH}_4$  : gold(III) more than 4.8), the absorption decreased slightly, then remained constant. Furthermore, the coloration changed from red to blue with increased reaction time. This result indicated that gold nanoparticle formation rate and gold nanoparticle aggregation or seed growth nucleation greatly depend on the concentration of  $\text{NaBH}_4$  [151, 152]. Thus, 0.6 mM  $\text{NaBH}_4$  was selected for further use.

**Table 4.3** Mole ratio of sodium borohydride and gold(III) ion

Au <sup>3+</sup> ( $\mu\text{M}$ )	Au <sup>3+</sup> ( $\mu\text{mol}$ )	NaBH <sub>4</sub> (mM)	NaBH <sub>4</sub> ( $\mu\text{mol}$ )	Mole ratio NaBH <sub>4</sub> :Au <sup>3+</sup>
125	0.5	0.2	0.8	1.60
125	0.5	0.4	1.6	3.20
125	0.5	0.6	2.4	4.80
125	0.5	0.8	3.2	6.40
125	0.5	1.0	4	8.00
125	0.5	1.2	4.8	9.60
125	0.5	1.4	5.6	11.20
125	0.5	1.6	6.4	12.80
125	0.5	1.8	7.2	14.40
125	0.5	2.0	8	16.00

**Figure 4.11** Effect of the concentration of NaBH<sub>4</sub> on the formation of gold nanoparticle stabilized by 3-AEPE.

The reducibility of NaBH<sub>4</sub> toward gold(III) ions to form gold nanoparticles was compared with hydroxylamine hydrochloride (NH<sub>2</sub>OH·HCl) and ascorbic acid. Both of them are generally used to synthesize gold nanoparticles or to reduce other

metal ions, but the reduction reaction rate is very slow. Fan *et al.* [133] reported 4.5 mM  $\text{NH}_2\text{OH}\cdot\text{HCl}$  (molar ratio of  $\text{NH}_2\text{OH}\cdot\text{HCl}$  : gold(III) equal to 4.5) as providing the highest absorption of gold nanoparticles achieved from the direct reduction of  $\text{HAuCl}_4$  to gold nanoparticle forms. Reaction time virtually took 16 minutes for  $50 \mu\text{g L}^{-1}$  mercury(II) ion, but reaction completed too long if its concentration lower than  $50 \mu\text{g L}^{-1}$ .

The absorption spectra of gold nanoparticles stabilized by 3-AEPE reduced by the various reducing agents is shown in Figure 4.12. The concentration of  $\text{NaBH}_4$  (0.6 mM) is less than  $\text{NH}_2\text{OH}\cdot\text{HCl}$  (72 mM) and ascorbic acid (71 mM) by about 100 times. The result showed that the solution reduced by  $\text{NaBH}_4$  immediately appeared rose-red in coloration, but it did not appear rose-red in color when reducing with  $\text{NH}_2\text{OH}\cdot\text{HCl}$  and ascorbic acid, even when increasing the reaction time to more than 60 minutes. Apparently,  $\text{NH}_2\text{OH}\cdot\text{HCl}$  and ascorbic acid are not suitable reducing agents for this protocol. The mechanism of the formation of gold nanoparticles greatly depended on the reducing power of  $\text{NaBH}_4$  according to the standard reduction potential of gold(III)/gold(0) (+1.50 V),  $\text{NaBH}_4$  (-1.24 V),  $\text{NH}_2\text{OH}\cdot\text{HCl}$  (-0.4 V vs SHE) [153] and ascorbic acid (+0.13 V vs NHE) [101]. This indicated that ascorbic acid is too weak to reduce gold(III) to gold(0), in agreement with the previous report [101]. Nevertheless, both  $\text{NH}_2\text{OH}\cdot\text{HCl}$  and ascorbic acid can be used together with the citrate-reduction method for seeding growth of gold nanoparticles [153-156]. It was reported that  $\text{NH}_2\text{OH}\cdot\text{HCl}$  can also reduce gold(III) ions to bulk gold metal, though the reaction rate was low. For example, the SPR of gold nanoparticle formed using direct reduction as much lower in intensity and its coloration appeared an obvious pale-red (SPR band  $\sim 580$  nm), completing reaction time to more than 25 - 30 minutes for 2 - 20  $\mu\text{g L}^{-1}$  mercury(II) ions [133].

The absorbance of gold nanoparticles stabilized by 3-AEPE measured at a wavelength of 517 nm is shown in Figure 4.13. This result confirmed that  $\text{NaBH}_4$  is the most capable reducing agent. Its absorbance is higher than  $\text{NH}_2\text{OH}\cdot\text{HCl}$  and ascorbic acid by about  $\sim 9$  and  $\sim 150$ -fold, respectively.

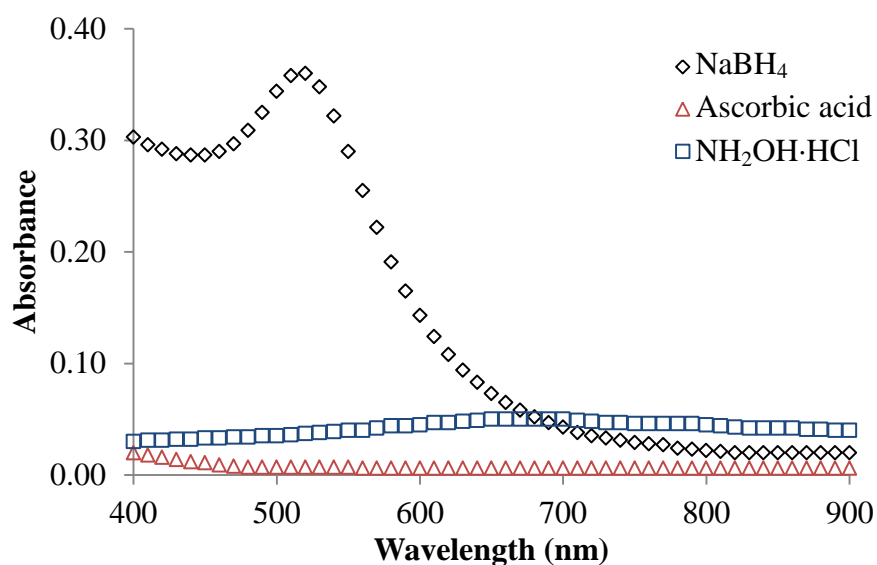


**Figure 4.12** Effect of different reducing agents on producing gold nanoparticles stabilized by 3-AEPE with 0.6 mM NaBH<sub>4</sub>, 72 mM NH<sub>2</sub>OH·HCl and 71 mM ascorbic acid. Experimental conditions: 125 μM gold(III), 0.3 mM 3-AEPE and 0.1% (v/v) Triton X-100.

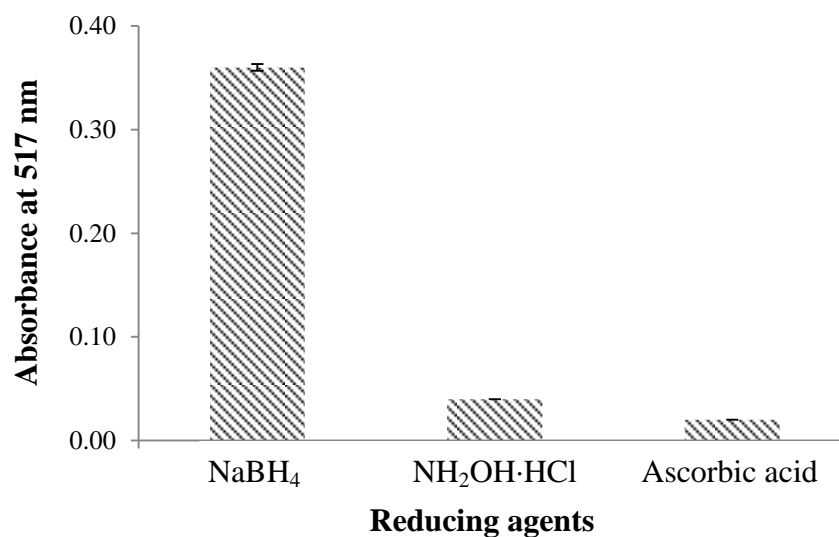


**Figure 4.13** Comparison of reducing agents on the formation of gold nanoparticles stabilized by 3-AEPE. Experimental conditions: 125 μM gold(III), 0.3 mM 3-AEPE, 0.1% (v/v) Triton X-100, 0.6 mM NaBH<sub>4</sub>, 72 mM NH<sub>2</sub>OH·HCl and 71 mM ascorbic acid.

#### 4.2.1.5 Effect of co-stabilizer concentration

Due to the instability and tendency of gold nanoparticles to aggregate, co-stabilizer has been used to prevent aggregation and to maintain the stability of gold nanoparticles. Non-ionic surfactants, such as Triton X-100, Tween 20 and Tween 80 were reported to enhance absorbance and be superior anionic and cationic surfactants for the direct reduction of gold nanoparticles [97, 133]. Non-ionic micelle forms are also known to increasingly produce fluorescent enhancements of metal-chelate complexes [157]. With this aspect, micelle solution might enhance the absorption by UV-vis too. Thus, Triton X-100 was selected for investigation.

The effect of co-stabilizer on the stability of gold nanoparticles against their aggregation was evaluated. By comparing absorption of gold nanoparticle stabilized by 3-AEPE and its coloration, Triton X-100 was used as a non-selective analyte co-stabilizer. The result showed that gold nanoparticles stabilized by 3-AEPE containing 0.1% (v/v) Triton X-100 revealed the highest absorption ( $\sim 0.319$ ) and remained slightly lower absorbance at increasing concentrations of 0.2 to 1.2% (v/v), as shown in Figure 4.14. However, the absorption of 3-AEPE-stabilized gold nanoparticles without Triton X-100 is as low as 0.115. It was indicated that the use of surfactant media can also enhance absorptibility in the spectra of 3-AEPE-stabilized gold nanoparticles by about 3 orders. This concentration of 0.1% (v/v) Triton X-100 is 1.5 mM, which is higher than its critical micelle concentration (CMC) of 0.22 - 0.24 mM by about 6 orders. At concentrations above CMC, non-ionic surfactant micelles are formed. This implied that 3-AEPE-stabilized gold nanoparticles are more soluble in solution and more intensive gold nanoparticles can distribute inside the micelle, leading to sensitivity enhancement. With concentrations of Triton X-100 in the range of 0.2 - 1.2 % (v/v) (3.09 - 18.5 mM), the absorption values at a wavelength of 517 nm decreased slightly and then remained constant. Thus, 0.1% (v/v) of Triton X-100 was selected as a co-stabilizer for all further work.

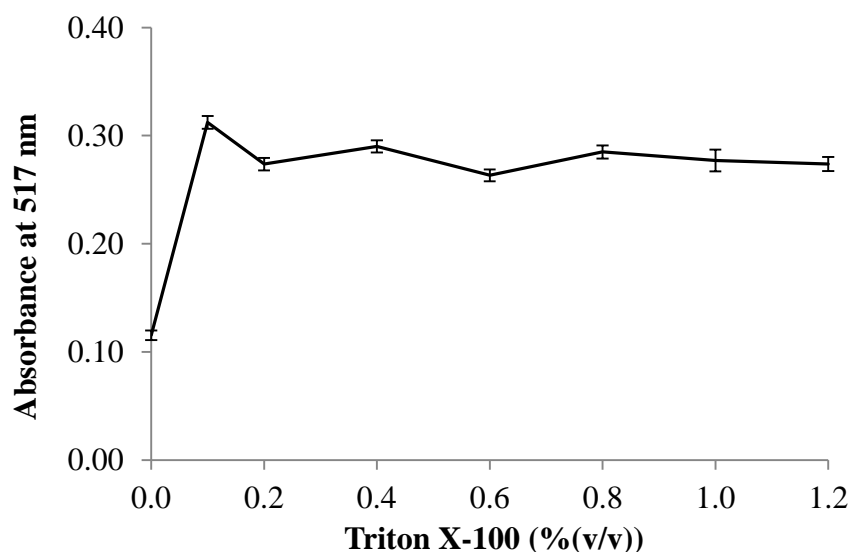


**Figure 4.14** Effect of Triton X-100 concentration on producing gold nanoparticles stabilized by 3-AEPE. Experimental conditions: 125  $\mu\text{M}$  gold(III), 0.3 mM 3-AEPE and 0.6 mM  $\text{NaBH}_4$ .

In this work, Triton X-100 was not only used to enhance sensitivity, but also acted as a co-stabilizer for maintaining the stability of 3-AEPE-stabilized gold nanoparticles in aqueous solution. Figure 4.15 shows different spectra of 3-AEPE-stabilized gold nanoparticles with and without 0.1% (v/v) of Triton X-100. Their absorption spectra in the absence of Triton X-100 (Figure 4.15 (a)) showed a red-shift to a longer wavelength quickly during the first minute, corresponding the solution color rapidly changed from red to purple, then deep-blue with increasing reaction times. However, the absorption spectra of 3-AEPE-stabilized gold nanoparticles with Triton X-100 did not significantly change in the red-shift region despite increasing reaction time up to 30 minutes (Figure 4.15 (b)). Therefore, the solution color remained rose-red. This indicated that Triton X-100 used as a co-stabilizer did not only reduce the aggregation degree of 3-AEPE-stabilized gold nanoparticles, but also enhanced the sensitivity. Accordingly, it was reasoned that micelle non-ionic surfactant has an important role in the distribution of 3-AEPE-stabilized gold nanoparticle in solution against aggregation. The rose-red color of 3-AEPE-stabilized gold nanoparticle solution is stable within 12 hours at room temperature.

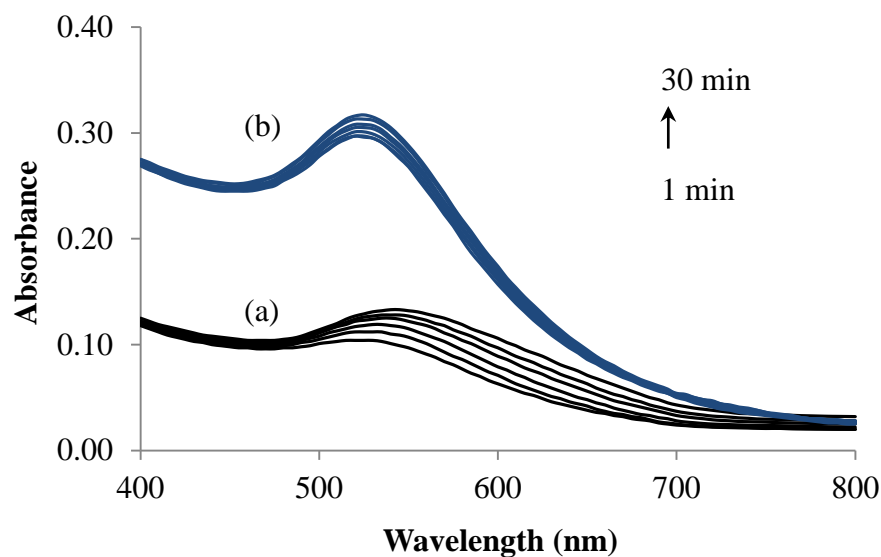


**Figure 4.15** The aggregation degree of 3-AEPE-stabilized gold nanoparticles without (a) and with (b) the inclusion of 0.1% (v/v) Triton X-100. Experimental conditions: 125  $\mu\text{M}$  gold(III), 0.3 mM 3-AEPE and 0.6 mM  $\text{NaBH}_4$ .

#### 4.2.1.6 Effect of reaction times

An important factor to be controlled the formation of gold nanoparticles is the reaction time. By maintaining constant concentrations of 125  $\mu\text{M}$  gold(III), 0.3 mM 3-AEPE, 0.1% (v/v) Triton X-100 and 0.6 mM  $\text{NaBH}_4$ , the reaction of 3-AEPE-stabilized gold nanoparticle without any mercury(II) ions (blank solution) but with  $\text{NaBH}_4$  occurred quickly within a few seconds after adding  $\text{NaBH}_4$ , resulting in a rose-red in coloration mentioned earlier. The absorption of blank solution was monitored after 30 minutes. It was found that the absorbance at a wavelength of 517 nm is slightly variable ( $\sim 0.32 - 0.34$  Abs.) because gold nanoparticles gradually occurred after direct reduction as shown in Figure 4.16 (transparent square,  $\square$ ), leading to SPR band change. Nevertheless, the rose-red color of the blank solution remained unchanged despite the reaction time increased.

Similarly, the absorbance of blank solution was also monitored at a wavelength of 680 nm, which is the same wavelength as the measurement of mercury(II) ion. The result showed that the absorbance of blank solution did not change significantly ( $\sim 0.047 - 0.052$  Abs.) as shown in Figure 4.16 (transparent

triangle,  $\Delta$ ). It was reasoned that gold nanoparticle stabilized by 3-AEPE in the presence of Triton X-100 remained stable in these conditions.

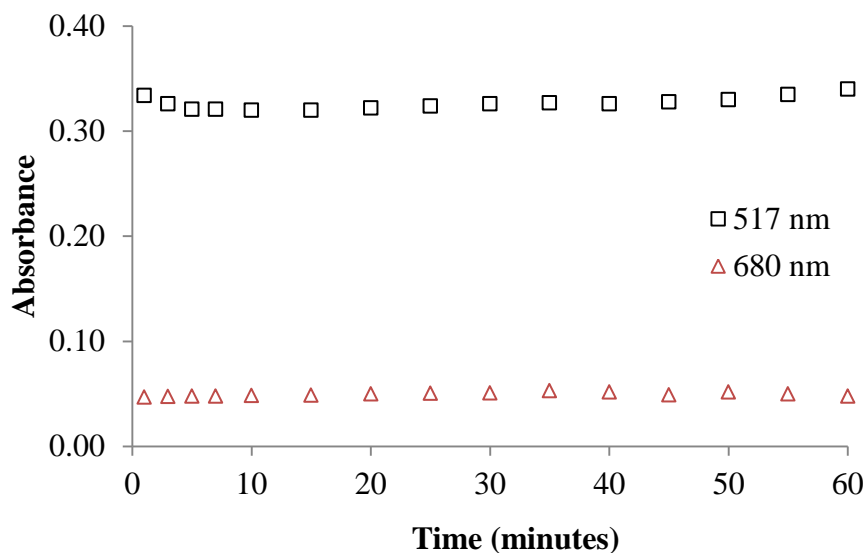


**Figure 4.16** The stability of 3-AEPE-stabilized gold nanoparticles without any mercury(II) ions ( $\Delta$  517 nm and  $\square$  680 nm). Experimental conditions: 125  $\mu\text{M}$  gold(III), 0.3 mM 3-AEPE, 0.1% (v/v) Triton X-100 and 0.6 mM  $\text{NaBH}_4$ .

The reaction time was studied by monitoring the absorption of 3-AEPE-stabilized gold nanoparticles in the presence of different concentrations of mercury(II) ions (0.5 - 5.0  $\mu\text{M}$ ). Figure 4.17 shows the absorbance of 3-AEPE-stabilized gold nanoparticles with various concentrations of mercury(II) ions when the reaction time increased from 1 to 30 minutes. It was indicated that the aggregation degree of 3-AEPE-stabilized gold nanoparticles slowly occurred when the concentration of mercury(II) ions was low ( $< 0.5 \mu\text{M}$ ). Meanwhile, the reaction could occur immediately at higher concentrations of mercury(II) ions ( $> 1.25 \mu\text{M}$ ). This result showed that the absorbance values obtained at a wavelength of 680 nm increased with also increase mercury(II) ions because the reduced  $\text{Hg}_{(l)}$  could likely deposit directly on the surface of gold nanoparticles to form an amalgam (Hg-Au alloys). Regardless, the reaction rate increased with increasing mercury(II) ions. As shown in Figure 4.18, the absorbance at a wavelength of 680 nm of 3-AEPE-stabilized gold nanoparticles increased within 5 - 10 minutes with the concentration of mercury(II) ions at less than

1.25  $\mu\text{M}$ , corresponding to a slow visual color change from red to purple, whereas their concentrations above 1.25  $\mu\text{M}$ , the increase occurred within a few seconds.

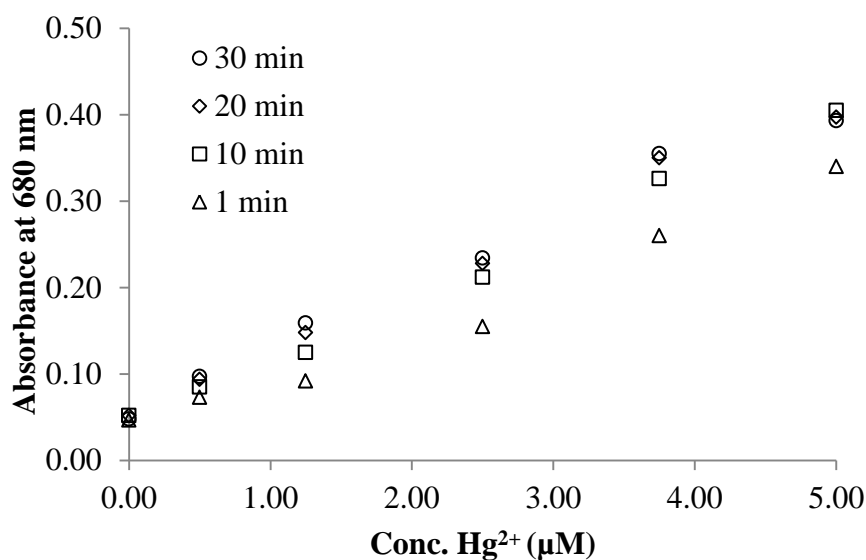


**Figure 4.17** Reaction times of 3-AEPE-stabilized gold nanoparticles in the presence of different concentrations of mercury(II) ions. Experimental conditions; 125  $\mu\text{M}$  gold(III), 0.3 mM 3-AEPE, 0.1% (v/v) Triton X-100 and 0.6 mM  $\text{NaBH}_4$ .

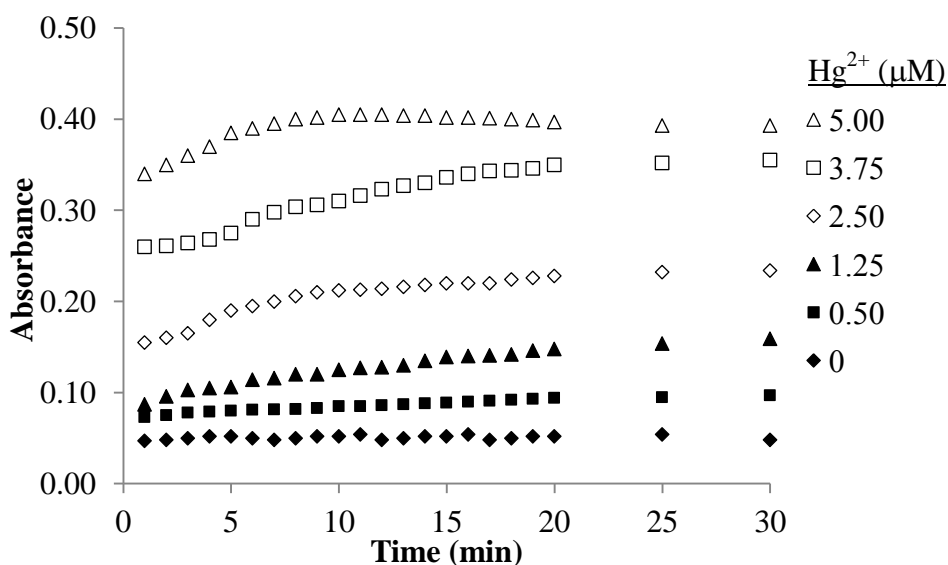


**Figure 4.18** Absorbance at 680 nm versus reaction times of 3-AEPE-stabilized gold nanoparticles in the presence of different concentrations of mercury(II) ions. Experimental conditions; 125  $\mu\text{M}$  gold(III), 0.3 mM 3-AEPE, 0.1% (v/v) Triton X-100 and 0.6 mM  $\text{NaBH}_4$ .

The optimum conditions for gold nanoparticle stabilization by 3-AEPE based colorimetric assays for monitoring mercury(II) ions are summarized in Table 4.4.

**Table 4.4** Optimum conditions of 3-AEPE-stabilized gold nanoparticle

<b>Parameters</b>	<b>Conditions</b>
Gold(III) ion	125 $\mu$ M
3-AEPE	0.3 mM
NaBH <sub>4</sub>	0.6 mM
Triton X-100	0.1% (v/v)
pH	1.2 - 2.0
Detection time	1 minute

#### **4.2.1.7 Characterization of 3-AEPE-stabilized gold nanoparticles**

The physical SPR property of gold nanoparticles and their interaction with mercury(II) ion can be investigated with a variety of tools, such as UV-vis spectroscopy, transmission electron microscopy (TEM), scanning electron microscopy (SEM), laser light scattering (LLS), dynamic light scattering (DLS), electrochemical methods, ICP-MS and others. UV-vis is the most widely used technique to characterize the optical properties of gold nanoparticles due to simple operation and common availability in laboratory. It is well known that gold nanoparticles display a maximum absorption band in the visible region at ~520 nm and so exhibit a rose-red color. For gold nanoparticles with mean diameters of 9, 15, 22, 48 and 99 nm, the SPR maximum bands,  $\lambda_{\text{max}}$ , were observed at 517, 520, 521, 533 and 575 nm, respectively [45]. In this work, UV-vis spectroscopy was used to characterize the 3-AEPE-stabilized gold nanoparticles before and after the addition of mercury(II) ions, as shown in Figure 4.19.

The characteristic SPR band of 3-AEPE-stabilized gold nanoparticles was observed in the spectrum at approximately 517 nm, corresponding to the observed rose-red color of the solution (Figure 4.19 (a)). It was also confirmed that gold

nanoparticles were formed. This was attributed to 3-AEPE-stabilized gold nanoparticle without mercury(II) ions preventing aggregation due to an electric field interaction between the gold nanoparticles and 3-AEPE ligand. To ensure the role of 3-AEPE ligand in the stability of gold nanoparticles, gold(III) ion was reduced by  $\text{NaBH}_4$  under the same conditions, but 3-AEPE was not added. It was found that the rose-red color of gold nanoparticles disappeared and the solution color turned deep-blue rapidly before precipitating. Therefore, 3-AEPE ligand is also indispensable in the formation and stabilization of gold nanoparticles that were direct reduced by  $\text{NaBH}_4$ . In agreement with a previous report [105], the gold nanoparticle spectra which were reduced by  $\text{NaBH}_4$  in the presence of polyethylene glycol (PEG) displayed a broadening band of 508 and 514 nm for 3 and 4 nm in diameter, respectively. The SPR band was distinctively observed with an average particle size of  $\sim 9$  nm.

On the other hand, the spectrum of 3-AEPE-stabilized gold nanoparticle in the presence of mercury(II) ion ( $5 \mu\text{M}$ ) is shown in Figure 4.19 (b). The color of the solution changed from colorless to blue immediately. This also displayed a red-shift and broadening of the SPR band.

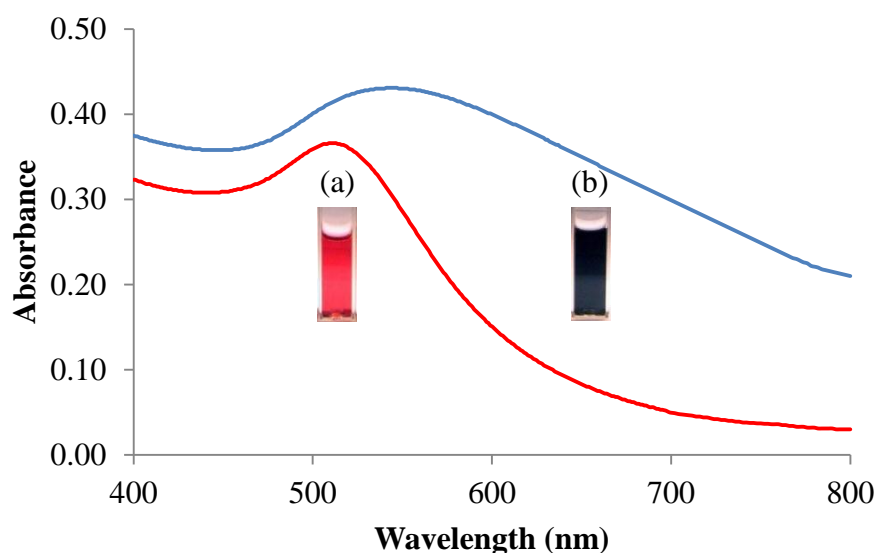


**Figure 4.19** UV-vis absorption spectra of 3-AEPE stabilized-gold nanoparticles in the (a) absence and (b) presence of  $5 \mu\text{M}$  mercury(II) ion.

In order to know both the shape and size of the gold nanoparticles, TEM was used to characterize the 3-AEPE-stabilized gold nanoparticles before and after the addition of mercury(II) ions. Figure 4.19 shows the TEM images of 3-AEPE-stabilized gold nanoparticles in the absence and presence of mercury(II) ions. The TEM image of 3-AEPE-stabilized gold nanoparticle without any mercury(II) ions is shown in Figure 4.19 (a) and displays typical shapes of regular and almost individual spherical particles with mean dispersed particle sizes of  $9 \pm 2$  nm in diameter. The average particle size was obtained by manual evaluation as shown in Figure 4.20. Thus, the average particle size of 3-AEPE-stabilized gold nanoparticles ( $\sim 9$  nm) is consistent with the SPR maximum band of 517 nm, as mentioned in the previous reports [45, 105]. The nanoparticles were not clearly observed as individual particles presented in the as-prepared gold nanoparticles because the reduction of gold(III) ions to gold nanoparticles with 3-AEPE ligand coordinated on the gold nanoparticle surfaces occurred simultaneously after the addition of  $\text{NaBH}_4$ . It was implied that gold nanoparticles were formed rapidly in solution. Although, most nanoparticles were capped by 3-AEPE ligand, some nanoparticles may not have been encapsulated on their surface. Nevertheless, we can summarize that 3-AEPE stabilized-gold nanoparticle was virtually formed under optimum conditions.

Figure 4.19 (b) shows the color of the 3-AEPE-stabilized gold nanoparticle solution in the presence of mercury(II) ions to be purple or blue due to aggregation and size increases of individual gold nanoparticle particles. It was indicated that mercury(II) ions can induce the 3-AEPE-stabilized gold nanoparticles to aggregate, as shown in Figure 4.20 (b). The 3-AEPE-stabilized gold nanoparticle was unstable with inclusion of mercury(II) ions because liquid mercury could be accelerated to join with gold nanoparticles as mercury-gold alloys. In addition, it is well known that both mercury(II) and liquid mercury exhibit tendencies to bind with a strong affinity to the surface of gold nanoparticles through amalgamation or nucleation [97, 133, 147, 149, 158]. Thus, after reduction of mercury(II) and gold(III) with  $\text{NaBH}_4$ , the reduced liquid mercury is directly deposited onto the surface of gold nanoparticles to form an amalgam. However, 3-AEPE ligand cannot perform the role of stabilization and aggregation prevention in these conditions.

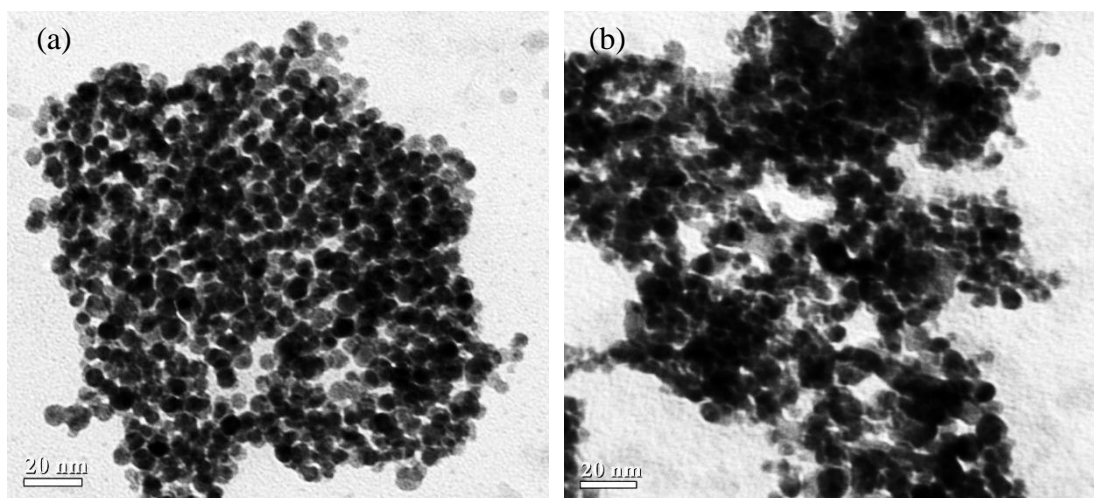


**Figure 4.20** TEM images (450,000 x magnification) of the 3-AEPE-stabilized gold nanoparticle solution in the (a) absence and (b) presence of 5  $\mu\text{M}$  mercury(II) ion.

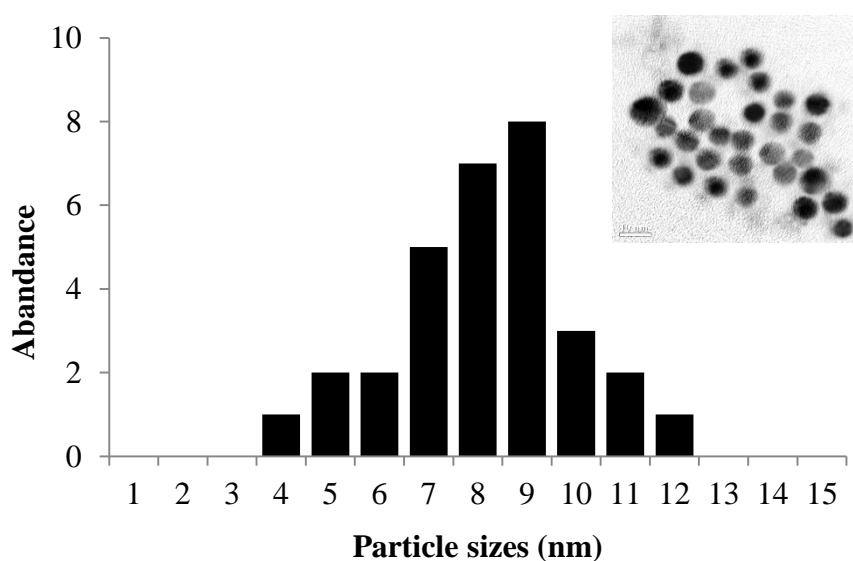
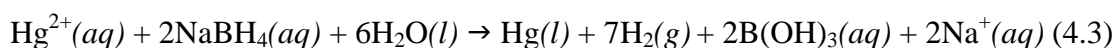
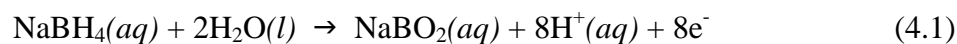


**Figure 4.21** Size distributions and (*insert*) typical TEM image of 3-AEPE-stabilized gold nanoparticle with average diameter of  $9 \pm 2$  nm.

The mechanism of 3-AEPE-stabilized gold nanoparticle was described for both in the absence (blank) and presence of mercury(II) ion. It was reasoned that 3-AEPE molecules display the indispensable role of stabilization and preventing the aggregation of gold nanoparticles in the absence of mercury(II) ions. It was confirmed that 3-AEPE molecules could greatly stabilize gold nanoparticles from aggregation as

evidenced by the SPR band at 517 nm and the rose-red appearance of the solution (Figure 4.19 (a)). The possible mechanism explaining such behavior is that 3-AEPE molecules only shield around gold nanoparticles by electrostatic repulsion between protonated ammonium and positively charged hydrogen ions ( $H^+$ ) in acidic aqueous solution; meanwhile, coordination could form through gold-sulfur (Au-S) bonds. 3-AEPE-stabilized gold nanoparticle formation is depicted in Figure 4.22. As previously demonstrated by Liu *et al.* [93], terminated quaternary ammonium displays a stabilizing role in acidic solutions and terminated thiol group was also capped onto the surface of the gold nanoparticles.

The reduction of gold(III) ions to gold(0) and mercury(II) ions to liquid mercury by  $NaBH_4$  is detailed in Eq. 4.1 - 4.3. It is apparent from equation (4.1) and (4.2) that 2.82 moles of trivalent gold can be reduced to metallic gold nanoparticles with one mole of  $NaBH_4$ .



Conversely, in the presence of mercury(II) ions, the solution turned blue rapidly after addition of  $NaBH_4$  due to the reduced liquid mercury likely to be directly combined onto the surface of gold nanoparticles through the formation of solid amalgam (Au-Hg alloys). The reaction of gold-mercury alloy is described in Eq. 4.4 and 4.5 [133, 147, 158].



This phenomenon was confirmed by analysis of the 3-AEPE-stabilized gold nanoparticles containing mercury (Au-Hg alloys) particles collected on a membrane using a laser ablation inductively coupled plasma mass spectrometer (LA-ICP-MS), which revealed that gold (197 amu Au) and mercury (202 amu Hg) were found on the membrane, and that the higher the mercury(II) concentration in the solution, the greater the mercury content found in the 3-AEPE-stabilized gold nanoparticles on the

membrane (see in Figure A.4). From this, the mechanism of 3-AEPE-stabilized gold nanoparticles for the detection of mercury(II) ions can be depicted in Figure 4.23.

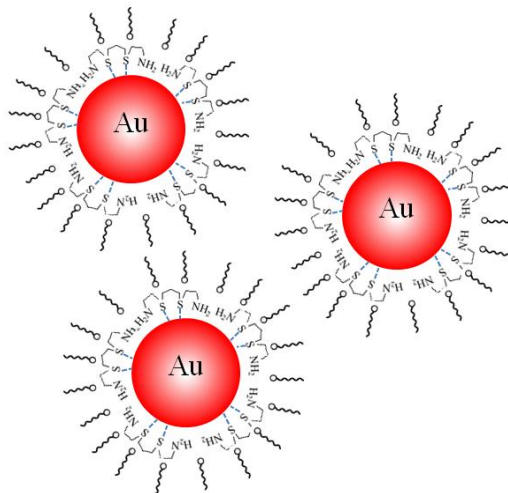


**Figure 4.22** The possibility of forming of 3-AEPE-stabilized gold nanoparticles under conditions of 125  $\mu\text{M}$  gold(III), 0.3 mM 3-AEPE, 0.1% (v/v) Triton X-100 and 0.6 mM  $\text{NaBH}_4$ .

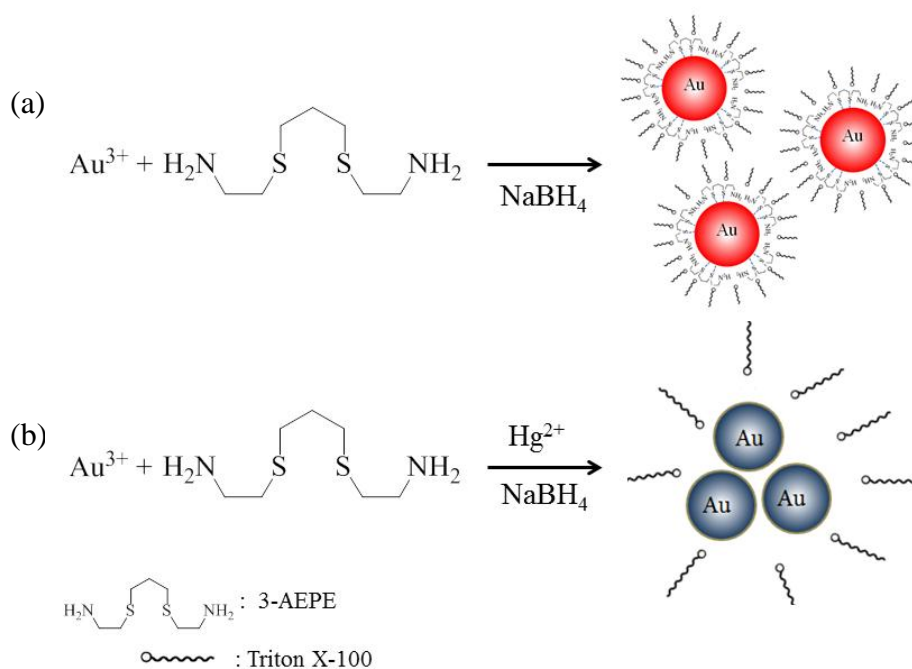


**Figure 4.23** The proposed mechanism of 3-AEPE-stabilized gold nanoparticle formation in the (a) absence and (b) presence of mercury(II) ions, under conditions of 125  $\mu\text{M}$  gold(III), 0.3 mM 3-AEPE, 0.1% (v/v) Triton X-100 and 0.6 mM  $\text{NaBH}_4$ .

#### 4.2.1.8 Selectivity and sensitivity

After obtaining optimum conditions, the selectivity of 3-AEPE-stabilized gold nanoparticles toward mercury(II) ions over other metal ions was evaluated. Selectivity for the target analyte is an extremely important aspect for a colorimetric sensor, especially in heavy metal analysis. The colorimetric response of the 3-AEPE stabilized-gold nanoparticles in the presence of various environmentally relevant and potentially competing ions, such as lead(II), cadmium(II), copper(II), cobalt(II), zinc(II), manganese(II), nickel(II), chromium(III), iron(III), aluminium(III), magnesium(II), calcium(II), potassium(I) and sodium(I), each at a concentration of 250  $\mu\text{M}$ , 100 times greater than that of the mercury(II) ions, was individually evaluated under identical conditions.

The absorption spectra of 3-AEPE-stabilized gold nanoparticles with all competing cations did not show any significant shift to a longer wavelength as shown in Figure 4.24 and their solutions did not exhibit any detectable colorimetric response upon the addition of the other tested cation salts on their own, except for a weakly positive response by cadmium(II) ion as depicted in Figure 4.24 (*inset*). This implied that only mercury(II) ions caused the aggregation of 3-AEPE stabilized-gold nanoparticles, resulting in a color change to blue within a few seconds, although cadmium(II) and copper(II) ions showed a pale-purple in color indicating a very slight interfering effect. However, it remained easy to distinguish mercury(II) ions from other metal ions by naked-eye observation. Figure 4.25 shows the absorbance at 680 nm of 3-AEPE-stabilized gold nanoparticles in the absence (blank) and presence of all competing metal ions at concentrations higher than mercury(II) ion by about 100 times. Selectivity can be described in two possible aspects;

(i) According to the hard and soft acids and bases (HSAB) theory [107], 3-AEPE has two sulfur atoms (dithia) and two  $-\text{NH}_2$  groups (diaza) that can provide a hydrophilic interface and display great binding affinities toward mercury(II) ions which are soft acid metal ions.

(ii) According to the formation of gold-mercury alloys, only reduced mercury could combine; meanwhile, other metallic ions did not interact on the surface of gold nanoparticles unlike reduced liquid mercury [97, 133].

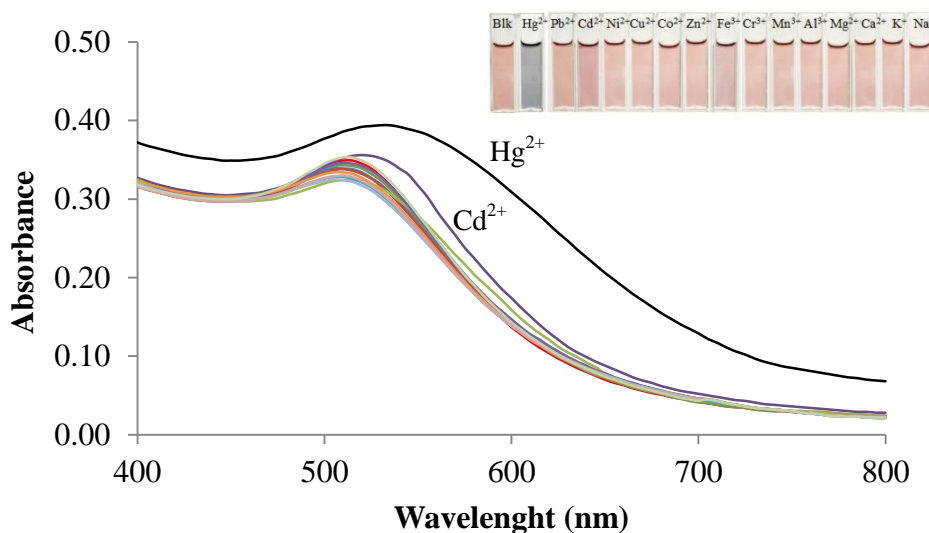


**Figure 4.24** Absorption spectra of 3-AEPE-stabilized gold nanoparticles in the presence of various metal ions (250  $\mu\text{M}$ ) or 2.5  $\mu\text{M}$  mercury(II) and (*inset*) the corresponding photo images, under conditions of 125  $\mu\text{M}$  gold(III), 0.3 mM 3-AEPE, 0.1% (v/v) Triton X-100 and 0.6 mM  $\text{NaBH}_4$ .

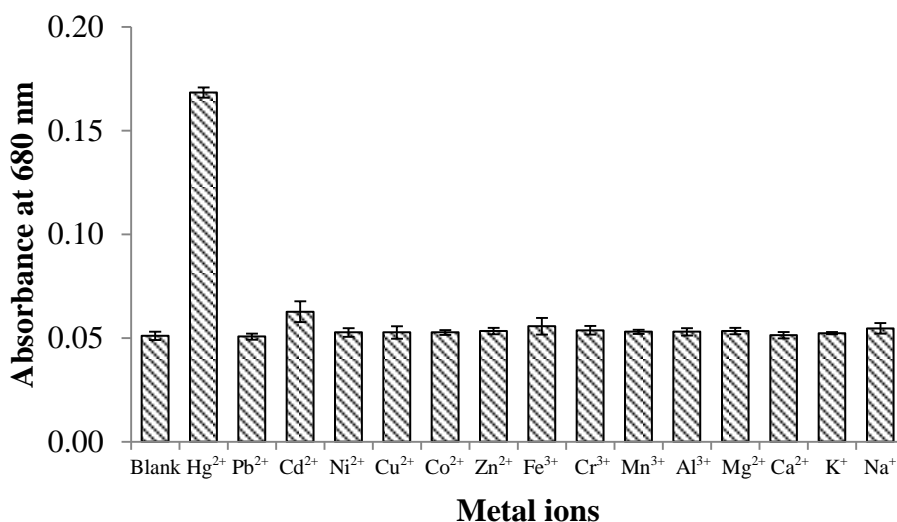


**Figure 4.25** Absorbance at 680 nm of 3-AEPE-stabilized gold nanoparticles in the presence of various metal ions (250  $\mu\text{M}$ ) or 2.5  $\mu\text{M}$  mercury(II) ( $n=3$ ), under conditions of 125  $\mu\text{M}$  gold(III), 0.3 mM 3-AEPE, 0.1% (v/v) Triton X-100 and 0.6 mM  $\text{NaBH}_4$ .

#### 4.2.1.9 Calibration curve for mercury(II) ions

According to above-mentioned procedures, the colorimetric response of 3-AEPE-stabilized gold nanoparticles in the absence of mercury(II) ions was to appear rose-red in color immediately. The calibration curve was done using different concentrations of mercury(II) ions in the range of 0 - 10.0  $\mu\text{M}$ . As shown in Figure 4.26, colorimetric responses became to be purple and blue with increase concentrations of mercury(II) ions. It was implied that the color of solution revealed from the aggregation of 3-AEPE-stabilized gold nanoparticles is proportionally related to concentrations of mercury(II) ions. Above 1.25  $\mu\text{M}$  mercury(II), the color of 3-AEPE-stabilized gold nanoparticle solution were immediately observed by naked eye to change to blue in coloration within a few seconds, while the faint-purple color of solution slowly appeared for concentrations of mercury(II) ions lower than 1.25  $\mu\text{M}$ . On the other hand, at higher concentrations of mercury(II) ( $>10 \mu\text{M}$ ), the solution became almost transparent rapidly due to the precipitation of the aggregated gold nanoparticles, in agreement with a previous report [92]. The absorption spectra of 3-AEPE-stabilized gold nanoparticles with different mercury(II) ions are depicted in Figure 4.27.

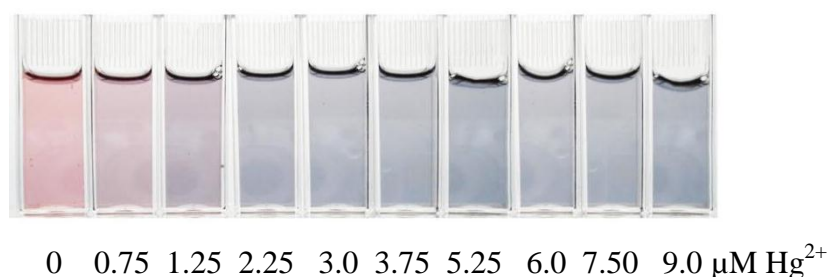


**Figure 4.26** Colorimetric responses of 3-AEPE-stabilized gold nanoparticle solution upon the addition of various concentration of mercury(II) ion.

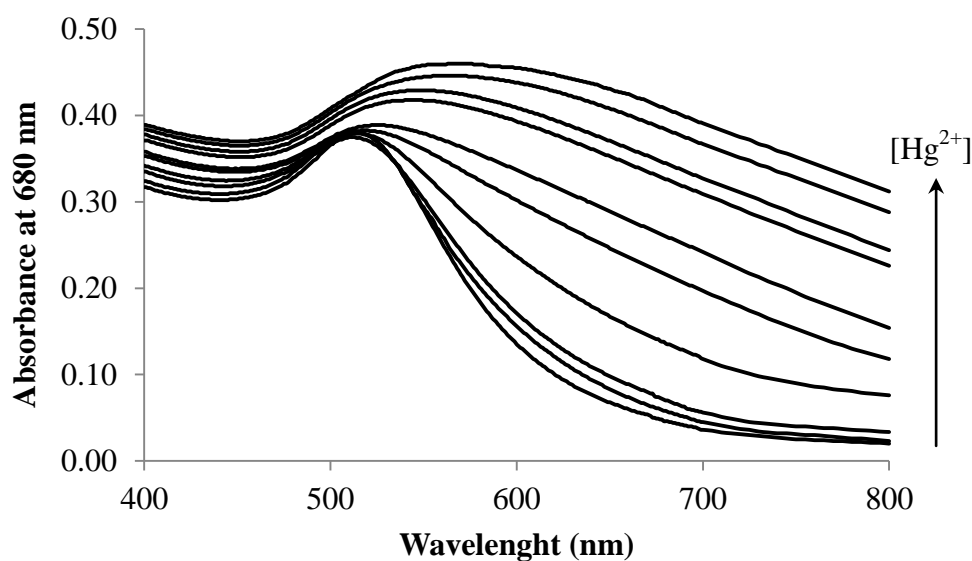


**Figure 4.27** Absorption spectra of 3-AEPE-stabilized gold nanoparticle solution upon the addition of various concentrations of mercury(II) ions.

The calibration curves of 3-AEPE-stabilized gold nanoparticles with different concentrations of mercury(II) ions (0 - 10.0  $\mu\text{M}$ ) were also plotted using the relationship between mercury(II) concentrations and their absorbance at wavelengths of 650, 660, 670, 680, 690 and 700 nm, as shown in Figure 4.27. This indicated that their curves obtained from each wavelength were similar. The absorption of 3-AEPE-stabilized gold nanoparticles with concentrations of mercury(II) ions of 0 - 1.25  $\mu\text{M}$  and 5.25 - 10.0  $\mu\text{M}$  showed a little proportionally increased, while its absorbance at 1.25 - 5.25  $\mu\text{M}$  mercury(II) ions showed linearity with better slope values as shown in Table 4.5. Therefore, calibration curve of 3-AEPE-stabilized gold nanoparticles can be divided into three levels of mercury(II) concentrations, including low (0 - 1.25  $\mu\text{M}$ ), medium (1.25 - 5.25  $\mu\text{M}$ ) and high (5.25 - 10.0  $\mu\text{M}$ ). Due to the aggregation of 3-AEPE-stabilized gold nanoparticles depending on the concentrations of mercury(II) ions, at low concentrations ( $< 1.25 \mu\text{M}$ ) could slow induce gold nanoparticle aggregation in agreement with previous report [133]. By comparing any wavelength, a wavelength at 680 nm provided the acceptable linearity, especially medium and high levels providing both better sensitivity and linearity. Thus, calibration curve of this protocol was also constructed at a wavelength of 680 nm as shown in Figure 4.29

and linearity curve of different mercury(II) concentration levels is depicted in Figure 4.30.

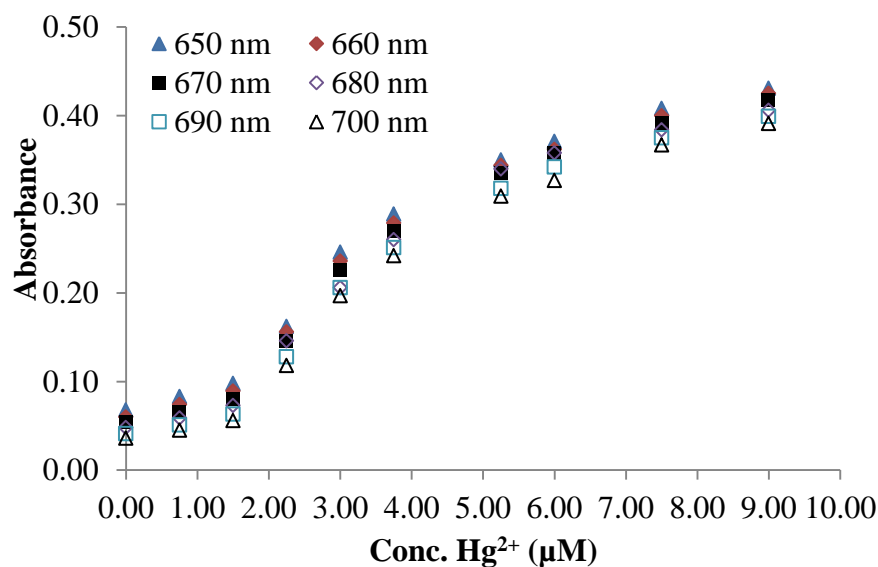


**Figure 4.28** The relationship between the concentrations of mercury(II) ions and their absorptions of 3-AEPE-stabilized gold nanoparticles at different wavelengths.

**Table 4.5** Linearity ranges of different mercury(II) concentration levels at different measuring wavelengths

$\lambda$ (nm)	0 - 1.25 $\mu\text{M Hg}^{2+}$		1.25 - 5.25 $\mu\text{M Hg}^{2+}$		5.25 - 10.0 $\mu\text{M Hg}^{2+}$	
	Linear Eq.	$R^2$	Linear Eq.	$R^2$	Linear Eq.	$R^2$
650	$0.02x + 0.068$	0.999	$0.0841x + 0.103$	0.991	$0.0328x + 0.351$	0.974
660	$0.0193x + 0.059$	0.999	$0.0844x + 0.094$	0.993	$0.0337x + 0.343$	0.978
670	$0.0173x + 0.053$	0.992	$0.0845x + 0.084$	0.993	$0.0335x + 0.336$	0.984
680	$0.0167x + 0.0475$	0.995	$0.0864x + 0.075$	0.996	$0.032x + 0.339$	0.99
690	$0.0147x + 0.041$	0.997	$0.0844x + 0.067$	0.995	$0.0316x + 0.321$	0.971
700	$0.0133x + 0.336$	0.997	$0.084x + 0.058$	0.995	$0.0372x + 0.332$	0.975

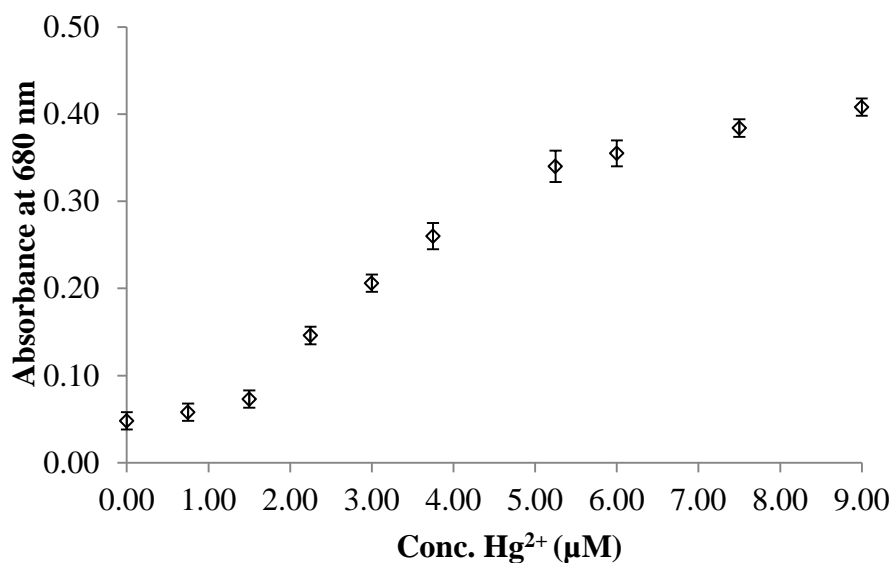


**Figure 4.29** Absorption values of 3-AEPE-stabilized gold nanoparticles at a wavelength of 680 nm versus mercury(II) concentrations.

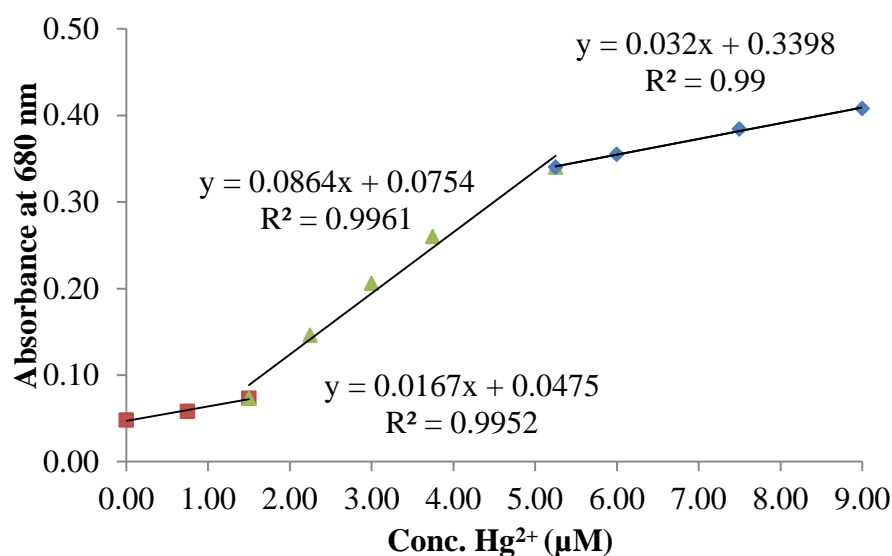


**Figure 4.30** Three levels of calibration curves of 3-AEPE-stabilized gold nanoparticles.

#### 4.2.2 Gold nanoparticles stabilized by 4-AEBE

In order to consider the efficiency of other dithia-diaza ligands for stabilizing gold nanoparticles, 4-AEBE was used instead of 3-AEPE. The effect of gold(III) ions, 4-AEBE and NaBH<sub>4</sub> were investigated by varying their concentrations. While, the

concentration of Triton X-100 was fixed at 0.1 % (v/v). Other experimental conditions, such as pH, mixing time and rate, measurement time and pattern of the addition of the reducing agent were done with the same procedure as gold nanoparticles stabilized by 3-AEPE (Section 4.2.1).

#### 4.2.2.1 Effect of gold(III) concentration

The investigation of concentrations of gold(III) ion solution affecting the formation of gold nanoparticles was done by the same procedure as 3-AEPE, but 3-AEPE was replaced with a constant 0.3 mM 4-AEBE. The concentrations of  $\text{NaBH}_4$  and Triton X-100 were 0.6 mM and 0.1% (v/v), respectively. It was found that concentration of gold(III) ions at 125  $\mu\text{M}$  (mole ratio of gold(III) ions :  $\text{NaBH}_4$  equal to 0.2) displayed characteristic SPR band greatly and its coloration became rose-red immediately as shown in Figure 4.31. This result was the same as 3-AEPE-stabilized gold nanoparticles. Thus, concentration of gold(III) ions of 125  $\mu\text{M}$  was great optimum condition.

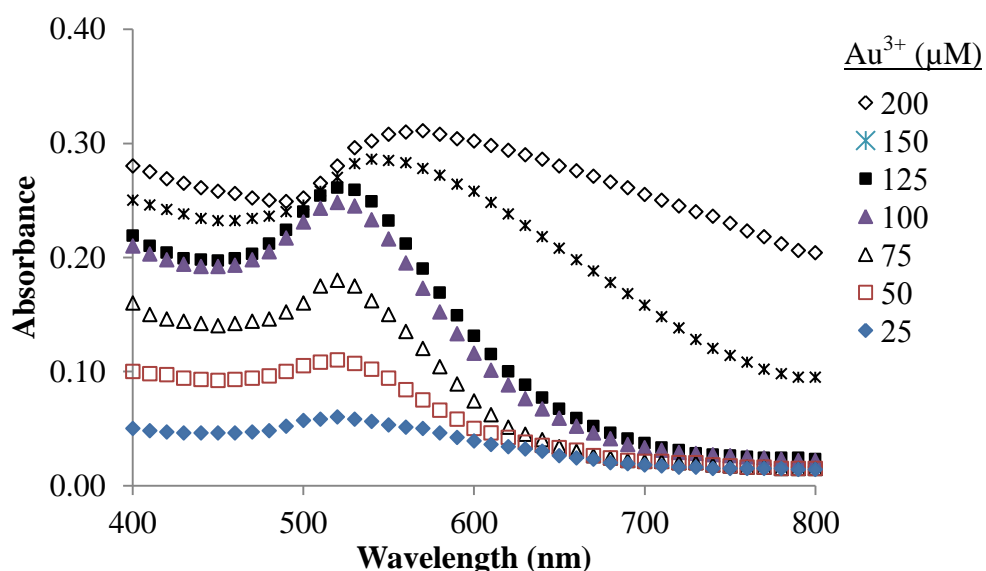


**Figure 4.31** Effect of the concentration of gold(III) solution on the formation of gold nanoparticle stabilized by 4-AEBE.

#### 4.2.2.2 Effects of 4-AEBE concentration

The mole ratio of gold(III) ions and 4-AEBE (range of 0.1 - 1.0 mM) is shown in Table 4.6, while the concentrations of 125  $\mu\text{M}$  gold(III), 0.1% (v/v) Triton X-100 and 0.6 mM  $\text{NaBH}_4$  were constant. The absorption spectra of 4-AEBE-stabilized gold nanoparticle solution achieved using various concentrations of 4-AEBE are showed in Figure 4.32. Although, the absorbance at a wavelength of 517 nm increased when increasing 4-AEBE concentrations, their solution color changed from rose-red to purple, except at 0.4 mM. The coloration of its solution could be obviously observed comparing to other concentrations. Thus, 0.4 mM 4-AEBE was selected for further studies, which with 125  $\mu\text{M}$  gold(III) yields a 0.78 : 1 mole ratio of gold(III) : 4-AEBE.

**Table 4.6** Mole ratio of gold(III) ion and 4-AEBE

$\text{Au}^{3+}$ ( $\mu\text{M}$ )	$\text{Au}^{3+}$ ( $\mu\text{mol}$ )	4-AEBE (mM)	4-AEBE ( $\mu\text{mol}$ )	Mole ratio $\text{Au}^{3+}$ :4-AEBE
125	0.5	0.1	0.04	12.5
125	0.5	0.2	0.16	3.13
125	0.5	0.3	0.36	1.39
125	0.5	0.4	0.64	0.78
125	0.5	0.6	1.44	0.35
125	0.5	0.8	2.56	0.20
125	0.5	1.0	4.00	0.13

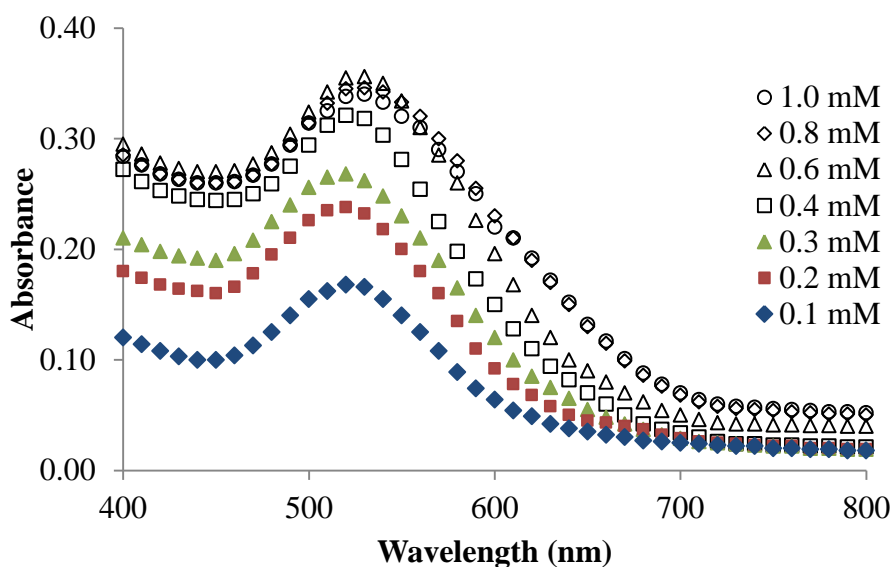


**Figure 4.32** Effect of the concentration of 4-AEBE ligand on the formation of gold nanoparticle stabilized by 4-AEBE.

#### 4.2.2.3 Effect of $\text{NaBH}_4$ concentration

The influence of  $\text{NaBH}_4$  concentration was performed by the same procedure as 3-AEPE, as mentioned in Table 4.3 as described in Section 4.2.1.4. Figure 4.33 shows the absorbance of 4-AEBE-stabilized gold nanoparticles at a wavelength of 517 nm with various the concentrations of  $\text{NaBH}_4$ . It was found that the results of this experiment were similar to the one of 3-AEPE. Thus, the concentration of  $\text{NaBH}_4$  on the formation of 4-AEBE-stabilized gold nanoparticles was 0.6 mM (mole ratio of  $\text{NaBH}_4$  : gold(III) of 4.8). The concentration of  $\text{NaBH}_4$  was similar to 3-AEPE-stabilized gold nanoparticles.

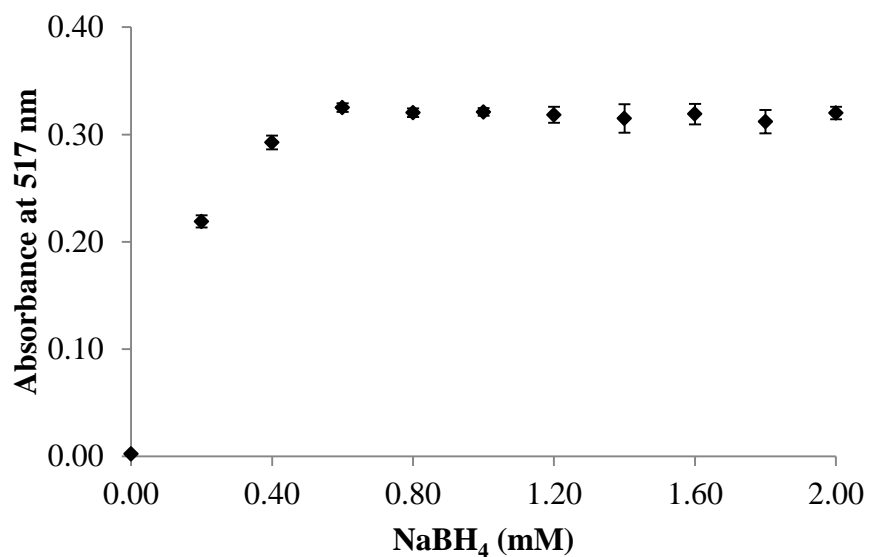


**Figure 4.33** Effect of the concentration of NaBH<sub>4</sub> on the formation of gold nanoparticle stabilized by 4-AEBE.

After optimization of 4-AEBE-stabilized gold nanoparticles, we obtained the suitable concentrations of gold(III) ions, 4-AEBE and NaBH<sub>4</sub>. The optimum condition of 4-AEBE-stabilized gold nanoparticles is summarized in Table 4.7.

**Table 4.7** Optimum conditions of 4-AEBE-stabilized gold nanoparticles

Parameters	Conditions
Gold(III) ion	125 $\mu$ M
4-AEBE	0.4 mM
NaBH <sub>4</sub>	0.6 mM
Triton X-100	0.1% (v/v)
pH	1.2 - 2.0
Detection time	1 minute

#### 4.2.2.4 Characterization of 4-AEBE-stabilized gold nanoparticles

After obtained optimum conditions as shown in Table 4.7, 125  $\mu\text{M}$  gold(III) ions, 0.4 mM 4-AEBE, 0.6 mM  $\text{NaBH}_4$  and 0.1%(v/v) Triton X-100, 4-AEBE-stabilized gold nanoparticle was characterized using UV-vis and TEM techniques with the absence and presence of mercury(II) ions. This result showed that 4-AEBE-stabilized gold nanoparticle solution in the absence of mercury(II) ions (blank) appeared rose-red in coloration obviously, while its coloration became deep-blue rapidly with the presence of mercury(II) ions. This implied that 4-AEBE can be a stabilizer to prevent the aggregation of gold nanoparticles, similar to 3-AEPE. TEM images of 4-AEBE-stabilized gold nanoparticles in the absence and presence of mercury(II) ion are shown in Figure 4.34. This result showed that 4-AEBE-stabilized gold nanoparticles without mercury(II) ions displayed typical shapes of regular and almost individual spherical particles with mean dispersed particle sizes of  $\sim 9$  nm in diameter, which is consistent with the SPR maximum band of 517 nm, similar to 3-AEPE-stabilized gold nanoparticles, but interparticular distances could be observed, while the distanced observed from the 3-AEPE system were closer apparently.

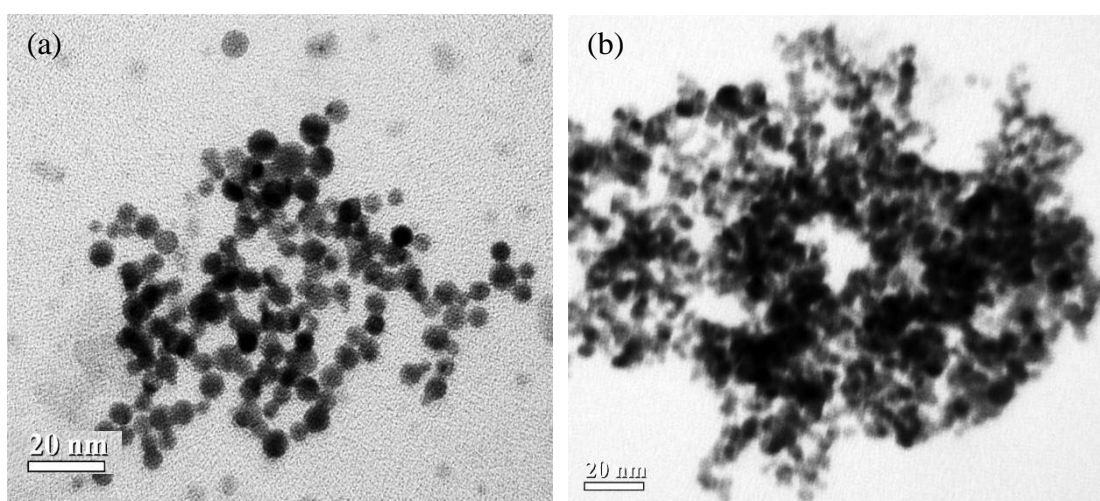


**Figure 4.34** TEM images (450,000x magnification) of 4-AEBE-stabilized gold nanoparticle solution in the (a) absence and (b) presence of 5  $\mu\text{M}$  mercury(II) ion.

#### 4.2.2.5 Calibration of 4-AEBE-stabilized gold nanoparticles

The calibration curve of 4-AEBE-stabilized gold nanoparticles was done using different concentrations of mercury(II) ions in the range of 0 - 10.0  $\mu\text{M}$ . The coloration became purple and deep-blue when the concentrations of mercury(II) ions increased, similar to 3-AEPE-stabilized gold nanoparticles as described in Section 4.2.1.9. Similarly, Figure 4.35 shows the linearity of 4-AEBE-stabilized gold nanoparticles with three levels of mercury(II) concentrations, including low (0 - 2.5  $\mu\text{M}$ ), medium (2.5 - 6.0  $\mu\text{M}$ ) and high (6.0 - 10.0  $\mu\text{M}$ ) levels. The calibration curves of gold nanoparticles stabilized by 3-AEPE and 4-AEBE were constructed to compare with intra-day. These results showed that 3-AEPE-stabilized gold nanoparticles revealed much more sensitive than 4-AEBE-stabilized gold nanoparticles, by considering from their slopes of each mercury(II) concentration levels, as shown in Table 4.8. Sensitivities of three concentration levels of mercury(II) ions between 3-AEPE-stabilized gold nanoparticle and 4-AEBE-stabilized gold nanoparticle were compared by their slopes. It was found that the slope of 3-AEPE was higher than 4-AEBE by about 6, 7.5 and 8 orders for low, medium and high concentration levels.

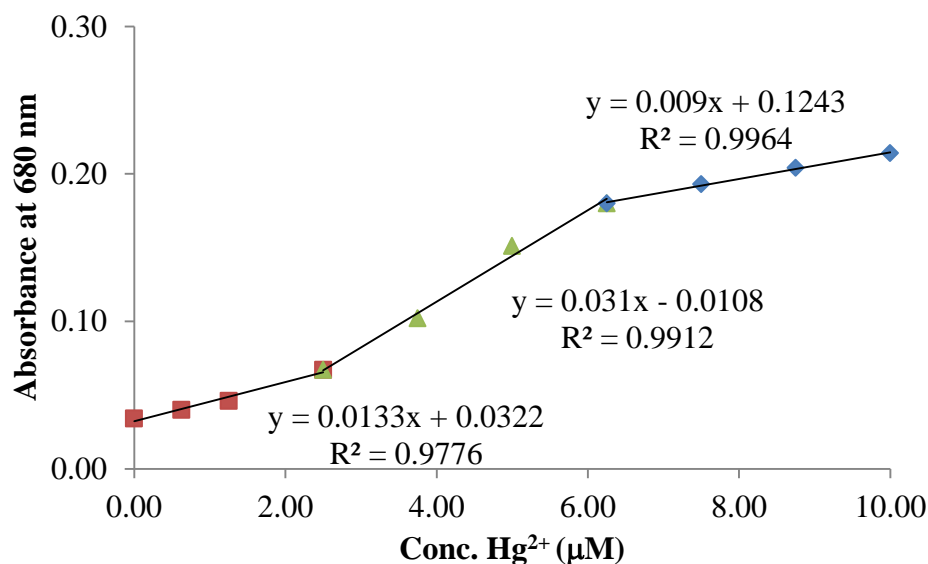


**Figure 4.35** The calibration curve of 4-AEBE-stabilized gold nanoparticles.

**Table 4.8** Linearity ranges of different mercury concentration levels of gold nanoparticles stabilized by 3-AEPE and 4-AEBE

Ligands	0 - 1.25 $\mu\text{M}$ $\text{Hg}^{2+}$		1.25 - 5.25 $\mu\text{M}$ $\text{Hg}^{2+}$		5.25 - 12.0 $\mu\text{M}$ $\text{Hg}^{2+}$	
	Linear Eq.	$R^2$	Linear Eq.	$R^2$	Linear Eq.	$R^2$
3-AEPE	$0.0905x + 0.050$	0.996	$0.3432x + 0.007$	0.994	$0.1028x + 0.227$	0.997
4-AEBE	$0.0149x + 0.043$	0.990	$0.046x + 0.008$	0.993	$0.0129x + 0.168$	0.994

### 4.2.3 Gold nanoparticles stabilized by 5-AEPE

Apart from 4-AEBE ligand, 5-AEPE was used instead of 3-AEPE in order to be a stabilizer for gold nanoparticles. Only the effects of concentrations of gold(III) ions, 5-AEPE and  $\text{NaBH}_4$  were investigated by varying their concentrations. Meanwhile, the concentration of Triton X-100 was maintained at 0.1 % (v/v). Other experimental conditions, such as pH, mixing time and rate, measurement time and the pattern of the addition of the reducing agent were done using the same procedure as 3-AEPE-stabilized gold nanoparticles as described in Section 4.2.1.

#### 4.2.3.1 Effect of gold(III) concentration

The effect of the concentration of gold(III) ion solution was done by the same procedure as 3-AEPE, but 3-AEPE was replaced with 5-AEPE. The concentration of gold(III) ion solution was investigated with a constant concentration of 0.6 mM 5-AEPE, 0.8 mM  $\text{NaBH}_4$  and 0.1% (v/v) Triton X-100. As shown in Figure 4.36, the concentration of gold(III) ions at 125  $\mu\text{M}$  (mole ratio of gold(III) ions :  $\text{NaBH}_4$  was 0.15) displayed the characteristic of SPR band greatly and its coloration became rose-red immediately, exhibiting the same result as 3-AEPE-stabilized gold nanoparticles.

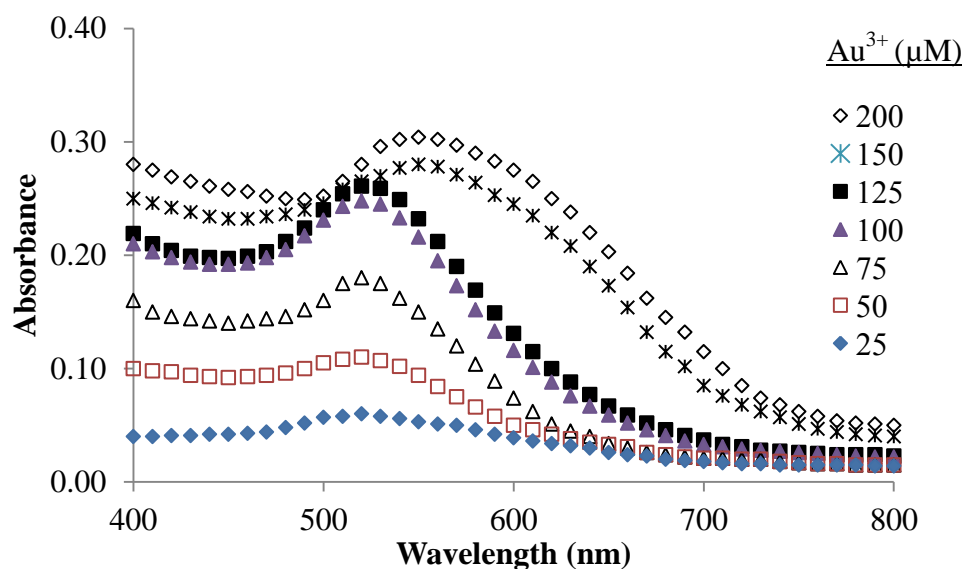


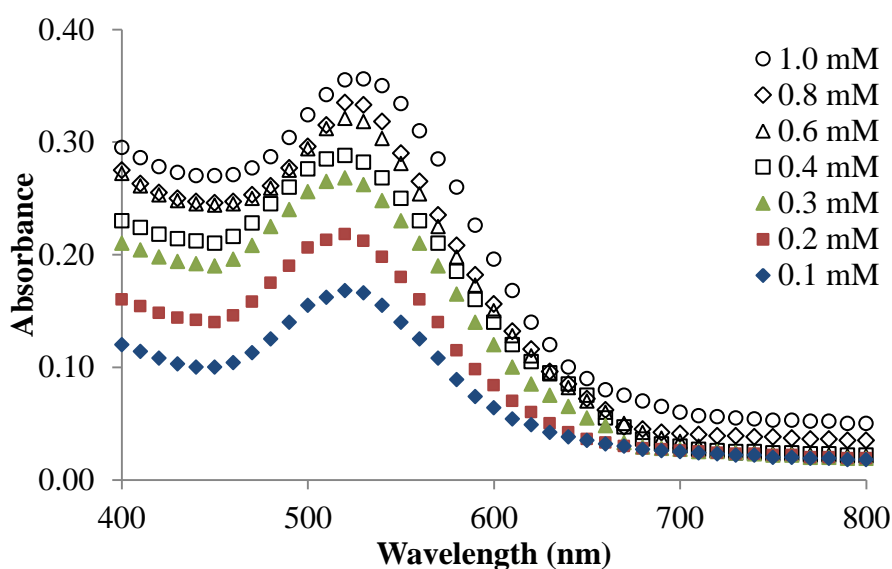
**Figure 4.36** Effect of the concentration of gold(III) solution on the formation of gold nanoparticle stabilized by 5-AEPE.

#### 4.2.3.2 Effects of 5-AEPE concentration

The mole ratio of gold(III) ions and 5-AEPE (ranging from 0.1 to 1.0 mM) is shown in Table 4.9, while the concentrations of 125  $\mu\text{M}$  gold(III), 0.1% (v/v) Triton X-100 and 0.6 mM  $\text{NaBH}_4$  were constant. The absorption spectra of 5-AEPE-stabilized gold nanoparticle solution achieved from 0.6 mM 5-AEPE concentrations showed the highest absorbance at a wavelength of 517 nm (Figure 4.37) and the solution showed rose-red color. The coloration of its solution could be obviously observed comparing to other concentrations. Thus, 0.6 mM 5-AEPE was selected for further studies, which with 125  $\mu\text{M}$  gold(III) yields a 0.35 : 1 mole ratio of gold(III) : 5-AEPE.

**Table 4.9** Mole ratio of gold(III) ion and 5-AEPE

Au <sup>3+</sup> ( $\mu$ M)	Au <sup>3+</sup> ( $\mu$ mol)	5-AEPE (mM)	5-AEPE ( $\mu$ mol)	Mole ratio Au <sup>3+</sup> :5-AEPE
125	0.5	0.1	0.04	12.5
125	0.5	0.2	0.16	3.13
125	0.5	0.3	0.36	1.39
125	0.5	0.4	0.64	0.78
125	0.5	0.6	1.44	0.35
125	0.5	0.8	2.56	0.20
125	0.5	1.0	4.00	0.13

**Figure 4.37** Effect of the concentration of 5-AEPE ligand on the formation of gold nanoparticle stabilized by 5-AEPE.

#### 4.2.3.3 Effect of NaBH<sub>4</sub> concentration

The influence of NaBH<sub>4</sub> concentration was studied by the same procedure as that of 3-AEPE, as mentioned in Table 4.3 (Section 4.2.1.4). It was found that the results of this experiment are shown in Figure 4.38. Thus, the concentration of NaBH<sub>4</sub> on the formation of 5-AEPE-stabilized gold nanoparticles was 0.8 mM (mole ratio of NaBH<sub>4</sub> : gold(III) of 6.4).

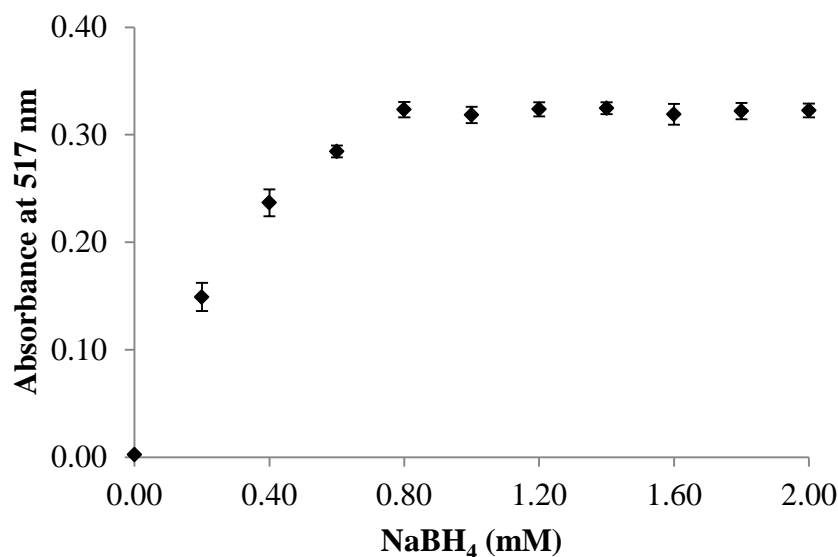


**Figure 4.38** Effect of the concentration of NaBH<sub>4</sub> on the formation of gold nanoparticle stabilized by 5-AEPE.

After optimization of 5-AEPE-stabilized gold nanoparticles, we obtained the suitable concentrations of gold(III) ions, 5-AEPE and NaBH<sub>4</sub>. The optimum condition of 4-AEPE-stabilized gold nanoparticles is summarized in Table 4.10.

**Table 4.10** Optimum conditions of 5-AEPE-stabilized gold nanoparticles

Parameters	Conditions
Gold(III) ion	125 $\mu$ M
5-AEPE	0.6 mM
NaBH <sub>4</sub>	0.8 mM
Triton X-100	0.1%(v/v)
pH	1.2-2.0
Detection time	1 minute

#### 4.2.3.4 Characterization of 5-AEPE-stabilized gold nanoparticles

Similar to 3-AEPE and 4-AEPE, 5-AEPE-stabilized gold nanoparticles were characterized using UV-vis and TEM techniques with the absence and presence of

mercury(II) ions. This result showed that 5-AEPE-stabilized gold nanoparticle solution in the absence of mercury(II) ions (blank) appeared rose-red in coloration, while its coloration became deep-blue rapidly with the presence of mercury(II) ions. This implied that 5-AEPE could be a good stabilizer to prevent the aggregation of gold nanoparticles, similar to 3-AEPE and 4-AEBE ligands. TEM images of 5-AEPE-stabilized gold nanoparticles in the absence and presence of mercury(II) ion are shown in Figure 4.39, showing typical shapes of regular and almost individual spherical particles, in case of without mercury(II) ion (Figure 4.39 (a)). This result is consistent with those 3-AEPE and 4-AEBE. On the other hand, the aggregated gold nanoparticles was obviously observed with the presence of 5  $\mu\text{M}$  mercury(II) ions.

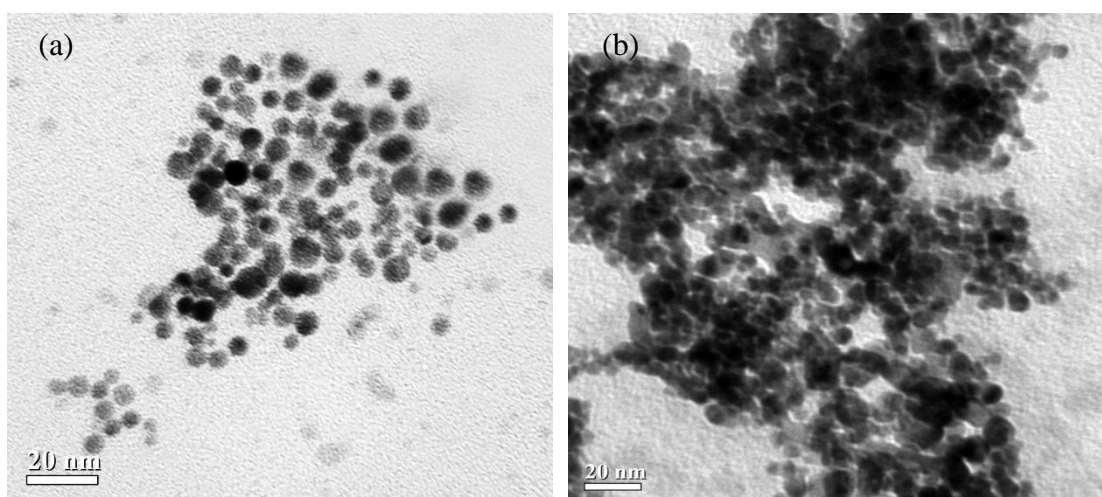


**Figure 4.39** TEM images (450,000x magnification) of the 5-AEPE-stabilized gold nanoparticle solution in the (a) absence and (b) presence of 5  $\mu\text{M}$  mercury(II) ion.

#### 4.2.3.5 Calibration of 5-AEPE-stabilized gold nanoparticle

The calibration curve of 5-AEPE-stabilized gold nanoparticles was done using different concentrations of mercury(II) ions in the range of 0 - 15.0  $\mu\text{M}$ . The coloration became purple and deep-blue with increasing the concentrations of mercury(II) ions, similar to 3-AEPE-stabilized gold nanoparticles as described in Section 4.2.1.9. Similarly, Figure 4.40 shows the linearity of 5-AEPE-stabilized gold nanoparticles with two levels of mercury(II) concentrations with low (0 - 2.5  $\mu\text{M}$ ) and high levels (2.5 - 15.0  $\mu\text{M}$ ). Although, each level of 5-AEPE-stabilized gold

nanoparticles showed low sensitivity, their levels give wider linear dynamic ranges (LDR) comparing linearity of 3-AEPE-stabilized gold nanoparticles and 4-AEBE-stabilized gold nanoparticles. This result indicated that 5-AEPE ligand was able to stabilize gold nanoparticles superior to 3-AEPE and 4-AEBE ligands. It was implied that the length of dithia-diaza ligand chain affected the stabilization of gold nanoparticles. The longer ligand chain, the more effective stabilization ability toward gold nanoparticles.

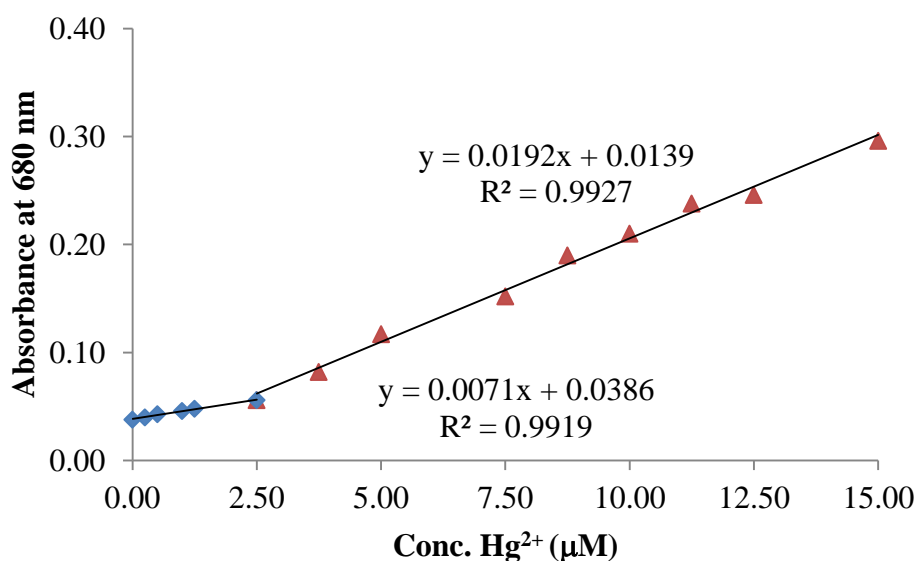


**Figure 4.40** The calibration curve of 5-AEPE-stabilized gold nanoparticles.

#### 4.2.4 Gold nanoparticles stabilized by cysteamine hydrochloride

Apart from three dithia-diaza ligands (3-AEPE, 4-AEBE and 5-AEPE), cysteamine hydrochloride was studied for stabilizing gold nanoparticles. Liu *et al.* [100] used a cysteamine hydrochloride as a precursor reagent to prepare a thymine acetamidoethanethiol ligand. The terminated thiol group of ligand was functionalized on the surface of gold nanoparticles.

The concentration of gold(III) ion solution, NaBH<sub>4</sub> and Triton X-100 was fixed at 125 μM (1000 μL of 0.5 mM), 0.6 mM (300 μL of 4 mM) and 0.1%(v/v), respectively. The concentration of cysteamine hydrochloride was varied in the range of 0.125 - 1.25 mM. (100 μL - 1000 μL of 5.0 mM). It was found that the coloration of all solutions turned blue rapidly after the addition of reducing agent. This implied

that cysteamine hydrochloride could not stabilize gold nanoparticles, unlike three dithia-diaza ligands.

### 4.3 Method validation

After obtaining optimum conditions for this proposed method, the method was validated by establishing the performance characteristics related to the accuracy and precision, which was reported in term of percentage of recovery and percentage of relative standard deviation (%RSD), respectively. The lowest detectable concentration was represented in term of the limit of detection (LOD). Among three dithia-diaza ligands, 3-AEPE was used to validate analytical method because 3-AEPE-stabilized gold nanoparticles provided the highest sensitivity.

#### *Limit of detection*

Under optimum conditions, the limit of detection was estimated using three times of the standard deviation ( $3\sigma$ ) of blank (3-AEPE-stabilized gold nanoparticles in the absence of mercury(II) ions). It was found that the lowest detectable concentration of mercury(II) ion is as low as 35 nM ( $7 \mu\text{g L}^{-1}$ ), whilst the limit of detection with naked eye method under observation within a minute is 1.25  $\mu\text{M}$  ( $250 \mu\text{g L}^{-1}$ ). With the naked eye assay, when the concentration of mercury(II) ions is lower than 1.25  $\mu\text{M}$ , no apparent color changes occurred during the reaction time of 1 - 10 minutes. However, when the reaction proceeded over 10 minutes, the solution color could be observed a significant difference in coloration between 3-AEPE-stabilized gold nanoparticle solution in the presence of 0.5  $\mu\text{M}$  ( $100 \mu\text{g L}^{-1}$ ) mercury(II) ion and blank solution. Thus, the lowest detectable concentration of mercury(II) was suggested at 0.5  $\mu\text{M}$  by naked eye detection.

#### *Reproducibility*

3-AEPE-stabilized gold nanoparticle solution in the presence of mercury(II) ion of 2.5  $\mu\text{M}$  ( $0.5 \text{ mg L}^{-1}$ ) was done repeatedly with the same condition. It was found that although the coloration of each experiment appeared no significant difference

using naked eye observation, but their absorption spectra obtained from UV-vis showed the significant difference. We also discovered that the factors that lead to effect on absorption spectrum were the addition rate of the reducing agent, mixing time and measurement time. First, three patterns of the addition of the reducing agent were investigated among from rapid or sudden, normal (drop-by-drop) and slow dropping. We found that the sudden adding pattern led to deep-blue color in solution. On the other hand, both later patterns caused purple in color, but the color of 3-AEPE-stabilized gold nanoparticle solution using drop-by-drop could easily be observe and also provided higher absorption values. Thus, the drop-by-drop pattern of addition of reducing agent was done for all experiments in this work.

Second, the degree of aggregation depending on reaction time, mixing time and measurement time were directly influenced to the formation of gold nanoparticle and its stabilization. We found that the suitable mixing time is 30 seconds and measurement time was recorded within 60 seconds after the addition of reducing agent. Then, reproducibility was performed by repeating 11 times under optimum conditions. The result showed that the percentage of relative standard deviation was less than 2%. Consequently, the proposed method for the detection of mercury(II) ion displays high precision, being consistent with the recommended from the literature (see Table 2.1).

### ***Accuracy***

In this part, the accuracy of this proposed colorimetric method was represented as the percentage of recovery. The different concentrations of mercury(II) ions of 0.45, 0.60, 1.05, and 1.25 mg L<sup>-1</sup> were used to evaluate the recovery. We found that the recovery was found in the range of 90.7 - 106.7%. The results showed that the accuracy of this proposed method in mercury(II) ion detection were acceptable, according to the widely used criteria of analyte recovery in different concentration levels (see Table 2.1).

### *Matrix-matched calibration*

A series of the concentrations of mercury(II) ion was spiked into real drinking water sample. Then, the procedure was done using the same calibration curve. Figure 4.41 shows the comparison of linearity of calibration (solid shapes) and spiked standard (transparent shapes) curves. It indicated that the relative response was not significantly different. It could imply that an operative matrix in sample had no effect for the detection of mercury(II) ions in real samples (bottled drinking water).

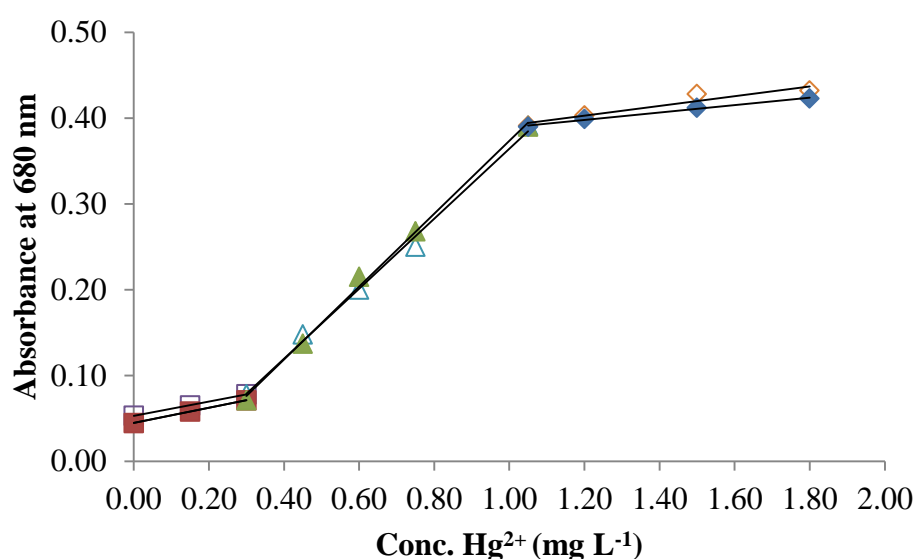


**Figure 4.41** Standard addition curve (solid and transparent shapes represent the calibration and matrix-matched curves, respectively)

### **4.4 Application in real drinking water**

The proposed method was applied to determine mercury(II) ions in real samples (bottled drinking water). It was found that the color of 3-AEPE-stabilized gold nanoparticle solution remains red in color, indicating that mercury(II) ions concentration in samples was below the limit of detection. This result was consistent with the result obtained from inductively coupled plasma-optical emission spectrophotometer (ICP-OES). The total concentration of mercury did not detect with a detection limit of 2  $\mu\text{g L}^{-1}$ .

To obtain the accuracy of this proposed method, the samples were also spiked by the different concentrations of mercury(II) ions. The spiked sample was then performed by the procedure of the proposed method. The results are shown in Table 4.11. The recoveries of mercury(II) ions from spiked samples at different concentration levels were acceptable. Thus, the proposed method can be used to determine mercury(II) ions in bottled drinking water samples.

**Table 4.11** Determination of mercury(II) ions in real samples

Sample	Added conc. (mg L <sup>-1</sup> )	Found conc. (mg L <sup>-1</sup> )	Recovery (%)
Bottled drinking water 1	-	n.d.	-
	0.45	0.46 (±0.004)	101.3
	0.60	0.60 (±0.025)	100.3
	1.05	1.04 (±0.019)	98.7
	1.25	1.09 (±0.052)	90.7
Bottled drinking water 2	-	n.d.	-
	0.45	0.42 (±0.016)	92.7
	0.60	0.64 (±0.030)	107.7
	1.05	1.08 (±0.020)	102.9
	1.25	1.22 (±0.030)	101.6
Bottled drinking water 3	-	n.d.	-
	0.45	0.52 (±0.45)	90.8
	0.60	0.71 (±0.3)	99.5
	1.05	1.18 (±0.35)	101.3
	1.25	1.39 (±0.20)	106.7

## 4.5 Extraction of mercury(II) ions by ionic liquid

### 4.5.1 Synthesis and characterization of ionic liquid

An ionic liquid 1-butyl-3-methylimidazolium hexafluorophosphate, also known as  $[C_4mim][PF_6]$  or Bmim- $PF_6$ , was synthesized by alkylation of 1-butyl-3-methylimidazolium chloride and hexafluorophosphoric acid. As the ionic liquid,  $[C_4mim][PF_6]$  is viscous, colorless, hydrophobic and non-water soluble. The  $^1H$ -NMR spectrum of  $[C_4mim][PF_6]$  recorded in  $CDCl_3$  is depicted in Figure 4.42. The  $^1H$ -NMR spectrum was obtained in chemical shifts as follows :  $\delta$  (ppm) 0.85 (t, 3H,  $J = 7.2$ ), 1.22 (sept, 2H,  $J = 7.5$ ), 1.81 (pen, 2H,  $J = 7.6$ ), 3.84 (s, 3H), 4.04 (t, 2H,  $J = 4.0$ ), 7.21 (t,  $J = 1.8$ ), 7.32 (t, 1H,  $J = 1.8$ ) and 8.25 (s, 1H). This result showed that the ionic liquid  $[C_4mim][PF_6]$  was successfully synthesized.

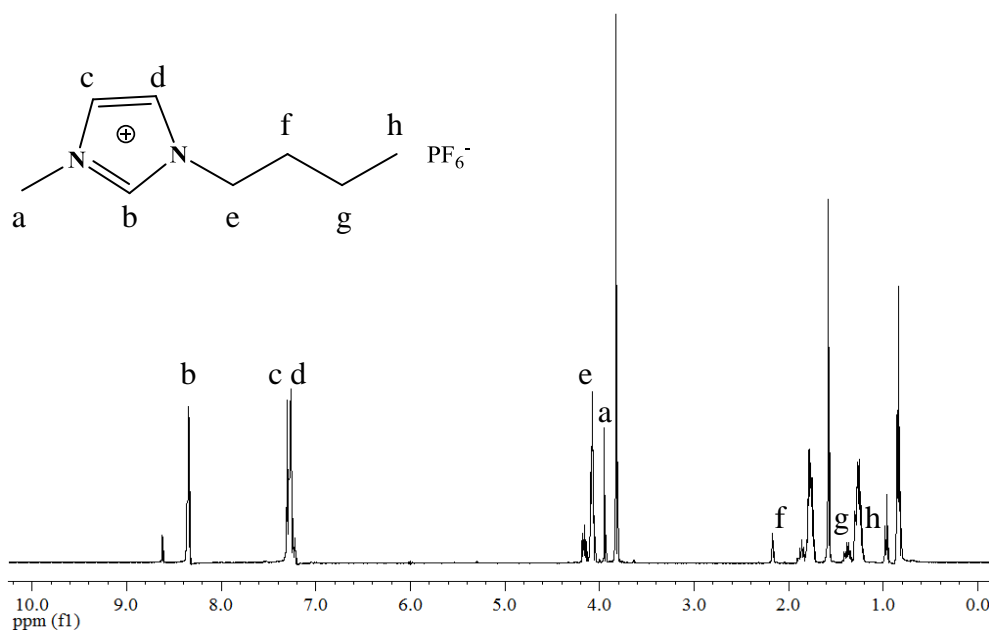


**Figure 4.42** The  $^1H$ -NMR spectrum of an ionic liquid  $[C_4mim][PF_6]$  in  $CDCl_3$ .

#### 4.5.2 Optimization of the extraction of mercury(II) ions by ionic liquid

For all experiments in this section, deionized water-saturated with ionic liquid [C<sub>4</sub>mim][PF<sub>6</sub>] (sat. DI water) was used instead of deionized water. Deionized water saturated with ionic liquid [C<sub>4</sub>mim][PF<sub>6</sub>] was prepared by stirring ionic liquid [C<sub>4</sub>mim][PF<sub>6</sub>] in deionized water until it saturated.

##### 4.5.2.1 Effect of the volume of ionic liquid

The effects of an ionic liquid [C<sub>4</sub>mim][PF<sub>6</sub>] on the extraction of mercury(II) ions was investigated by varying volume in the range of 1 - 5 mL. A 20 mL of 100 µg L<sup>-1</sup> mercury(II) ions and ionic liquid [C<sub>4</sub>mim][PF<sub>6</sub>] were stirred thoroughly for 20 minutes. After centrifuging for 5 minutes at 2500 rpm, the solution was collected and then measured using CV-AAS. It was found that the percentages of extraction efficiency (%EE) were very low within the range of 15 - 25%. This result was consistent with the previous reports [121, 159] stated that the extraction efficiency of mercury(II) ions was very low due to its relatively high water solubility when the volume of ionic liquid [C<sub>4</sub>mim][PF<sub>6</sub>] was smaller than 25 mL. Thus, organic chelators were used to complex with mercury(II) ion before extraction using ionic liquids. In this work, 3-AEPE was employed as a chelating agent to form a complex with mercury(II) ion. The solution was stirred for 5 minutes before extraction with ionic liquid [C<sub>4</sub>mim][PF<sub>6</sub>]. However, the result revealed low extraction efficiency in the range of 19 - 26%. This result implied that low concentrations of mercury(II) ions were transfer into ionic liquid [C<sub>4</sub>mim][PF<sub>6</sub>] phase because the initial concentration of mercury(II) ion was very low 10 times lower than that was used in the literature [121, 159] leading to low concentration gradient that is a main driving force for the extraction.

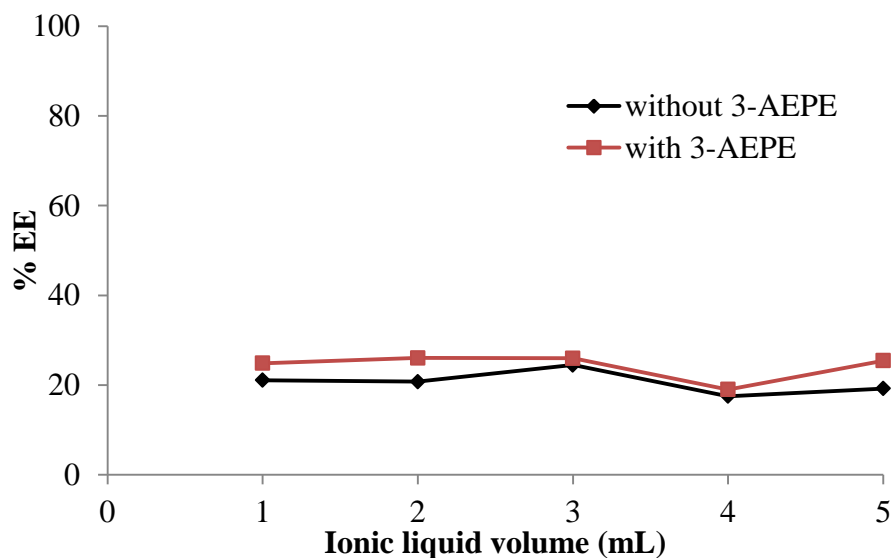


**Figure 4.43** Effect of ionic liquid volumes on the extraction efficiency of mercury(II) ions using ionic liquid  $[C_4mim][PF_6]$  in the absence and presence of 3-AEPE.

#### 4.5.2.2 Effect of pH

The influence of the pH value on the extraction of mercury(II) ions was investigated by varying 2 to 10 by using 5% (v/v)  $HNO_3$  and 0.1 M NaOH as pH adjusting agents. Similarly, 20 mL of  $100 \mu g L^{-1}$  mercury(II) ions and 1 mL of ionic liquid  $[C_4mim][PF_6]$  was performed until the upper aqueous phase was obtained. The extraction efficiencies were compared between the extraction in the absence and presence of 1 mL of 1 mM 3-AEPE as shown in Figure 4.44. Both experimental conditions showed similar behavior, with extraction efficiencies in the pH ranges of 4 - 7 in the range of 30 - 32% and 34 - 40 % for the absence and presence of 3-AEPE, respectively. Meanwhile, extraction efficiencies were lower than 20 % when the pH of solution was less than 7 due to mercury(II) ion precipitation in alkaline solution.

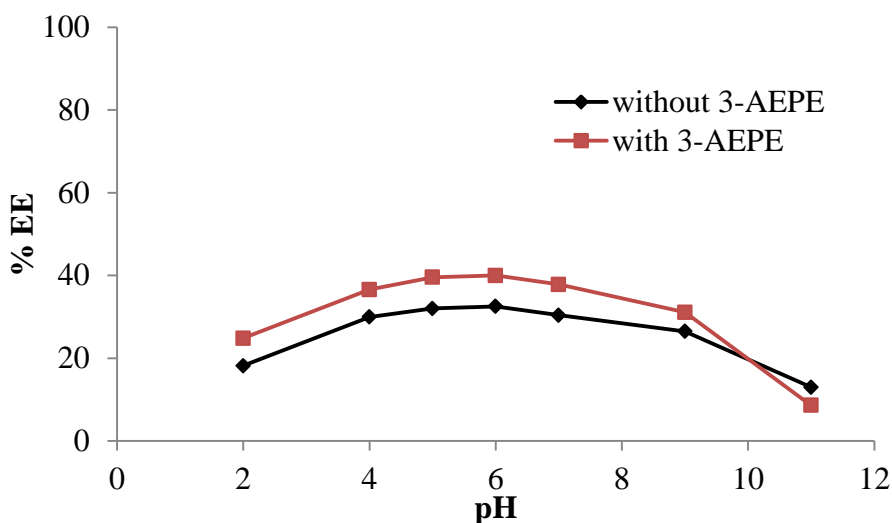


**Figure 4.44** Effect of pH on the extraction efficiency of mercury(II) ions using ionic liquid  $[C_4mim][PF_6]$  in the absence and presence of 3-AEPE.

#### 4.5.2.3 Effect of the concentration of 3-AEPE

The concentration of 3-AEPE was varied in the range of 0 - 222 mM, while maintaining the concentration of mercury(II) ions at 446 mM and 1 mL of ionic liquid  $[C_4mim][PF_6]$ . The result is shown in Figure 4.45. It was found that the highest extraction efficiency of mercury(II) ions were the ratio of 3-AEPE and mercury(II) ions over 0.8.

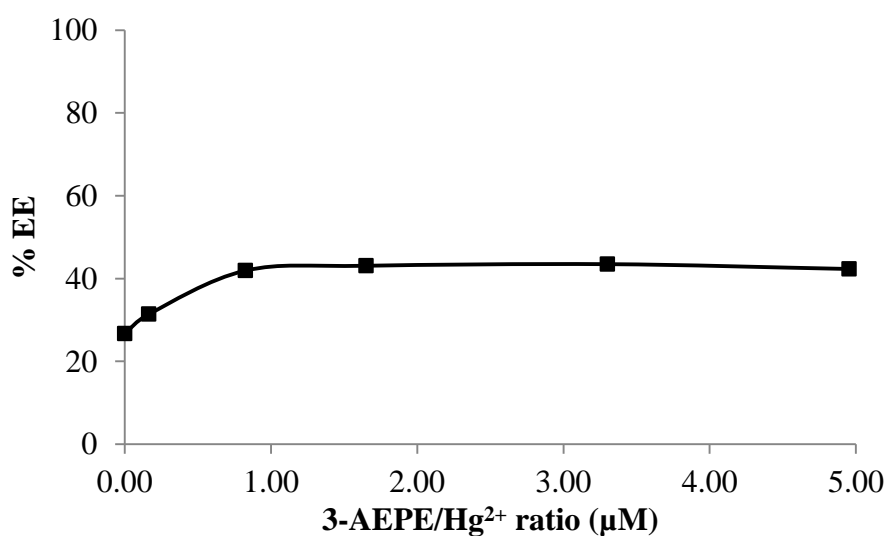


**Figure 4.45** Effect of the concentration of 3-AEPE on the extraction efficiency of mercury(II) ions using ionic liquid  $[C_4mim][PF_6]$ .

#### 4.5.2.4 Effects of extraction times

The extraction time was varied in the range of 15 - 120 minutes. While maintaining constant volume of 1 mL of ionic liquid  $[\text{C}_4\text{mim}][\text{PF}_6]$  and 1 mL of 1 mM 3-AEPE, 20 mL of  $100 \mu\text{g L}^{-1}$  mercury(II) ions at pH 4 were added and allowed to react until the upper aqueous phase was obtained. In both cases, the results showed that extraction efficiencies increased slightly and then remained constant with extraction time over 30 minutes as shown in Figure 4.46. The extraction efficiency of mercury(II) ions in the absence and presence of 3-AEPE was slightly different.

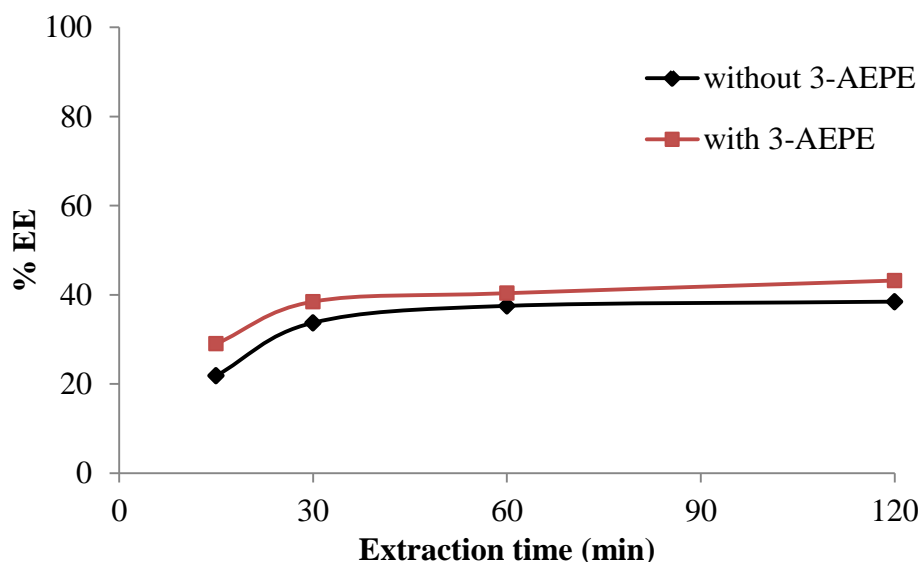


**Figure 4.46** Effect of extraction time on the extraction efficiency of mercury(II) ions using ionic liquid  $[\text{C}_4\text{mim}][\text{PF}_6]$  in the absence and presence of 3-AEPE.

In this work, the extraction efficiency of mercury(II) ions using an ionic liquid  $[\text{C}_4\text{mim}][\text{PF}_6]$  in the absence and presence of 3-AEPE was low (less than 40 %). It was indicated that a small concentration of mercury(II) ions and a neutral complex of mercury(II)-3-AEPE was distributed in ionic liquid phase. This result is consistent with a previous report by Germani *et al.* [118]. The distribution ratio of mercury(II) ions in an ionic liquid  $[\text{C}_4\text{mim}][\text{PF}_6]$  was 0.84. Under stirring at a constant temperature of 60 °C, mercury(II) ions did not transfer instantaneously into an ionic liquid  $[\text{C}_4\text{mim}][\text{PF}_6]$  in the absence of any chelating agent. However, the transfer of mercury(II) ions into an ionic liquid phase can occur completely if the

extraction time was extended over 30 hours. This equilibrium time is too long for analytical purposes. However, a neutral mercury(II)-3-AEPE complex was tried to form by mixing mercury(II) ions with 3-AEPE ligand prior to be extracted by the ionic liquid, the high extraction efficiency was expected. Unfortunately in this work, 3-AEPE-Hg(II) complex could be low extracted into the ionic liquid [C<sub>4</sub>mim][PF<sub>6</sub>] at room temperature. This unsatisfactory result could be attributed to high water solubility of the ligand and the complex, thus they preferred to be solvated by water molecules in the aqueous phase rather than moving to the ionic liquid phase.

## CHAPTER V

### CONCLUSION

Dithia-diaza ligands (3-AEPE, 4-AEPE and 5-AEPE) were synthesized and used as a stabilizer for preventing aggregation of gold nanoparticles obtained from direct reduction by  $\text{NaBH}_4$ . Gold(III) ion ( $\text{HAuCl}_4$  form) containing dithia-diaza ligands and non-ionic-surfactant was reduced to form gold nanoparticles and simultaneously stabilized by dithia-diaza ligands.

Without mercury(II) ions, 3-AEPE-stabilized gold nanoparticle in the presence of Triton X-100 appeared a rose-red in coloration upon addition of  $\text{NaBH}_4$ , showing the SPR absorption band at 517 nm. The average sizes of 3-AEPE-stabilized gold nanoparticles obtained from TEM displayed individual particles in diameter of 9 nm. The results obtained from UV-vis and TEM techniques confirmed that 3-AEPE can stabilize gold nanoparticles by direct reduction using  $\text{NaBH}_4$  against their aggregation. While, 3-AEPE-stabilized gold nanoparticle solution in the presence of mercury(II) became purple and blue immediately when addition of the reducing agent within a few second. The optimum conditions of the concentrations of gold(III) ions, 3-AEPE, Triton X-100 and  $\text{NaBH}_4$  were 125  $\mu\text{M}$ , 0.3 mM, 0.1%(v/v) and 0.6 mM, respectively. For quantitative colorimetric analysis by UV-vis, 3-AEPE-stabilized gold nanoparticle solution in the presence of mercury(II) was measured at a wavelength of 680 nm. By comparing with other metal ions that concentration higher than mercury(II) ion by about 100 times, only mercury(II) ion can induce to aggregate of gold nanoparticles, resulting solution turns to blue, while the solution containing other metal ions remained rose-red in coloration. The calibration curve was constructed at a wavelength of 680 nm with various concentrations of mercury(II) ions. The linearity depended on the concentrations of mercury(II) ion was divided into three levels of, including low (0 - 1.25  $\mu\text{M}$ ), medium (1.25 - 5.25  $\mu\text{M}$ ) and high (5.25 - 10.0  $\mu\text{M}$ ). The limit of detection was estimated to be 35 nM (7  $\mu\text{g L}^{-1}$ ), with a relative standard deviation of 1.3% ( $n = 11$ ). The acceptable recoveries of spiked samples were found in the range of 90.7 - 106.7%.

Similarly, 4-AEBE and 5-AEPE ligands were able to stabilize gold nanoparticles from aggregation. The coloration of gold nanoparticle stabilized by 4-AEBE and 5-AEPE was rose-red and purple color with the absence and presence of mercury(II) ions, respectively. The optimum conditions of 4-AEBE-stabilized gold nanoparticle was the same as 3-AEPE, except the concentration of 4-AEBE of 0.4 mM. The calibration curve was divided into three levels similar to 3-AEPE, but their sensitivities were lower than 3-AEPE with 6, 7.5 and 8 orders for low, medium and high levels, respectively. For 5-AEPE-stabilized gold nanoparticle, the optimal concentrations of 5-AEPE and NaBH<sub>4</sub> were 0.6 mM and 0.8 mM, respectively. The calibration curve was divided into two levels, including low (0 - 2.5 μM) and high (2.5 - 15.0 μM).

3-AEPE ligand displays a stabilizer to protect gold nanoparticles from aggregation and at the same time to be highly selective recognition to mercury(II) ion over other metal ions. This method offers advantages of simplicity, rapidity, cost effectiveness and no requirement of any sophisticated instruments and it is alternatively possible method for mercury(II) monitoring in drinking water. Moreover, this method has several potential advantages as optical sensor, especially no as-prepared gold nanoparticles synthesis and shorter observation time.

The extraction efficiencies of mercury(II) ions using the ionic liquid [C<sub>4</sub>mim][PF<sub>6</sub>] in the absence and presence of 3-AEPE were less than 40%. Thus, the extraction using ionic liquid [C<sub>4</sub>mim][PF<sub>6</sub>] was not appropriate for mercury(II) ions.

### **Suggestion for further works**

Although, this proposed method is a novel colorimetric and naked eye methods for detection of mercury(II) ions in bottled drinking water, limit of detection of this protocol is higher than that recommended acceptable value of mercury(II) in drinking water (2 μg L<sup>-1</sup>). Thus, preconcentration steps have required improving sensitivity of this proposed method.

## REFERENCES

- [1] Baeyens, W. Speciation of mercury in different compartments of the environment. Trends in Analytical Chemistry. 11 (1992): 245-254.
- [2] Leermakers, M.; Baeyens, W.; Quevauviller, P. and Horvat, M. Mercury in environmental samples: speciation, artifacts and validation. Trends in Analytical Chemistry. 24 (2005): 383-393.
- [3] Kubán, P.; Pelcová, P.; Margetinová, J. and Kubán, V. Mercury speciation by CE: an update. Electrophoresis. 30 (2009): 92-99.
- [4] Stoichev, T.; Amouroux, D.; Martin-Doimeadios, R.C.R.; Monperrus, M.; Donard, O.F.X. and Tsaley, D.L. Speciation analysis of mercury in aquatic environment. Applied Spectroscopy Reviews. 41 (2006): 591-619.
- [5] Counter, S.A. and Buchanan, L.H. Mercury exposure in children - a review. Toxicology and Applied Pharmacology. 198 (2004): 209-230.
- [6] Hernandez Córdoba, M.; López García, I. and Sánchez-Pedreño, C. Spectrophotometric determination of mercury with thiocyanate and Rhodamine B. Microchimica Acta. 84 (1984): 467-475.
- [7] Mudakavi, J.R. Spectrophotometric determination of trace amounts of mercury with phenanthroline and eosin. Analyst. 109 (1984): 1577-1579.
- [8] Chatterjee, S.; Pillai, A. and Gupta, V.K. Spectrophotometric determination of mercury in environmental sample and fungicides based on its complex with *o*-carboxy phenyl diazoamino *p*-azobenzene. Talanta. 57 (2002): 461-465.
- [9] Khan, H.; Ahmed, M.J. and Bhangar, M.I. A simple spectrophotometric determination of trace level mercury using 1,5-diphenylthiocarbazone solubilized in micelle. Analytical Sciences. 21 (2005): 507-512.
- [10] Manzoori, J.L.; Sorouraddin, M.H. and Haji Shabani, A.M. Determination of mercury by cold vapour atomic absorption spectrometry after preconcentration with dithizone immobilized on surfactant-coated alumina. Journal of Analytical Atomic Spectrometry. 13 (1998): 305-308.
- [11] Balarama Krishna, M.V.; Karunasagar, D.; Rao, S.V. and Arunachalam, J. Preconcentration and speciation of inorganic and methyl mercury in

- waters using polyaniline and gold trap-CVAAS. Talanta. 68 (2005): 329-335.
- [12] Río Segade, S. and Tyson, J.F. Determination of inorganic mercury and total mercury in biological and environmental samples by flow injection-cold vapor-atomic absorption spectrometry using sodium borohydride as the sole reducing agent. Spectrochimica Acta Part B: Atomic Spectroscopy. 58 (2003): 797-807.
- [13] Swift, R.P. and Campbell, J.E. An atomic fluorescence-based method for ultratrace mercury detection in environmental samples. Spectroscopy. 8 (1993): 38-47.
- [14] Scifres, J.; Cheema, V.; Wasko, M. and McDaniel, W. Determination of ultratrace-level total mercury in sediment and tissue by microwave digestion and atomic fluorescence detection: Part 2. American Environmental Laboratory. 7 (1995): 1-2.
- [15] Jagtap, R.; Krikowa, F.; Maher, W.; Foster, S. and Ellwood, M. Measurement of methyl mercury(I) and mercury(II) in fish tissues and sediments by HPLC-ICPMS and HPLC-HGAAS. Talanta. 85 (2011): 49-55.
- [16] Yang, H.; Zhou, Z.; Li, F.; Yi, T. and Huang, C. New Hg<sup>2+</sup> and Ag<sup>+</sup> selective colorimetric sensor based on thiourea subunits. Inorganic Chemistry Communications. 10 (2007): 1136-1139.
- [17] Tan, J. and Yan, X.P. 2,1,3-Benzoxadiazole-based selective chromogenic chemosensor for rapid naked-eye detection of Hg<sup>2+</sup> and Cu<sup>2+</sup>. Talanta. 76 (2008): 9-14.
- [18] Sheng, R.; Wang, P.; Liu, W.; Wu, X. and Wu, S. A new colorimetric chemosensor for Hg<sup>2+</sup> based on coumarin azine derivative. Sensors and Actuators B: Chemical. 128 (2008): 507-511.
- [19] Yan, Y.; Hu, Y.; Zhao, G. and Kou, X. A novel azathia-crown ether dye chromogenic chemosensor for the selective detection of mercury(II) ion. Dyes and Pigments. 79 (2008): 210-215.
- [20] Wanichacheva, N.; Siriprumpoothum, M.; Kamkaew, A. and Grudpan, K. Dual optical detection of a novel selective mercury sensor based on 7-

- nitrobenzo-2-oxa-1,3-diazolyl subunits. Tetrahedron Letters. 50 (2009): 1783-1786.
- [21] Choi, M.J.; Kim, M.Y. and Chang, S.K. A new Hg<sup>2+</sup>-selective chromoionophore based on calix[4]arenediazacrown ether. Chemical Communications. (2011): 1664-1665.
- [22] Yu, Y.; Lin, L.R.; Yang, K.B.; Zhong, X.; Huang, R.B. and Zheng, L.S. *p*-Dimethylaminobenzaldehyde thiosemicarbazone: a simple novel selective and sensitive fluorescent sensor for mercury(II) in aqueous solution. Talanta. 69 (2006): 103-106.
- [23] Son, Y.A.; Hwang, J.H.; Wang, S.; Bae, J.S. and Kim, S.H. New fluorescent dye chemosensor for mercury ion (Hg<sup>2+</sup>) detection. Fibers and Polymers. 10 (2009): 272-274.
- [24] Song, C.; Zhang, X.; Jia, C.; Zhou, P.; Quan, X. and Duan, C. Highly sensitive and selective fluorescence sensor based on functional SBA-15 for detection of Hg<sup>2+</sup> in aqueous media. Talanta. 81 (2010): 643-649.
- [25] Hu, Z.Q.; Yang, X.D.; Cui, C.L.; Ding, L.; Lin, C.S.; Lu, H.Y. and Wang, L. 1,8-Anthracene disulfonamide: a simple but highly sensitive and selective fluorescent chemosensor for Hg<sup>2+</sup> in aqueous media. Sensors and Actuators B: Chemical. 145 (2010): 61-65.
- [26] Lai, Y.; Ma, Y.; Sun, L.; Jia, J.; Weng, J.; Hu, N.; Yang, W. and Zhang, Q. A highly selective electrochemical biosensor for Hg<sup>2+</sup> using hemin as a redox indicator. Electrochimica Acta. 56 (2011): 3153-3158.
- [27] Ensafi, A.A. and Fouladgar, M. Development of a spectrophotometric optode for the determination of Hg(II). IEEE Sensors Journal. 8 (2008): 347-353
- [28] Ensafi, A.A. and Fouladgar, M. A sensitive and selective bulk optode for determination of Hg(II) based on hexathiacyclooctadecane and chromoionophore V. Sensors and Actuators B: Chemical. 136 (2009): 326-331.
- [29] Tavallali, H. and NoroziKhah, H. Design of cold vapor system and assembled on atomic absorption spectrometer for mercury determination in several waste water samples. International Journal of ChemTech Research. 1 (2009): 390-393.

- [30] Martinis, E.M.; Bertón, P.; Olsina, R.A.; Altamirano, J.C. and Wuilloud, R.G. Trace mercury determination in drinking and natural water samples by room temperature ionic liquid based-preconcentration and flow injection-cold vapor atomic absorption spectrometry. Journal of Hazardous Materials. 167 (2009): 475-481.
- [31] Cheng, X.; Li, Q.; Li, C.; Qin, J. and Li, Z. Azobenzene-based colorimetric chemosensors for rapid naked-eye detection of mercury(II). Chemistry - A European Journal. 17 (2011): 7276-7281.
- [32] Cheng, Y.; Zhang, M.; Yang, H.; Li, F.; Yi, T. and Huang, C. Azo dyes based on 8-hydroxyquinoline benzoates: Synthesis and application as colorimetric Hg<sup>2+</sup>-selective chemosensors. Dyes and Pigments. 76 (2008): 775-783.
- [33] Liu, B. and Tian, H. A selective fluorescent ratiometric chemodosimeter for mercury ion. Chemical Communications. 41 (2005): 3156-3158.
- [34] Lee, M.H.; Cho, B.K.; Yoon, J. and Kim, J.S. Selectively chemodosimetric detection of Hg(II) in aqueous media. Organic Letters. 9 (2007): 4515-4518.
- [35] Lee, M.H.; Lee, S.W.; Kim, S.H.; Kang, C. and Kim, J.S. Nanomolar Hg(II) detection using Nile blue chemodosimeter in biological media. Organic Letters. 11 (2009): 2101-2104.
- [36] Leng, B.; Zou, L.; Jiang, J. and Tian, H. Colorimetric detection of mercuric ion (Hg<sup>2+</sup>) in aqueous media using chemodosimeter-functionalized gold nanoparticles. Sensors and Actuators B: Chemical. 140 (2009): 162-169.
- [37] Mulvaney, P. Surface plasmon spectroscopy of nanosized metal particles. Langmuir. 12 (1996): 788-800.
- [38] Link, S. and El-Sayed, M.A. Optical properties and ultrafast dynamics of metallic nanocrystals. Annual Review of Physical Chemistry. 54 (2003): 331-366.
- [39] Scaffardi, L.B.; Lester, M.; Skigin, D. and Tocho, J.O. Optical extinction spectroscopy used to characterize metallic nanowires. Nanotechnology. 18 (2007): 315402.

- [40] Huang, X.; Jain, P.K.; El-Sayed, I.H. and El-Sayed, M.A. Gold nanoparticles: interesting optical properties and recent applications in cancer diagnostics and therapy. Nanomedicine. 2 (2007): 681-693.
- [41] Kelly, K.L.; Coronado, E.; Zhao, L.L. and Schatz, G.C. The optical properties of metal nanoparticles: the influence of size, shape and dielectric environment. The Journal of Physical Chemistry B. 107 (2002): 668-677.
- [42] Willets, K.A. and Van Duyne, R.P. Localized surface plasmon resonance spectroscopy and sensing. Annual Review of Physical Chemistry. 58 (2007): 267-297.
- [43] Link, S. and El-Sayed, M.A. Size and temperature dependence of the plasmon absorption of colloidal gold nanoparticles. The Journal of Physical Chemistry B. 103 (1999): 4212-4217.
- [44] Ghosh, S.K. and Pal, T. Interparticle coupling effect on the surface plasmon resonance of gold nanoparticles: from theory to applications. Chemical Reviews. 107 (2007): 4797-4862.
- [45] Daniel, M.C. and Astruc, D. Gold nanoparticles: assembly, supramolecular chemistry, quantum-size-related properties, and applications toward biology, catalysis, and nanotechnology. Chemical Reviews. 104 (2004): 293-346.
- [46] Myroshnychenko, V.; Rodriguez-Fernandez, J.; Pastoriza-Santos, I.; Funston, A.M.; Novo, C.; Mulvaney, P.; Liz-Marzan, L.M. and Garcia de Abajo, F.J. Modelling the optical response of gold nanoparticles. Chemical Society Reviews. 37 (2008): 1792-1805.
- [47] Link, S. and El-Sayed, M.A. Spectral properties and relaxation dynamics of surface plasmon electronic oscillations in gold and silver nanodots and nanorods. The Journal of Physical Chemistry B. 103 (1999): 8410-8426.
- [48] Moores, A. and Goettmann, F. The plasmon band in noble metal nanoparticles: an introduction to theory and applications. New Journal of Chemistry. 30 (2006): 1121-1132.
- [49] Underwood, S. and Mulvaney, P. Effect of the solution refractive index on the color of gold colloids. Langmuir. 10 (1994): 3427-3430.

- [50] Jain, P.K.; Lee, K.S.; El-Sayed, I.H. and El-Sayed, M.A. Calculated absorption and scattering properties of gold nanoparticles of different size, shape, and composition: applications in biological imaging and biomedicine. The Journal of Physical Chemistry B. 110 (2006): 7238-7248.
- [51] Liu, X.; Atwater, M.; Wang, J. and Huo, Q. Extinction coefficient of gold nanoparticles with different sizes and different capping ligands. Colloids and Surfaces B: Biointerfaces. 58 (2007): 3-7.
- [52] Maye, M.M.; Han, L.; Kariuki, N.N.; Ly, N.K.; Chan, W.B.; Luo, J. and Zhong, C.J. Gold and alloy nanoparticles in solution and thin film assembly: spectrophotometric determination of molar absorptivity. Analytica Chimica Acta. 496 (2003): 17-27.
- [53] Sato, K.; Hosokawa, K. and Maeda, M. Rapid aggregation of gold nanoparticles induced by non-cross-linking DNA hybridization. Journal of the American Chemical Society. 125 (2003): 8102-8103.
- [54] Zhao, W.; Brook, M.A. and Li, Y. Design of gold nanoparticle-based colorimetric biosensing assays. ChemBioChem. 9 (2008): 2363-2371.
- [55] Kim, Y.; Johnson, R.C. and Hupp, J.T. Gold nanoparticle-based sensing of “spectroscopically silent” heavy metal ions. Nano Letters. 1 (2001): 165-167.
- [56] Lin, Y.W.; Huang, C.C. and Chang, H.T. Gold nanoparticle probes for the detection of mercury, lead and copper ions. Analyst. 136 (2011): 863-871.
- [57] Kimling, J.; Maier, M.; Okenve, B.; Kotaidis, V.; Ballot, H. and Plech, A. Turkevich method for gold nanoparticle synthesis revisited. The Journal of Physical Chemistry B. 110 (2006): 15700-15707.
- [58] Kumar, S.; Gandhi, K.S. and Kumar, R. Modeling of formation of gold nanoparticles by citrate method. Industrial & Engineering Chemistry Research. 46 (2006): 3128-3136.
- [59] Brust, M.; Walker, M.; Bethell, D.; Schiffrin, D.J. and Whyman, R. Synthesis of thiol-derivatised gold nanoparticles in a two-phase liquid-liquid system. Journal of the Chemical Society, Chemical Communications. (1994): 801-802.

- [60] Brust, M.; Fink, J.; Bethell, D.; Schiffrin, D.J. and Kiely, C. Synthesis and reactions of functionalised gold nanoparticles. Journal of the Chemical Society, Chemical Communications. (1995): 1655-1656.
- [61] Dumur, F.; Guerlin, A.; Dumas, E.; Bertin, D.; Gigmes, D. and Mayer, C. Controlled spontaneous generation of gold nanoparticles assisted by dual reducing and capping agents. Gold Bulletin. 44 (2011): 119-137.
- [62] Templeton, A.C.; Chen, S.; Gross, S.M. and Murray, R.W. Water-soluble, isolable gold clusters protected by tiopronin and coenzyme a monolayers. Langmuir. 15 (1998): 66-76.
- [63] Knecht, M. and Sethi, M. Bio-inspired colorimetric detection of  $\text{Hg}^{2+}$  and  $\text{Pb}^{2+}$  heavy metal ions using Au nanoparticles Analytical and Bioanalytical Chemistry. 394 (2009): 33-46.
- [64] Sardar, R. and Shumaker-Parry, J.S. Asymmetrically functionalized gold nanoparticles organized in one-dimensional chains. Nano Letters. 8 (2008): 731-736.
- [65] Giersig, M. and Mulvaney, P. Preparation of ordered colloid monolayers by electrophoretic deposition. Langmuir. 9 (1993): 3408-3413.
- [66] Yonezawa, T. and Kunitake, T. Practical preparation of anionic mercapto ligand-stabilized gold nanoparticles and their immobilization. Colloids and Surfaces A: Physicochemical and Engineering Aspects. 149 (1999): 193-199.
- [67] Templeton, A.C.; Wuelfing, W.P. and Murray, R.W. Monolayer-protected cluster molecules. Accounts of Chemical Research. 33 (2000): 27-36.
- [68] DeLong, R.K.; Reynolds, C.M.; Malcolm, Y.; Schaeffer, A.; Severs, T. and Wanekaya, A. Functionalized gold nanoparticles for the binding, stabilization, and delivery of therapeutic DNA, RNA, and other biological macromolecules Nanotechnology, Science and Applications 3(2010): 53-63.
- [69] Miyake, Y.; Togashi, H.; Tashiro, M.; Yamaguchi, H.; Oda, S.; Kudo, M.; Tanaka, Y.; Kondo, Y.; Sawa, R.; Fujimoto, T.; Machinami, T. and Ono, A. Mercury(II)-mediated formation of thymine-Hg(II)-thymine base pairs

- in DNA duplexes. Journal of the American Chemical Society. 128 (2006): 2172-2173.
- [70] Chiu, T.C. and Huang, C.C. Aptamer-functionalized nano-biosensors. Sensors. 9 (2009): 10356-10388.
- [71] Lee, J.S.; Han, M.S. and Mirkin, C.A. Colorimetric detection of mercuric ion ( $\text{Hg}^{2+}$ ) in aqueous media using DNA-functionalized gold nanoparticles. Angewandte Chemie International Edition. 46 (2007): 4093-4096.
- [72] Xue, X.; Wang, F. and Liu, X. One-step, room temperature, colorimetric detection of mercury ( $\text{Hg}^{2+}$ ) using DNA/nanoparticle conjugates. Journal of the American Chemical Society. 130 (2008): 3244-3245.
- [73] Liu, C.W.; Hsieh, Y.T.; Huang, C.C.; Lin, Z.H. and Chang, H.T. Detection of mercury(II) based on  $\text{Hg}^{2+}$ -DNA complexes inducing the aggregation of gold nanoparticles. Chemical Communications. (2008): 2242-2244.
- [74] Li, D.; Wieckowska, A. and Willner, I. Optical analysis of  $\text{Hg}^{2+}$  ions by oligonucleotide-gold-nanoparticle hybrids and DNA-based machines. Angewandte Chemie International Edition. 47 (2008): 3927-3931.
- [75] Lee, J.S. and Mirkin, C.A. Chip-based scanometric detection of mercuric ion using DNA-functionalized gold nanoparticles. Analytical Chemistry. 80 (2008): 6805-6808.
- [76] Lu, N.; Shao, C. and Deng, Z. Colorimetric  $\text{Hg}^{2+}$  detection with a label-free and fully DNA-structured sensor assembly incorporating G-quadruplex halves. Analyst. 134 (2009): 1822-1825.
- [77] Liu, Z.D.; Li, Y.F.; Ling, J. and Huang, C.Z. A localized surface plasmon resonance light-scattering assay of mercury(II) on the basis of  $\text{Hg}^{2+}$ -DNA complex induced aggregation of gold nanoparticles. Environmental Science & Technology. 43 (2009): 5022-5027.
- [78] Li, T.; Dong, S. and Wang, E. Label-free colorimetric detection of aqueous mercury ion ( $\text{Hg}^{2+}$ ) using  $\text{Hg}^{2+}$ -modulated G-quadruplex-based DNAzymes. Analytical Chemistry. 81 (2009): 2144-2149.
- [79] Wu, J.; Li, L.; Zhu, D.; He, P.; Fang, Y. and Cheng, G. Colorimetric assay for mercury(II) based on mercury-specific deoxyribonucleic acid-

- functionalized gold nanoparticles. Analytica Chimica Acta. 694 (2011): 115-119.
- [80] Xu, Y.; Deng, L.; Wang, H.; Ouyang, X.; Zheng, J.; Li, J. and Yang, R. Metal-induced aggregation of mononucleotides-stabilized gold nanoparticles: an efficient approach for simple and rapid colorimetric detection of Hg(II). Chemical Communications. 47 (2011): 6039-6041.
- [81] Liu, C.W.; Huang, C.C. and Chang, H.T. Highly selective DNA-based sensor for lead(II) and mercury(II) ions. Analytical Chemistry. 81 (2009): 2383-2387.
- [82] Zhu, Z.; Su, Y.; Li, J.; Li, D.; Zhang, J.; Song, S.; Zhao, Y.; Li, G. and Fan, C. Highly sensitive electrochemical sensor for mercury(II) ions by using a mercury-specific oligonucleotide probe and gold nanoparticle-aided amplification. Analytical Chemistry. 81 (2009): 7660-7666.
- [83] Yu, C.J.; Cheng, T.L. and Tseng, W.L. Effects of Mn<sup>2+</sup> on oligonucleotide-gold nanoparticle hybrids for colorimetric sensing of Hg<sup>2+</sup>: Improving colorimetric sensitivity and accelerating color change. Biosensors and Bioelectronics. 25 (2009): 204-210.
- [84] Radhakumary, C. and Sreenivasan, K. Gold nanoparticles generated through "green route" bind Hg<sup>2+</sup> with a concomitant blue shift in plasmon absorption peak. Analyst. 136 (2011): 2959-2962.
- [85] Guo, Y.; Wang, Z.; Qu, W.; Shao, H. and Jiang, X. Colorimetric detection of mercury, lead and copper ions simultaneously using protein-functionalized gold nanoparticles. Biosensors and Bioelectronics. 26 (2011): 4064-4069.
- [86] Huang, C.C. and Chang, H.T. Parameters for selective colorimetric sensing of mercury(II) in aqueous solutions using mercaptopropionic acid-modified gold nanoparticles. Chemical Communications. 12 (2007): 1215-1217.
- [87] Yu, C.J. and Tseng, W.L. Colorimetric detection of mercury(II) in a high-salinity solution using gold nanoparticles capped with 3-mercaptopropionate acid and adenosine monophosphate. Langmuir. 24 (2008): 12717-12722.

- [88] Darbha, G.K.; Singh, A.K.; Rai, U.S.; Yu, E.; Yu, H. and Chandra, R.P. Selective detection of mercury(II) ion using nonlinear optical properties of gold nanoparticles. Journal of the American Chemical Society. 130 (2008): 8038-8043.
- [89] Rose, M.; Knaggs, M.; Owen, L. and Baxter, M. A review of analytical methods for lead, cadmium, mercury, arsenic and tin determination used in proficiency testing. Journal of Analytical Atomic Spectrometry. 16 (2001): 1101-1106.
- [90] Ma, M.; Wang, J. and Zheng, X. Enhancement of the colorimetric sensitivity of gold nanoparticles with triethanolamine to minimize interparticle repulsion. Microchimica Acta. 172 (2011): 155-162.
- [91] Chai, F.; Wang, C.; Wang, T.; Ma, Z. and Su, Z. L-cysteine functionalized gold nanoparticles for the colorimetric detection of  $\text{Hg}^{2+}$  induced by ultraviolet light. Nanotechnology. 21 (2010): 1-6.
- [92] Kim, Y.R.; Mahajan, R.K.; Kim, J.S. and Kim, H. Highly sensitive gold nanoparticle-based colorimetric sensing of mercury(II) through simple ligand exchange reaction in aqueous media. ACS Applied Materials & Interfaces. 2 (2010): 292-295.
- [93] Liu, D.; Qu, W.; Chen, W.; Zhang, W.; Wang, Z. and Jiang, X. Highly sensitive, colorimetric detection of mercury(II) in aqueous media by quaternary ammonium group-capped gold nanoparticles at room temperature. Analytical Chemistry. 82 (2010): 9606-9610.
- [94] Hirayama, T.; Taki, M.; Kashiwagi, Y.; Nakamoto, M.; Kunishita, A.; Itoh, S. and Yamamoto, Y. Colorimetric response to mercury-induced abstraction of triethylene glycol ligands from a gold nanoparticle surface. Dalton Transactions. 35 (2008): 4705-4707.
- [95] Hung, Y.L.; Hsiung, T.M.; Chen, Y.Y.; Huang, Y.F. and Huang, C.C. Colorimetric detection of heavy metal ions using label-free gold nanoparticles and alkanethiols. The Journal of Physical Chemistry C. 114 (2010): 16329-16334.

- [96] Chai, F.; Wang, C.; Wang, T.; Li, L. and Su, Z. Colorimetric detection of  $Pb^{2+}$  using glutathione functionalized gold nanoparticles. ACS Applied Materials & Interfaces. 2 (2010): 1466-1470.
- [97] Lin, C.Y.; Yu, C.J.; Lin, Y.H. and Tseng, W.L. Colorimetric sensing of silver(I) and mercury(II) ions based on an assembly of Tween 20-stabilized gold nanoparticles. Analytical Chemistry. 82 (2010): 6830-6837.
- [98] Si, S.; Kotal, A. and Mandal, T.K. One-dimensional assembly of peptide-functionalized gold nanoparticles: an approach toward mercury ion sensing. The Journal of Physical Chemistry C. 111 (2007): 1248-1255.
- [99] Aragay, G.; Pons, J.; Ros, J. and Merkoci, A. Aminopyrazole-based ligand induces gold nanoparticle formation and remains available for heavy metal ions sensing. a simple mix and detect approach. Langmuir. 26 (2010): 10165-10170.
- [100] Xiangjun, L.; Xiaohong, C.; Tao, B.; Canliang, F. and Dihua, S. Visual detection of  $Hg^{2+}$  with high selectivity using thymine modified gold nanoparticles. Analytical Sciences. 26 (2010): 1169-1172.
- [101] Jana, N.R.; Gearheart, L. and Murphy, C.J. Seeding growth for size control of 5-40 nm diameter gold nanoparticles. Langmuir. 17 (2001): 6782-6786.
- [102] Chen, X.; Zu, Y.; Xie, H.; Kemas, A.M. and Gao, Z. Coordination of mercury(II) to gold nanoparticle associated nitrotriazole towards sensitive colorimetric detection of mercuric ion with a tunable dynamic range. Analyst. 136 (2011): 1690-1696.
- [103] Amendola, V. and Meneghetti, M. Size evaluation of gold nanoparticles by UV-vis spectroscopy. The Journal of Physical Chemistry C. 113 (2009): 4277-4285.
- [104] Yu, L. and Andriola, A. Quantitative gold nanoparticle analysis methods: A review. Talanta. 82 (2010): 869-875.
- [105] Philip, D. Synthesis and spectroscopic characterization of gold nanoparticles. Spectrochimica Acta Part A. 71 (2008): 80-85.

- [106] Haiss, W.; Thanh, N.T.K.; Aveyard, J. and Fernig, D.G. Determination of size and concentration of gold nanoparticles from UV-Vis spectra. Analytical Chemistry. 79 (2007): 4215-4221.
- [107] Pearson, R.G. Hard and soft acids and bases. Journal of the American Chemical Society. 85 (1963): 3533-3539.
- [108] Ho, T.L. Hard soft acids bases (HSAB) principle and organic chemistry. Chemical Reviews. 75 (1975): 1-20.
- [109] Puanngam, M. and Unob, F. Preparation and use of chemically modified MCM-41 and silica gel as selective adsorbents for Hg(II) ions. Journal of Hazardous Materials. 154 (2008): 578-587.
- [110] Phothitontimongkol, T.; Siebers, N.; Sukpirom, N. and Unob, F. Preparation and characterization of novel organo-clay minerals for Hg(II) ions adsorption from aqueous solution. Applied Clay Science. 43 (2009): 343-349.
- [111] Jainae, K.; Sanuwong, K.; Nuangjamnong, J.; Sukpirom, N. and Unob, F. Extraction and recovery of precious metal ions in wastewater by polystyrene-coated magnetic particles functionalized with 2-(3-(2-aminoethylthio)propylthio)ethanamine. Chemical Engineering Journal. 160 (2010): 586-593.
- [112] Nutthanara, P.; Ngeontae, W.; Imyim, A. and Kreethadumrongdat, T. Cyclic dithia/diaza with dual schiff base linkage functionalized polymers for heavy metal adsorption. Journal of Applied Polymer Science. 116 (2010): 801-809.
- [113] Wanichacheva, N.; Kamkaew, A.; Watpathomsub, S.; Lee, V.S. and Grudpan, K. 2-[3-(2-Aminoethylsulfanyl)propylsulfanyl]ethanamine bearing dansyl subunits: an efficient, simple, and rapid fluorometric sensor for the detection of mercury(II) ions. Chemistry Letters. 39 (2010): 1099-1101.
- [114] Zhao, H.; Xia, S. and Ma, P. Use of ionic liquids as "green" solvents for extractions. Journal of Chemical Technology & Biotechnology. 80 (2005): 1089-1096.

- [115] Visser, A.E.; Swatloski, R.P.; Griffin, S.T.; Hartman, D.H. and Rogers, R.D. Liquid/liquid extraction of metal ions in room temperature ionic liquid. Separation Science and Technology. 36 (2001): 785-804.
- [116] Han, D. and Row, K.H. Recent applications of ionic liquids in separation technology. Molecules. 15 (2010): 2405-2426.
- [117] Wei, G.T.; Yang, Z. and Chen, C.J. Room temperature ionic liquid as a novel medium for liquid/liquid extraction of metal ions. Analytica Chimica Acta. 488 (2003): 183-192.
- [118] Germani, R.; Mancini, M.V.; Savelli, G. and Spreti, N. Mercury extraction by ionic liquids: temperature and alkyl chain length effect. Tetrahedron Letters. 48 (2007): 1767-1769.
- [119] Visser, A.E.; Swatloski, R.P.; Reichert, W.M.; Mayton, R.; Sheff, S.; Wierzbicki, A.; Davis, J.J.H. and Rogers, R.D. Task-specific ionic liquids for the extraction of metal ions from aqueous solutions. Chemical Communications. (2001): 135-136.
- [120] Visser, A.E.; Swatloski, R.P.; Reichert, W.M.; Mayton, R.; Sheff, S.; Wierzbicki, A.; Davis, J.H. and Rogers, R.D. Task-specific ionic liquids incorporating novel cations for the coordination and extraction of  $\text{Hg}^{2+}$  and  $\text{Cd}^{2+}$ : synthesis, characterization, and extraction studies. Environmental Science & Technology. 36 (2002): 2523-2529.
- [121] Li, Z.; Wei, Q.; Yuan, R.; Zhou, X.; Liu, H.; Shan, H. and Song, Q. A new room temperature ionic liquid 1-butyl-3-trimethylsilylimidazolium hexafluorophosphate as a solvent for extraction and preconcentration of mercury with determination by cold vapor atomic absorption spectrometry. Talanta. 71 (2007): 68-72.
- [122] Pourreza, N. and Ghanemi, K. Solid phase extraction of cadmium on 2-mercaptobenzothiazole loaded on sulfur powder in the medium of ionic liquid 1-butyl-3-methylimidazolium hexafluorophosphate and cold vapor generation-atomic absorption spectrometric determination. Journal of Hazardous Materials. 178 (2010): 566-571.
- [123] Dadfarnia, S.; Haji Shabani, A.M.; Shirani Bidabadi, M. and Jafari, A.A. A novel ionic liquid/micro-volume back extraction procedure combined with

- flame atomic absorption spectrometry for determination of trace nickel in samples of nutritional interest. Journal of Hazardous Materials. 173 (2010): 534-538.
- [124] Tsalev, D.L.; Sperling, M. and Welz, B. On-line microwave sample pre-treatment for hydride generation and cold vapour atomic absorption spectrometry. Part 2. Chemistry and applications. Analyst. 117 (1992): 1735-1741.
- [125] Skoog, D.A.; Holler, F.J. and Crouch, S.R. Principles of instrumental analysis. 6<sup>th</sup> Ed. Thomson Brooks/Cole. 2007
- [126] Ingle, J.D. and Crouch, S.R. Spectrochemical analysis. Prentice Hall: New Jersey, 1988.
- [127] Huber, L. Validation and qualification in analytical laboratories. Interpharm Press: Illinois, 1999.
- [128] Lou, T.; Chen, Z.; Wang, Y. and Chen, L. Blue-to-red colorimetric sensing strategy for Hg<sup>2+</sup> and Ag<sup>+</sup> via redox-regulated surface chemistry of gold nanoparticles. ACS Applied Materials & Interfaces. 3 (2011): 1568-1573.
- [129] Xu, X.; Wang, J.; Jiao, K. and Yang, X. Colorimetric detection of mercury ion (Hg<sup>2+</sup>) based on DNA oligonucleotides and unmodified gold nanoparticles sensing system with a tunable detection range. Biosensors and Bioelectronics. 24 (2009): 3153-3158.
- [130] Huang, C.C. and Tseng, W.L. Role of fluorosurfactant-modified gold nanoparticles in selective detection of homocysteine thiolactone: remover and sensor. Analytical Chemistry. 80 (2008): 6345-6350.
- [131] Wang, Y.; Yang, F. and Yang, X. Colorimetric biosensing of mercury(II) ion using unmodified gold nanoparticle probes and thrombin-binding aptamer. Biosensors and Bioelectronics. 25 (2010): 1994-1998.
- [132] Yang, X.; Liu, H.; Xu, J.; Tang, X.; Huang, H. and Tian, D. A simple and cost-effective sensing strategy of mercury(II) based on analyte-inhibited aggregation of gold nanoparticles. Nanotechnology. 22 (2011): 275503.
- [133] Fan, A.; Ling, Y.; Lau, C. and Lu, J. Direct colorimetric visualization of mercury (Hg<sup>2+</sup>) based on the formation of gold nanoparticles. Talanta. 82 (2010): 687-692.

- [134] Ding, N.; Zhao, H.; Peng, W.; He, Y.; Zhou, Y.; Yuan, L. and Zhang, Y. A simple colorimetric sensor based on anti-aggregation of gold nanoparticles for  $\text{Hg}^{2+}$  detection. Colloids and Surfaces A: Physicochemical and Engineering Aspects. 395 (2012): 161-167.
- [135] Chen, L.; Lou, T.; Yu, C.; Kang, Q. and Chen, L. *N*-1-(2-Mercaptoethyl)thymine modification of gold nanoparticles: a highly selective and sensitive colorimetric chemosensor for  $\text{Hg}^{2+}$ . Analyst. 136 (2011): 4770-4773.
- [136] Liu, Z.; Hu, J.; Tong, S.; Cao, Q. and Yuan, H. Colorimetric detection of  $\text{Hg}^{2+}$  ions in aqueous media using CA-Au NPs. Spectrochimica Acta Part A: Molecular and Biomolecular Spectroscopy. 97 (2012): 737-740.
- [137] Li, L.; Li, B.; Qi, Y. and Jin, Y. Label-free aptamer-based colorimetric detection of mercury ions in aqueous media using unmodified gold nanoparticles as colorimetric probe. Analytical and Bioanalytical Chemistry. 393 (2009): 2051-2057.
- [138] Yang, X.; Liu, H.; Xu, J.; Tang, X.; Huang, H. and Danbi, T. A simple and cost-effective sensing strategy of mercury (II) based on analyte-inhibited aggregation of gold nanoparticles. Nanotechnology. 22 (2011): 1-6.
- [139] Zhang, F.; Zeng, L.; Yang, C.; Xin, J.; Wang, H. and Wu, A. A one-step colorimetric method of analysis detection of  $\text{Hg}^{2+}$  based on an in situ formation of Au@HgS core-shell structures. Analyst. 136 (2011): 2825-2830.
- [140] Qing, Z.; He, X.; Wang, K.; Zou, Z.; Yang, X.; Huang, J. and Yan, G. Colorimetric multiplexed analysis of mercury and silver ions by using a unimolecular DNA probe and unmodified gold nanoparticles. Analytical Methods. (2012):
- [141] Lou, T.; Chen, L.; Zhang, C.; Kang, Q.; You, H.; Shen, D. and Chen, L. A simple and sensitive colorimetric method for detection of mercury ions based on anti-aggregation of gold nanoparticles. Analytical Methods. 4 (2012): 488-491.

- [142] Chansuvarn, W. and Imyim, A. Visual and colorimetric detection of mercury(II) ion using gold nanoparticles stabilized with a dithia-diaza ligand. Microchimica Acta. 176 (2012): 57-64.
- [143] Choudhury, S.B.; Ray, D. and Chakravorty, A. Sulfur-ligated nickel oxidation states. Chemistry of family of  $Ni^zS_2N_4$  ( $z = +2, +3, +4$ ) complexes incorporating hexadentate thioether-imine-oxime binding. Inorganic Chemistry. 30 (1991): 4354-4360.
- [144] Huddleston, J.G.; Willauer, H.D.; Swatloski, R.P.; Visser, A.E. and Rogers, R.D. Room temperature ionic liquids as novel media for 'clean' liquid-liquid extraction. Chemical Communications. (1998): 1765-1766.
- [145] Alvarez, M.M.; Khoury, J.T.; Schaaff, T.G.; Shafigullin, M.N.; Vezmar, I. and Whetten, R.L. Optical absorption spectra of nanocrystal gold molecules. The Journal of Physical Chemistry B. 101 (1997): 3706-3712.
- [146] Leopold, K.; Foulkes, M. and Worsfold, P. Methods for the determination and speciation of mercury in natural waters-A review. Analytica Chimica Acta. 663 (2010): 127-138.
- [147] Lisha, K.P.; Anshup and Pradeep, T. Towards a practical solution for removing inorganic mercury from drinking water using gold nanoparticles. Gold Bulletin. 42 (2009): 144-152.
- [148] Samal, A.; Sreeprasad, T. and Pradeep, T. Investigation of the role of  $NaBH_4$  in the chemical synthesis of gold nanorods. Journal of Nanoparticle Research. 12 (2010): 1777-1786.
- [149] Leopold, K.; Foulkes, M. and Worsfold, P.J. Gold-coated silica as a preconcentration phase for the determination of total dissolved mercury in natural waters using atomic fluorescence spectrometry. Analytical Chemistry. 81 (2009): 3421-3428.
- [150] Zhang, Y.; Li, B. and Chen, X. Simple and sensitive detection of dopamine in the presence of high concentration of ascorbic acid using gold nanoparticles as colorimetric probes. Microchimica Acta. 168 (2010): 107-113.
- [151] Zhang, Z. and Wu, Y. Investigation of the  $NaBH_4$ -induced aggregation of Au nanoparticles. Langmuir. 26 (2010): 9214-9223.

- [152] Wagner, J.; Tshikhudo, T.R. and Köhler, J.M. Microfluidic generation of metal nanoparticles by borohydride reduction. Chemical Engineering Journal. 135, Supplement 1 (2008): S104-S109.
- [153] Brown, K.R. and Natan, M.J. Hydroxylamine seeding of colloidal Au nanoparticles in solution and on surfaces. Langmuir. 14 (1998): 726-728.
- [154] Jana, N.R.; Gearheart, L. and Murphy, C.J. Evidence for seed-mediated nucleation in the chemical reduction of gold salts to gold nanoparticles. Chemistry of Materials. 13 (2001): 2313-2322.
- [155] Gole, A. and Murphy, C.J. Seed-mediated synthesis of gold nanorods: role of the size and nature of the seed. Chemistry of Materials. 16 (2004): 3633-3640.
- [156] Cao, L.; Zhu, T. and Liu, Z. Formation mechanism of nonspherical gold nanoparticles during seeding growth: Roles of anion adsorption and reduction rate. Journal of Colloid and Interface Science. 293 (2006): 69-76.
- [157] Sanz-Medel, A.; Fernandez Perez, M.M.; De la Guardia Cirugeda, M. and Dominguez, J.L.C. Metal chelate fluorescence enhancement by nonionic micelles: surfactant and auxiliary ligand nature influence on the niobium-lumogallion complex. Analytical Chemistry. 58 (1986): 2161-2166.
- [158] Rex, M.; Hernandez, F.E. and Campiglia, A.D. Pushing the limits of mercury sensors with gold nanorods. Analytical Chemistry. 78 (2005): 445-451.
- [159] Hirayama, N.; Deguchi, M.; Kawasumi, H. and Honjo, T. Use of 1-alkyl-3-methylimidazolium hexafluorophosphate room temperature ionic liquids as chelate extraction solvent with 4,4,4-trifluoro-1-(2-thienyl)-1,3-butanedione. Talanta. 65 (2005): 255-260.

## **APPENDIX**

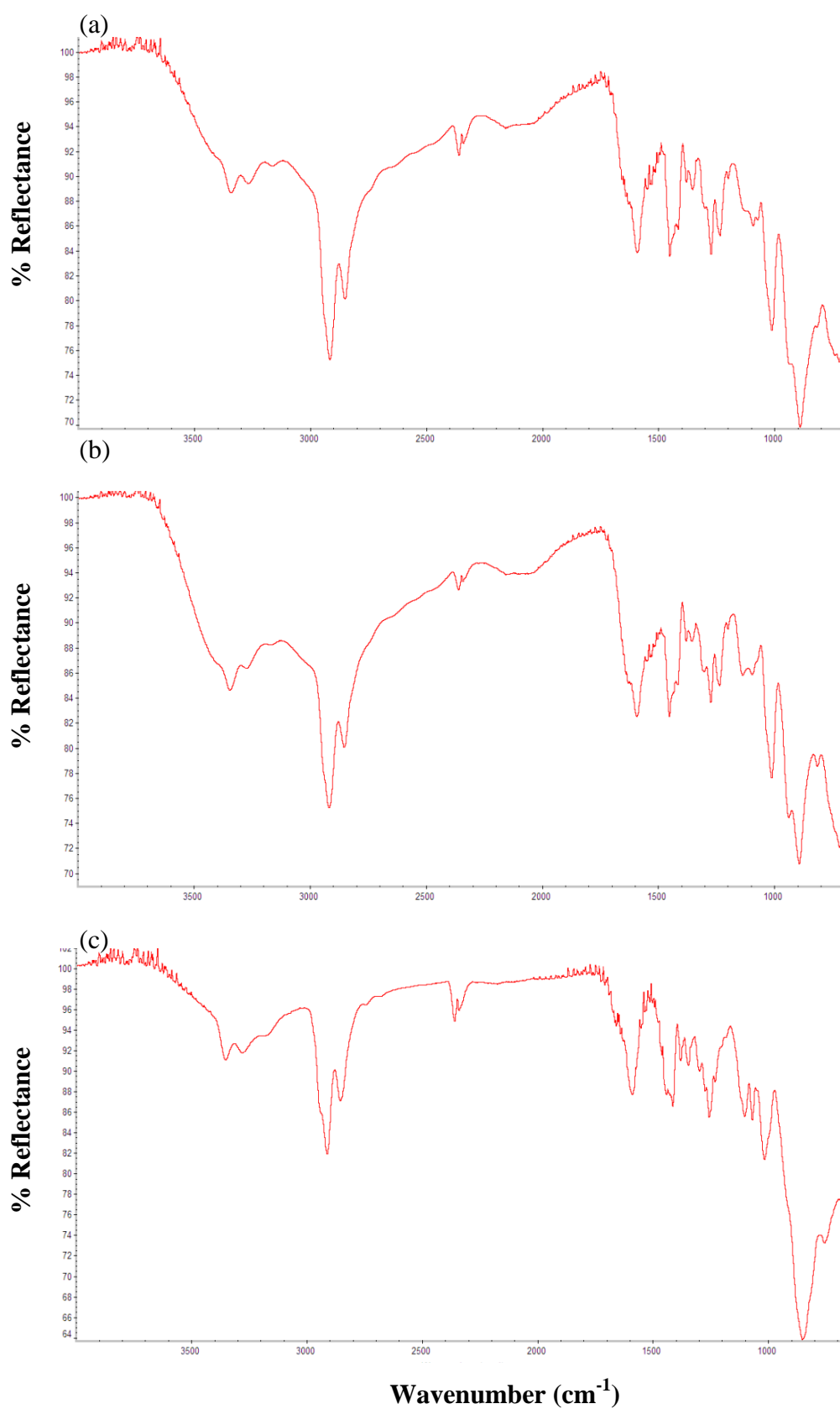


**Figure A.1** FT-IR spectra of three dithia-diaza ligands (a) 3-AEPE, (b) 4-AEBE and (c) 5-AEPE.

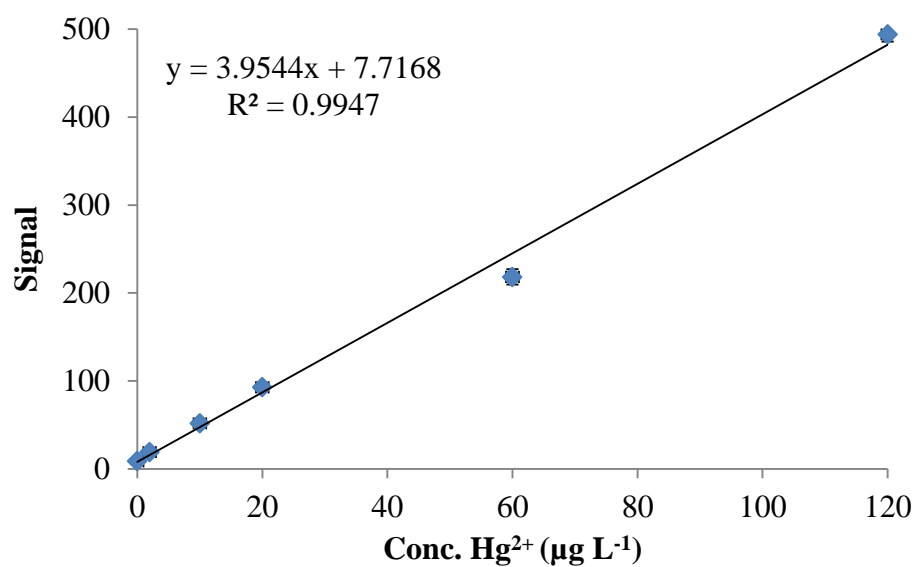


**Figure A.2** Calibration curve of mercury from ICP-OES.

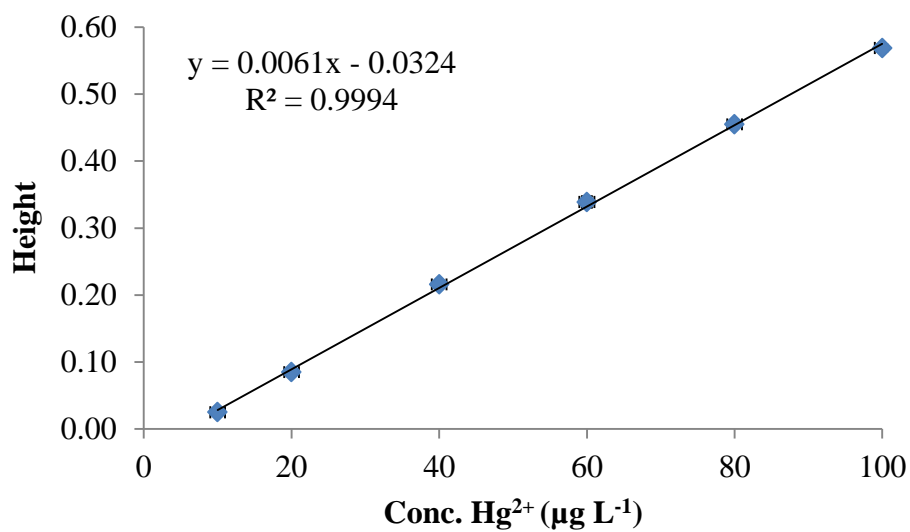
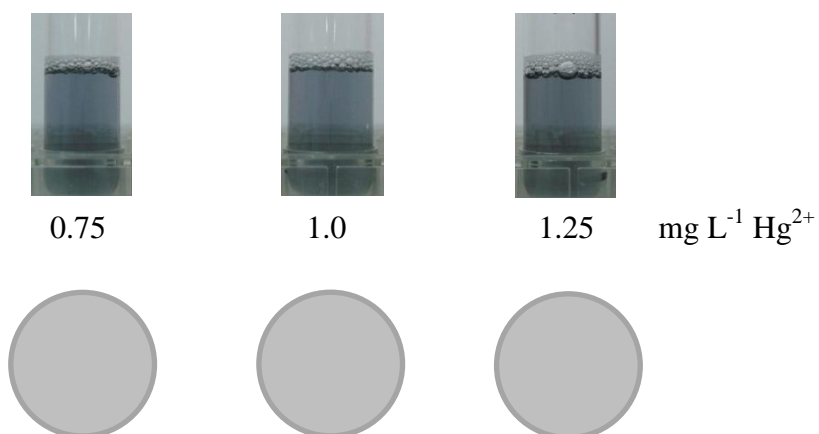


**Figure A.3** Calibration curve of mercury from flow injection CV-AAS.



Element	Signal (count/second)		
$^{202}\text{Hg}$	476.68	630.02	656.68
$^{197}\text{Au}$	3.33	16.67	16.67

**Figure A.4** Pictures of blue solutions and membranes (0.22  $\mu\text{M}$ ) after the filtration and mercury (202 amu) and gold (197 amu) contents from LA-ICP-MS of 3-AEPE-stabilized gold nanoparticles with different concentration of mercury(II) ions.

## VITA

Mr. Woravith Chansuvarn was born on February 5, 1977 in Suphanburi, Thailand. He received a Bachelor's degree of Science in Chemistry from Rajabhat Institute Kanchanaburi in 2003. He received a Master's degree of Science in Chemistry (Analytical Chemistry) from Chiang Mai University in 2005. Since 2008, he has been a graduate student at the Department of Chemistry Chulalongkorn University and a member of Environmental Analysis Research Unit (EARU) under supervision of Assistant Professor Dr. Apichat Imyim. He finished his Doctor of Philosophy (Chemistry) in the Academic Year 2012. He has been working as a lecturer at Faculty of Science and Technology, Rajamangala University of Technology Phra Nakhon (RMUTP), Bangkok. His present address is 1381 Pibulsongkram Road, Bang-Sue, Bangkok, Thailand, 10800. Contact number is 0-2913-2424 ext. 195. E-mail: woravith.c@rmutp.ac.th.

### Publication

1. Woravith Chansuvarn and Apichat Imyim, Visual and colorimetric detection of mercury(II) ion using gold nanoparticles stabilized with a dithia-diaza ligand. *Microchimica Acta*. 176 (2012) 57-64.